Norges miljø- og
biovitenskapelige
universitet

Master's Thesis 2016 30 ECTS
Department of Mathematical Sciences and Technology

Using Open Circuit Voltage Relaxation for Analyzing Material Behaviors in a Half-Cell

Tor Kristian Vara
Environmental Physics and Renewable Energy

Preface

This thesis is a part of the master degree Environmental Physics and Renewable Energy at the Norwegian University of Life Sciences (NMBU), and was carried out during the fall semester of the year 2016. The idea of identifying a cell's parameters by fitting the open circuit voltage relaxation, originated from the Energy Systems department at the Institute for Energy Technology (IFE).

I want to thank my external supervisor at IFE, Jan Petter Mæhlen, for being a positive and calm person. Jan Petter Mæhlen helped me with everything from Python-related problems to giving insightful ideas and discussions. It was truly motivating and fun to have Jan Petter as a supervisor. I also want to thank my internal supervisor, Espen Olsen, at NMBU. Espen Olsen was of great help regarding the process and layout of the thesis. His concrete opinions and experience in how to conduct a good thesis has been valuable.

There are many people at IFE I want to thank. Martin Kirkengen for his invaluable knowledge that arose many ideas and theories. I also want express my gratitude to Martin Kirkengen for introducing me to a lot of useful theory about lithium-ion batteries through his Battery Technology course at Universitetssenteret på Kjeller (UNIK). A thanks to Allen, for his questions, opinions and knowledge, which lead to interesting discussions and many theories. I owe a great thank you to Hanne Andersen for taking her time to make the cells used in my thesis. Furthermore, I would like to thank Preben Vie for conducting the electrochemical impedance spectroscopy (EIS) and showing enthusiastic interest for my thesis. I also want to thank everyone that helped me with any questions I had and for including me during my time at IFE.

I want to thank my family and friends for incredible support during my thesis and in general. A special thanks to my girlfriend for her encouragement and many corrections. Lastly, I want to thank all my friends at NMBU for an amazing five years at Ås.

Ås, 2016-12-15

_____

Tor Kristian Vara

Abstract

The possibility of using the open circuit voltage relaxation to understand material behaviors in a battery cell was examined in this thesis. The aim was to develop a method to interpret the activities occurring in a battery, without the use of other experimental methods. The impact could be less work with expensive and time-consuming experiments.

Seven lithium-ion cells with silicon as active material on the negative electrode and lithium metal as the counter electrode, were made. Three cells contained electrolyte additives, and five without. An EIS study was carried out on one of the cells with additives. The rest of the cells were used for open circuit analysis. An equivalent circuit with two resistance-capacitance (RC) parallels connected in series was used as a cell model. The RC-circuits represented the charge transfer and diffusion polarization in a cell. Apparent RC-parameters for the cells were found by using the cell model and Levenberg-Marquardt least square minimization.

Python was used as programming tool to develop a subprogram for the Python package, `cellpy`. The program fitted the cell model's voltage to the measured open circuit voltage by iterating the model's RC-parameters. The best parameters obtained from the fit were compared with the impedance found in the EIS study, and are displayed in Fig. 1. The method developed in this thesis was concluded to be useful in analyzing the cell's material behaviors regarding the charge transfer process.

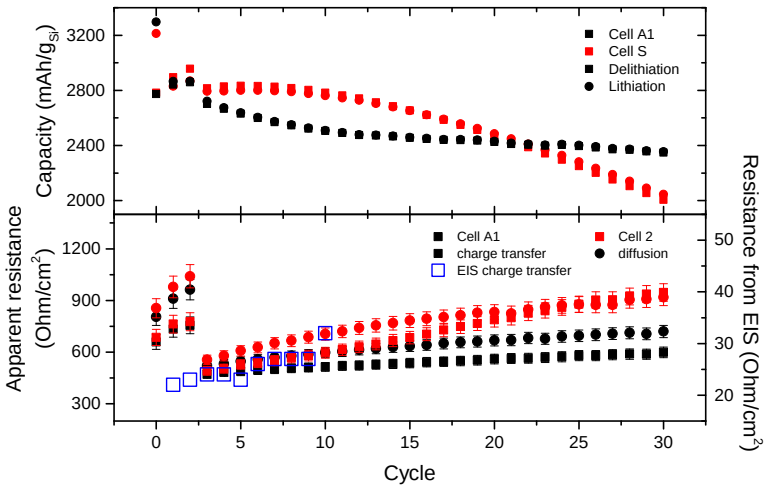

Figure 1: Main result. Comparison between specific capacity, apparent resistance from the fit and charge transfer resistance from EIS. The EIS cell and cell A1 had electrolyte additives.

Sammendrag

Hensikten med oppgaven var å undersøke muligheten for å bruke åpen krets relaksasjonsspenningsdata til å forstå oppførselen til materialene i en battericelle. Målet var å utvikle en metode for å analysere aktivitetene i et batteri, uten bruk av dyre og tidskrevende eksperimenter.

Det ble lagd syv litium-ion battericeller med silisium som litium vert på den negative elektroden og rent litium metall som positive elektrodemateriale. Tre av cellene hadde additiver i elektrolytten, og resten var foruten. En av de tre cellene med additiver ble brukt i en elektrokjemisk impedans spektroskopi (EIS) studie. Analyse og parameter tilpassing av åpen krets relaksasjonsspenning ble utført på de resterende cellene. En ekvivalent krets med to motstand-kondensator paralleller koblet i serie ble brukt som en cellemodell for tilpasningsprosessen. En av parallellene representerte aktiveringsoverspenningen, mens konsentrasjonsoverspenningen var representert av den andre parallellkretsen. Tilpassingen av de tilsynelatende parameterne ble gjennomført med Levenberg-Marquardt minste kvadraters metode.

Programmeringsspråket Python ble brukt som et digitalt verktøy for å utvikle en ny funksjon til Python pakken, `cellpy`. Brukeren av programmet kan definere en cellemodell og tilpasse modellens åpen krets spenning til målte verdier. Figur 2 viser to av cellenes kapasiteter som funksjon av sykling, sammenlignet med tilpassede motstander og EIS resultatet. Aktiveringsoverspenningen tilpasset i denne oppgaven var nyttig i vurderingen av cellematerialenes oppførsel.

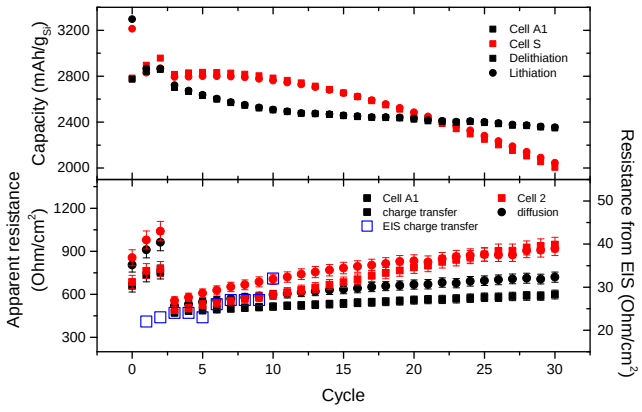

Figure 2: Hovedresultatet fra denne studien. EIS cellen og celle A1 hadde additiver i elektrolytten.

Contents

Nomenclature

Abbreviations

AC	Alternating Current [A]
a-Si	Amorphous Silicon Structure
CMC	CarboxyMethyl Cellulose
c-Si	Crystalline Silicon Structure
DL	Double-Layer
DMC	Dimethyl Carbonate
EC	Ethylene Carbonate
EDLC	Electrical Double-Layer Capacitor
EIS	Electrochemical Impedance Spectroscopy
Fig.	Figure
HF	Hydrogen Fluoride
IHP	Inner Helmholtz Plane
IR	Internal Resistance
KCL	Kirchhoff's Circuit Law
LCP	Lithium Cobalt Phosphate
Li	Lithium

LM	Levenberg-Marquardt
LMO	Lithium Manganese Oxide
NLLS	Non-Linear Least Square
OCV	open circuit voltage
OHP	Outer Helmholtz Plane
PC	Propylene Carbonate
redox	Reduction-Oxidation
redox	Reduction-Oxidation
SEI	Solid Electrolyte Interface
SHE	Standard Hydrogen Electrode
Si	Silicon
SOC	State of Charge
SOC	State of Charge

Symbols

$a_{oxidation}$	Activity from the oxidation reation
$a_{reduction}$	Activity from the reduction reaction
C	Capacitance [F]
E	Electric field [V/m]
e^-	Electron
ϵ	Dielectric constant
ϵ_0	Permittivity of vacuum
ϵ_r	Relative permittivity of medium
η	Coulombic efficiency

f	Frequancy [Hz]
ΔG^0	Standard change in Gibbs free energy [J]
ΔG^0	Standard change in Gibbs free energy [J]
ΔI	Difference in current [A]
I	Current [A]
I_0	Current amplitude
I_a	Applied AC current
R_{IR}	Internal resistance resistor [ohm]
j	Imaginary number
κ	Conductivity of solution [S/m]
d	Distance from electrode [m]
l	Length [m]
M^+	Metal-ion
M	Metal
ω_{max}	Maximum radial frequencys
ω	Radial frequency
ϕ	Shift in phase
φ	Overpotential (Polarization) [V]
Q	Charge [Ah]
Q_{in}	Amount of charge in [C]
Q_{out}	Amount of charge out [C]
Q_r	Reaction quotient

R	Resistance [Ohm]
R_g	Universal gas constant [J/(mol K)]
ρ	Charge density [C/m]
T	Temperature [K]
t	Time [s]
t_0	Start time [s]
τ	Time constant [s]
V	Electric potential [V]
V_0	Amplitude of a sinusoidal potential wave.
V_{cell}	Cell voltage [V]
V_i	Initial voltage in relaxation process [V]
V_{neg}	Negative electrode potential [V]
V_{pos}	Positive electrode potential [V]
V_{rlx}	Relaxation voltage
x	Number of electrons
Z	Impedance [Ohm]
$Z(Im)$	Imaginary impedance [Ohm]
$Z(Re)$	Real impedance [Ohm]

List of Figures

List of Tables

Chapter 1

Introduction

The demand for energy storage is increasing as the growth of technologies is continues. Today's batteries are used in numerous applications, all from gadgets and communication devices to grid-storage and operations in space. Although batteries, especially Li-ion batteries, receive a lot of attention in this "technological evolution", the batteries advancement are criticized for being too slow in contrast to the improvement of technologies and pressing matter of global warming [1].

Ever since Sony commercialized the Li-ion battery in 1991, there has been an increase in energy density of Li-ion batteries with 8-9 % per year [2][3]. Despite its incomparable high energy and power density, scientists are searching for a way to significantly improve the battery to keep up with today's society. Li-ion batteries have the potential to store more capacity than today's commercially available batteries [4].

The current negative electrode material used for hosting lithium in the Li-ion batteries is graphite. Graphite can store 372 mAh/g of charge capacity when holding one lithium per six carbon (LiC_6). Silicon (Si) can increase this charge capacity by a factor 10, as its ability to host lithium is much greater. In fact, a lithium-silicon (Li-Si) alloy of $Li_{15}Si_4$ can theoretically store 3579 mAh/g_{Si} [3]. The biggest challenge with Si as active material on the negative electrode is that its lattice expand up to 320 % when fully inserted by Li [5]. This cause the Li-ion battery with Si to die after about 100 cycles, which is low compared to the demand of about 1000 cycles [6][7].

1.1 Background

At research facilities, such as Institute of Energy Technology (IFE), it's common to sample the open circuit voltage (OCV) during battery cell testing. It has been observed that the OCV decay (relax) towards an equilibrium potential after charge and discharge. The decay imitates the discharge of a charged capacitor. The battery group at Institute of Energy Technology (IFE) proposed the idea of developing a program to fit a cell's or battery's impedance with a proposed model to the OCV-relaxation data.

1.1.1 Problem Formulation

This thesis will examine the open circuit voltage (OCV)-relaxation data from lithium-ion half-cells with silicon as an active anode material, and investigate the possibility of using these data to analyze how the materials in a cell behave. To achieve this, the following approach will be used:

- Making test cells with silicon as an active anode material. Some of the cells will have an improved electrolyte, to check that the cells behave accordingly.
- Design a representable cell model. The model will be based on theory of a cell's functioning.
- Derive an expression for the model's voltage during OCV-relaxation.
- Build a program in Python 2.7. The program has to accept a legitimate model, make a reasonable guess of initial parameters and fit the defined model's relaxation voltage to the measured OCV-relaxation data.
- Compare the cell model's impedance with results gained from performing an electrochemical impedance spectroscopy (EIS) on the test cells.
- Verify the developed method. It will be based on the cells' behaviors and correlations between the EIS study and fitted parameters.

The aim is to develop a new method to faster analyze the effect from altering a battery's material. The impact of a successful fitting of the OCV-relaxation data would indeed make research faster and easier for scientist, which would result in reduced workload and less expenses for research facilities.

1.2 Structure of the Report

The report is structured in the following way:

Chapter 2 will give a brief introduction to batteries in general. Then elaborate how a cell operate and the lithium-ion battery.

Chapter 3 describes how the cells are assembled and introduces the instruments used in this study. The development of a cell model and the programming will be further explained.

Chapter 4 is the results and discussion part of the report. The chapter will first discuss some general characterization graphs. Then display and discuss the fitted results and EIS study.

Chapter 5 summarizes the results and discussion, before announcing the conclusion.

Chapter 6 gives examples of further studies.

Chapter 2

Theory

It is important to examine the composition, purpose and parameters of a battery before introducing the theory about Li-ion battery with silicon (Si) as its negative electrode material. This chapter will give the required theory to analyze and discuss the results.

2.1 The Battery

A battery is a device that can store and convert chemical energy into electrical energy. What makes the battery device so popular, is the convenience of its production flexibility. It can be designed in a wide range of sizes and be used in numerous applications. This thesis will mainly focus on the rechargeable Li-ion battery, or more specifically, a Li-ion half cell with silicon as its negative electrode material. In this text, "cell" and "half-cell" refers to as an electrochemical cell and a “battery” is cells connected in series.

2.2 Components in an Electrochemical Cell

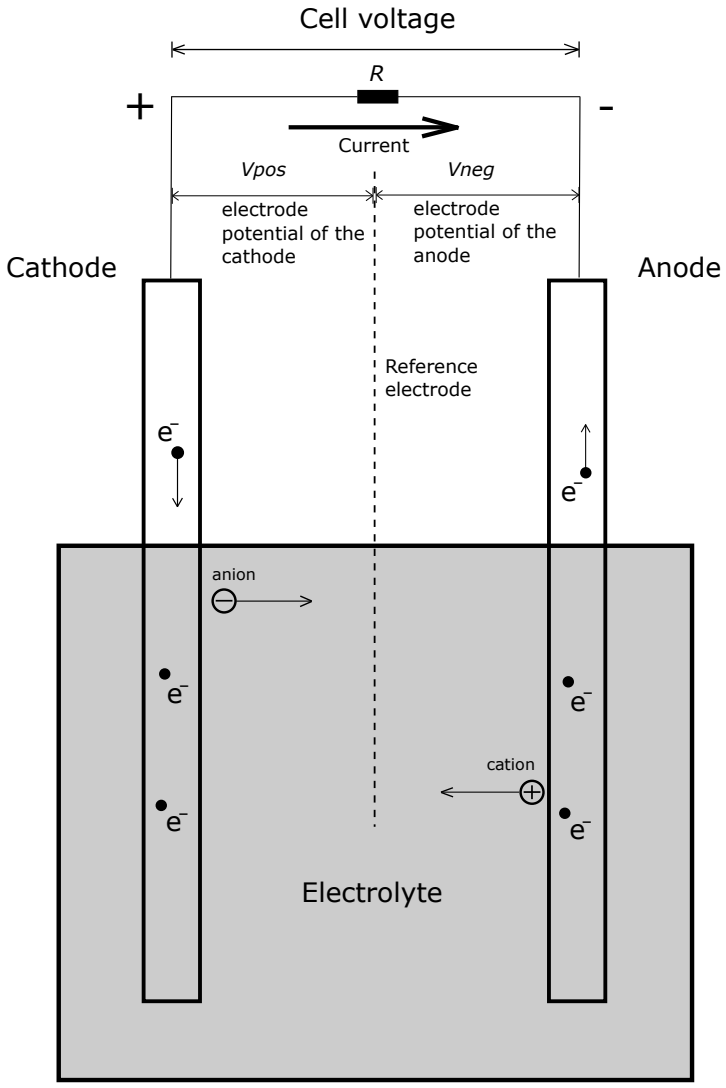

Figure 2.1: Fundamental operation of an electrochemical cell during discharge through a load R. Oxidation and reduction occurs respectively at the negative (anode) - and positive (cathode) electrode. The electrons move in an external circuit connected between the electrodes, while the ions (cations/ anions) move through the electrolyte. The cell voltage (V_{cell}) is the difference in the two electrode's electrical potentials (V_{pos} and V_{neg}) with respect to a reference electrode [8][9]

The basic components in a cell are the negative electrode (anode), positive electrode (cathode) and the electrolyte, as shown in Fig. 2.1. Figure 2.1 illustrates how electrons and ions move in a closed circuit cell during discharge. The reference electrode in Fig. 2.1 is not necessarily physically inside the cell, and is merely to show how the cell voltage is defined by the potential

difference between the two electrodes with respect to a reference, when soaked in an electrolyte [8]. The difference in electric potential causes a reduction-oxidation (redox) reaction on the electrodes, which respectively induces an electric current and ionic transfer through the external circuit and electrolyte [10].

2.2.1 Anode

The anode is defined as the electrode where oxidation appears. Oxidation happens when a cell's electrode loses electrons to an external circuit, or gains anions (negatively charged ions) from the electrolyte [8][11]. A simple example of a chemistry formula for oxidation half-reaction can be expressed as:

$$M \longrightarrow M^+ + e^- \tag{2.1}$$

where M is the metal, M^+ is the metal-ion, and e^- is the released electron. The half-reaction (2.1) can happen on either electrode in a cell, e.g., during discharge (situation in Fig. 2.1) the negative electrode is the cell's anode because it oxidizes. In this and other texts, the anode is referred to as the negative electrode of a battery or cell [10]. The anode's active material is preferably easily oxidized, but varies with the chemistry of the cell and the cell's requirements. This thesis will concentrate on silicon as active anode material in an Li-ion half-cell (see section 2.2.5).

2.2.2 Cathode

The cathode is the electrode where a reduction occurs. A reduction refers to when the electrode gains electrons or cations (positively charged ions) [8]. The cathode and anode are therefore always on opposite electrodes. The chemical formula for reduction is the same as half - reaction (2.1), but with the arrow facing the opposite way, as shown in reaction (2.2).

$$M^+ + e^- \longrightarrow M \tag{2.2}$$

During discharge (see Fig. 2.1), the cathode is defined as the positive electrode. The cathode is naturally assigned the role as the positive electrode because the anode is referred to as the negative electrode [10].

2.2.3 Electrolyte

Another essential component in a cell is the electrolyte. As described and illustrated in Fig. 2.1, the electrons released in reaction (2.1) travel through an external circuit, and the metal-ion is

transported through a liquid or solid electrolyte [8]. The electrolyte has to be ionic conductive and electronic isolating, otherwise the electrons would not be able to perform work on a load. If the electrolyte does not meet these criteria, it could ruin the cell by i.e., inducing an internal short circuit [9].

2.2.4 Separator

A critical component when dealing with liquid electrolytes is the separator (not illustrated in Fig. 2.1). Its task is as the name implies, to separate the electrodes and to make sure that there are no physical contacts between them. A separator is usually an electric isolating membrane that is ionic conductive. It should be as thin as possible while being chemically, electrochemically and mechanically strong - mechanically because it has to withstand e.g., physical tension, internal temperature rise, assembling process, etc. The accepted separator thickness for commercial batteries are ~2 μm. The porosity is important for the separator's ability to hold a liquid electrolyte, which will increase the ionic conductivity. For Li-ion batteries, the porosity is usually about 40 %. The pore size plays an important role in the separators' ability to actually separate the electrode materials. The pores have to be smaller than the electrodes' particles and the additives in the electrolyte. It is also desirable to have a separator that does not increase the resistance in the electrolyte too much. The permeability is a measure of how easily the particles are transported through the membrane and is important for the separator's contribution to increased resistance in an electrolyte. To ensure a long cycle life, the permeability has to be uniform on the separator's surface [12].

2.2.5 Half-cell

Fig. 2.1 shows a full cell with a working cathode and anode. A half-cell is, as the name implies, one or the other electrode in an electrolyte by itself [10]. To physically measure the activity and working voltage, an arbitrary reference electrode is required in the half-cell [8]. Using a half-cell for research purposes is favorable because it isolates each electrode, making it easier to analyze the electrode material's properties [10]. The relationship between the activities on the electrode and the cell's potential is important to understand in order to analyze the properties of an electrode [8].

2.3 Cell Voltage and Gibbs Free Energy

The cell voltage from Fig. 2.1, V_{cell}, can be expressed as the potential difference from the chemical reactions in the cell:

$$V_{cell} = V_{pos} - V_{neg} \tag{2.3}$$

V_{pos} and V_{neg} are respectively the electrical potential from the positive and negative electrode. Half-reactions (2.1) and (2.2) can be combined to a general reduction-oxidation (redox) reaction (2.4), which describe the reactions in a full cell.

$$M^{x-} + xe^{-} \longleftrightarrow M \tag{2.4}$$

x is the number of electrons involved in the redox reaction.

The change in Gibbs free energy (electrical work) for the activities occurring on an electrode is expressed in (2.5).

$$\Delta G = \Delta G^0 + R_g T \ln(\frac{a_{oxidation}}{a_{reduction}}) \tag{2.5}$$

where R_g is the universal gas constant (8.314 J/(K·mol)) and T is the temperature. $a_{oxidation}$ and $a_{reduction}$ are the activities, or concentrations, from the oxidation and reduction reactions. The change in Gibbs free energy is stated as the:

$$|\Delta G| \ = \ \text{charges passed} \ \times \ \text{equilibrium potential difference}$$

which yields the equation (2.6) [13].

$$\Delta G = -nFV_{eq} \tag{2.6}$$

n is the number of moles of electrons in the reaction, F is the Faraday constant (96 485 C/mol) and V_{eq} is the equilibrium electrode potential. The negative sign of ΔG^0 describes whether a reaction is spontaneous or not. The reaction occurs spontaneously if Eq. (2.6) is negative [14].

In equation (2.6), ΔG^0 is the "standard change in Gibbs free energy" under standard conditions (1 bar, 25°C and 1 mol/dm^3). The standard change in Gibbs free energy is expressed in Eq. (2.7) [8][10].

$$\Delta G^0 = -nFV_{eq}^0 \tag{2.7}$$

Nernst's well-known equation (2.8) is obtained when inserting Eq. (2.6) and (2.7) into Eq. (2.5).

$$V_{eq} = V_{eq}^{0} - \frac{RT}{nF}\ln(Q_r) \tag{2.8}$$

$Q_r = a_{oxidation} / \ a_{reduction}$ is known as the reaction quotient [10][8]. Nernst's equation (Eq. (2.9)) relates the equilibrium potential on an electrode to the activities of the chemical reactions. By using Eq. (2.3) and Nernst Eq. (2.8), the cell voltage can be linked to the redox reaction (2.4) occurring in a cell through Nernst's equation (2.9).

$$V_{cell} = V_{cell}^{0} - \frac{RT}{nF}\ln(Q_r) \tag{2.9}$$

2.4 Double-Layer Capacitance

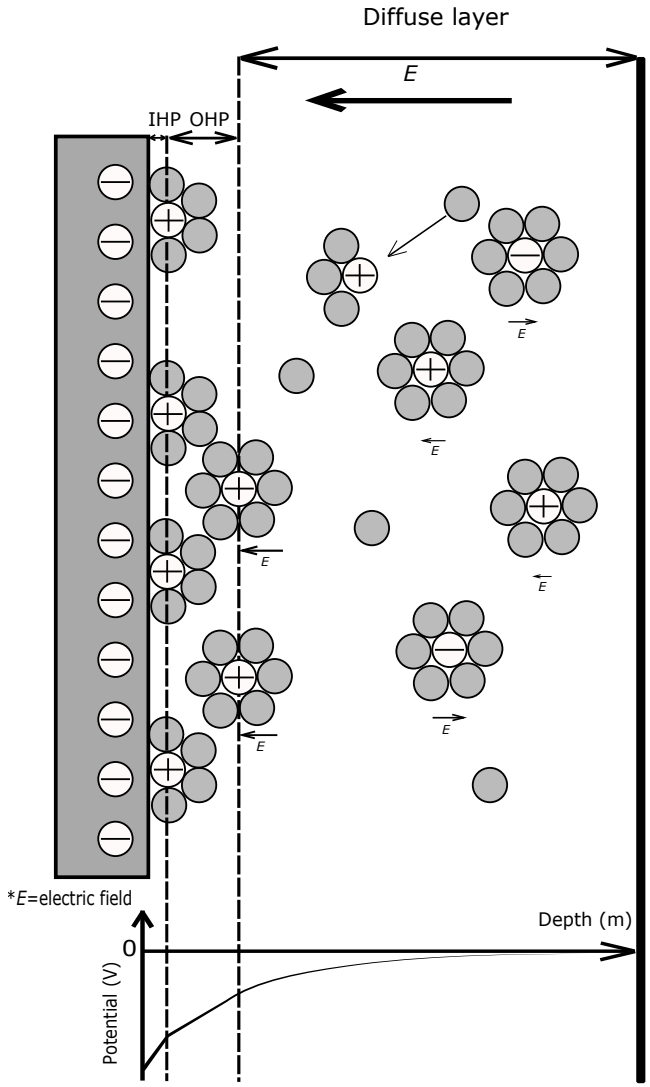

Figure 2.2: A simple illustration of the electrical double-layer (DL) on the interface of the electrode surface and electrolyte. IHP and OHP are the inner and outer Helmholtz plane defined by Grahame. The gray particles sticking to the ions are solvent molecules in the electrolyte. The potential drops linearly at IHP and exponentially with distance into the electrolyte [15]. The electric field (E) is induced by the difference of ion-concentration in the diffuse layer, electric field from IHP and OHP. E for IHP and OHP are not shown in the figure. The small electric field arrows indicate the contribution from each solvate compound [16][17].

This section covers the development of different double-layer (DL) models. The DL model is important to understand because it explains the capacitive behavior of a cell.

2.4.1 Inner Helmholtz Plane (IHP)

Hermann von Helmholtz first described in 1853 the formation of a double-layer (DL) between an electrode material and the electrolyte. At the interface of thes electrode surface and the electrolyte, the ions in the electrolyte interact with the active material in the electrode, forming a so-called "Inner Helmholtz Plane" (IHP) as shown in Fig. 2.2 [16]. Because of their difference in charges, an electric field arises. Poisson's equation for one dimension, explains the potential distribution between the planes.

$$\frac{\delta^2 V}{\delta d^2} = -\frac{\rho(d)}{\epsilon_r \epsilon_0} \tag{2.10}$$

V is the electric potential, d, the distance from the electrode, ρ is the charge density and ϵ_r and ϵ_0 are respectively the relative permittivity of medium and permittivity of vacuum [18]. Helmholtz assumed that the ions are point charges, thus the Poisson's equation (2.10) can be simplified to:

$$\frac{\delta^2 V}{\delta d^2} = 0 \tag{2.11}$$

The equation (2.11) suggests that the IHP functions in the same fashion as a capacitor, where the electrode surface and center of the ions behave as two parallel plates. The capacitor's ability to store energy is rated as the capacitance expressed in Eq. (2.12).

$$C = \frac{A\epsilon}{4\pi d} \tag{2.12}$$

A is the surface area of the electrode interface, ϵ is the relative permittivity of the electrolyte (also called the dielectric constant) and d is the distance between the two plates (the ion's radius) [16].

2.4.2 Development of Electric Double-Layer Models

The Helmholtz layer is under the assumptions that no interactions take place further into the electrolyte, and does not consider the concentration of the electrolyte. Gouy and Chapman introduced a diffuse model which explains the electrical double-layer capacitance (EDLC) as a function of distance into the electrolyte [18]. Stern then combined Helmholtz layer with the Gouy-Chapman diffuse layer, and Grahame introduced a third layer. Thus he defined the inner Helmholtz plane (IHP), outer Helmholtz plane (OHP) and diffuse layer (Fig. 2.2). The introduction of an outer Helmholtz plane showed that an absorbed ion loses some of its solvent

molecules to get closer to the electrode surface, and forms the IHP [16].

In the case of dipole solvent, Bockris, Devanathan and Müller proposed a model of the DL which includes the actions of the solvent particles. The dipoles are oriented because of the charges at the electrode surface. This forms a layer of solvent particles on the electrode as shown in Fig. 2.3. The solvent particles are also surrounding the ions in the electrolyte because of the ion's charge [15]. The ions, cations in Fig. 2.3, are sticking to the electrode surface, keeping its solvent depending on the solvent's dielectric constant [17]. In figure 2.3, the potential drops in the same way as shown in Fig. 2.2 [19].

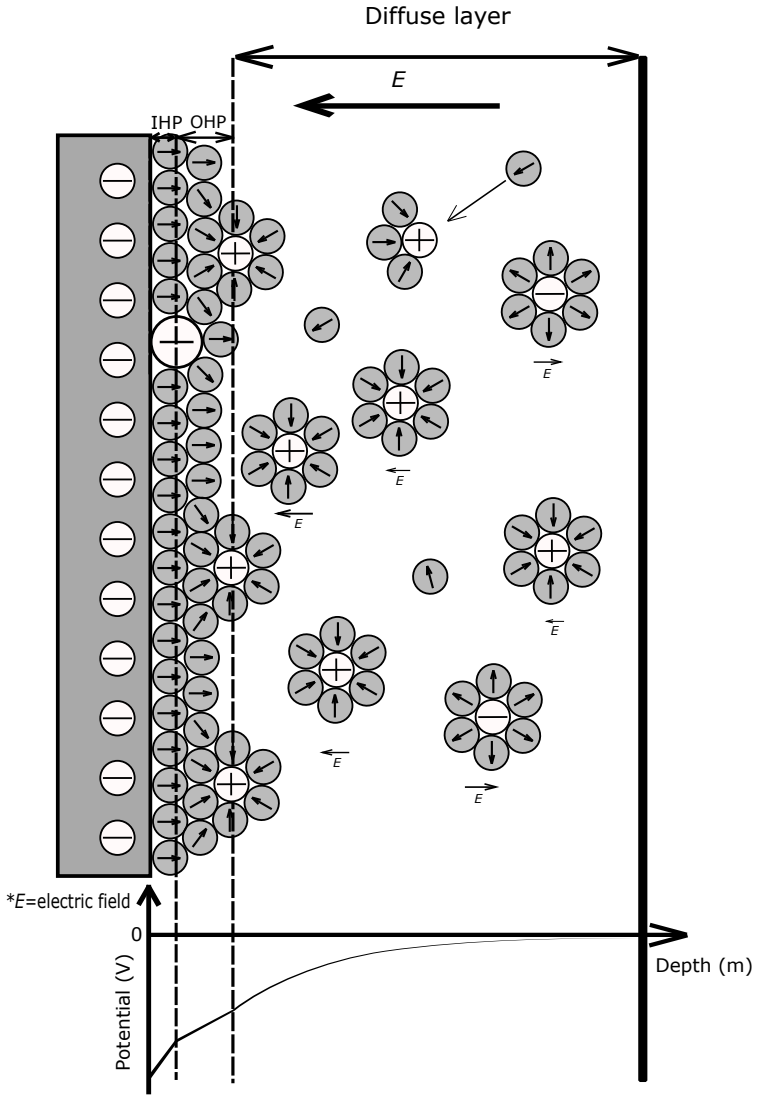

Figure 2.3: Bockris, Devanathan and Müller's model of the DL with details. The difference from this illustration and Fig. 2.2 is the polar solvent forming a layer at the electrode surface [16][17].

2.5 Characteristics and Parameters of a Cell

The choice of the battery depends on various factors affecting its performance. It is important to understand the cell's chemistry and parameters in order to analyze its performance during the desired situation. Some basic battery characteristics and parameters will be covered in this section.

2.5.1 Voltage and Polarization

The cell voltage (V_{cell}) is the potential difference between two electrodes in an electrolyte (described in section 2.2 and expressed in equation (2.3)) [8]. When the electrodes are not connected through an external circuit, the cell voltage is referred to as the relaxation voltage (V_{rlx}), and open circuit voltage (OCV) when fully relaxed (electrochemical equilibrium), that is when V_{rlx} = OCV. Written on a battery package is the nominal voltage. The actual operating voltage under load is called the working voltage, and is always lower than the OCV. The cut-off voltage is a term for the end voltage during discharge/charge of a cell. The cut-off voltage is designed for safety reasons [20].

When an electrode's electric potential changes from its equilibrium voltage (V_{eq}), it experiences polarization caused by a current flow. The magnitude of the deviation from the equilibrium voltage is equal to the polarization potential (overpotential) at the electrode [21]. The total polarization in the cell is the sum of the polarizations occurring at the electrodes. In Fig. 2.4 the potential difference between the ideal curve (OCV) and a characteristic curve, is caused by polarization [20].

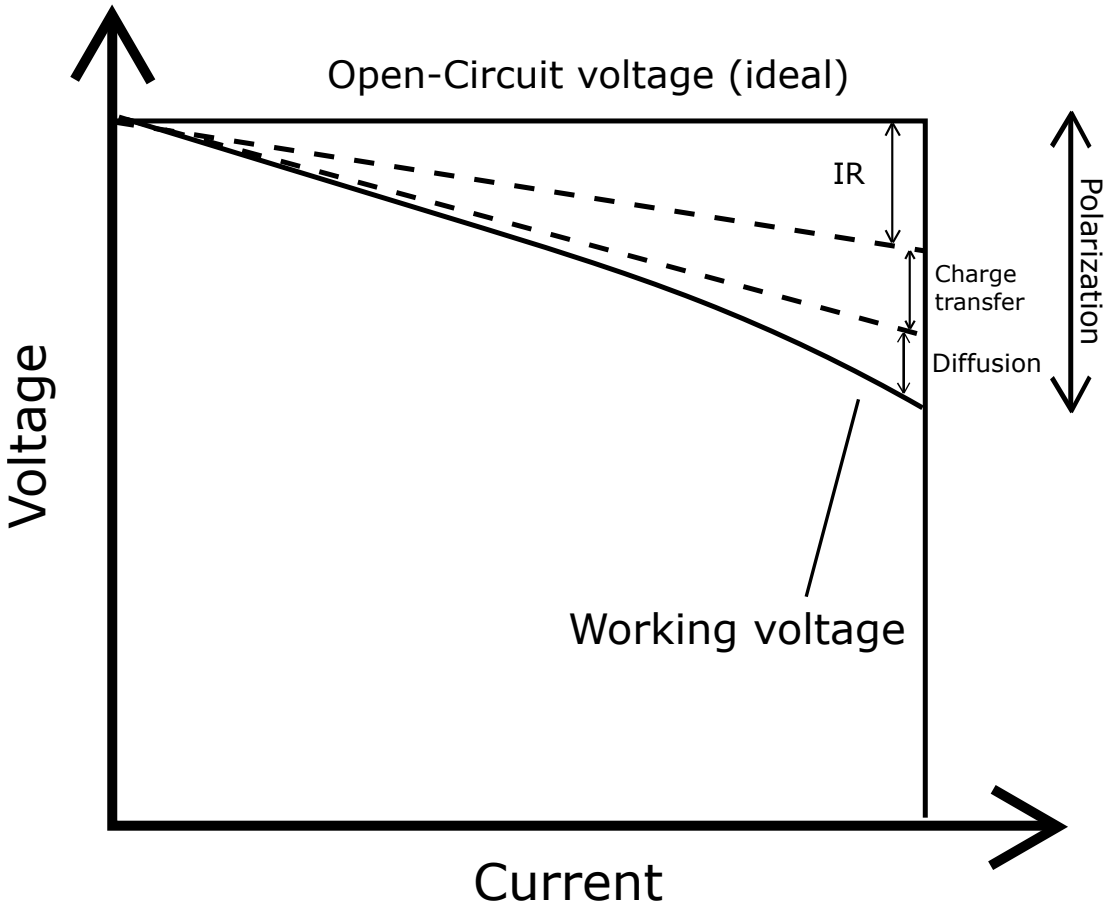

Figure 2.4: Ideal discharge of a cell and the polarizations [10]. IR = Internal Resistance.

The equilibrium voltage (OCV) can be expressed as:

$$\text{OCV} = V_{cell} - \Sigma V_{over\_pot} \tag{2.13}$$

ΣV_{over_pot} is the sum of all the polarizations in the cell and is illustrated as the overpotential in Fig. 2.4 [10]. A polarization is i.e. the ohmic loss caused by the resistance in the collectors and cables when electrons are moving from one electrode to the other. As soon as the cell is open (relaxation situation), the electron- and Li-ion movements are restrained because of resistance in the electrolyte surrounding the electrode. This causes a potential drop called the internal resistance (IR) drop, which is part of the reasons why the working voltage is always lower than the OCV [10].

The general expression for resistance in a ionic solution can be defined as in Eq. (2.14).

$$R = \frac{l}{\kappa A} \tag{2.14}$$

where l is the length the current has to travel, A the area and κ is called the conductivity of the solution. κ is a material property that indicates how easy it is to move ions through the solution. Another way to find the resistance is to use Ohm's law in Eq. (2.15).

$$V = RI \tag{2.15}$$

The electrolyte's IR-resistor equivalent can be calculated from Ohm's law (Eq.(2.15)).

$$R_{IR} = \frac{\Delta V_{cell}}{\Delta I} \tag{2.16}$$

ΔV_{cell} is the difference in cell voltage before and after the IR-drop and ΔI is the current during charge/discharge. The change in voltage caused by IR is linear. The Gibbs free energy for the redox reactions at the electrodes (Eq. (2.6)), have to be achieved before cell operation. After the activation of Gibbs free energy is reached, the ion-products from the redox reaction (2.4) have to move through the DL. The change in voltage is determined by the rate of the overall process just described, and is often referred to as charge transfer polarization, or activation polarization [9].

After the IR- and charge transfer polarizations have occurred, ion-diffusion can be considered as the only remaining thing. The diffuse layer in fig. 2.2 is, like the Stern layer, equivalent with an EDLC. The electric field in the diffuse layer is the result of a difference in ion-concentration in the electrolyte. The concentration difference leads ions to move toward the region with a lower concentration, and is called a "diffusion current". The induced electric field from the diffusion layer causes opposite-charged ions from the electrolyte to move in the opposite direction of the redox ion-products. The drift of these oppositely-charged ions will weaken the electric field, preventing the ion-products' motion. The lack of ion-products limits the reaction rates in a cell and contribute to diffusion polarization. The resistivity of the diffusion polarization depends material properties i.e. the viscosity of the electrolyte. Diffusion may also occur through the electrode, depending on the electrode's material properties like porosity [9]. The diffusion process into the

active electrode material may be calculated in first approximation by equation (2.17)

$$\Delta t \approx \frac{L^2}{3D_0\epsilon^\alpha} \tag{2.17}$$

where Δt is the time of diffusion into the active material of the electrode, L is the electrode thickness, D_0, the ion diffusion coefficient into the liquid electrolyte, ϵ is the porosity and α is the pore tortuosity of the electrode [6].

2.5.2 Impedance

Considering that a cell experience resistances, partly caused by moving charges, the cell can be expressed in an equivalent circuit that consist of resistors and capacitors. Eq. (2.18) is derived from Ohm's law (Eq. (2.15)).

$$I = C\frac{dV}{dt} \tag{2.18}$$

I is the current, C is the capacitance in Eq. (2.12) and dV/dt is the change in voltage [22]. Considering $I = dQ/dt$, where Q is charge, Eq. (2.18) may be expressed as in Eq. (2.19).

$$C = \frac{dQ}{dV} \tag{2.19}$$

Eq. (2.19) expresses how charges move when there is a change in voltage, and can be a useful representation of C when analyzing fast reactions and movements in a battery [23].
The capacitor has an imaginary impedance ($Z(Im)$) expressed Eq. (2.20). The capacitor's impedance consists of only a negative complex number, thus a voltage has a 90°phase shift offset from an alternating current (AC).

$$Z(Im) = -\frac{1}{j\omega C} \tag{2.20}$$

where $\omega = 2\pi f$ and f is the frequency of the applied AC. j is representing the imaginary unit $\sqrt{-1}$. The resistor parts of a battery in an equivalent circuit are ohmic losses described with Eq. (2.15), e.g. the IR-drop defined in Eq. (2.16) [22].

2.5.3 The Randles Circuit

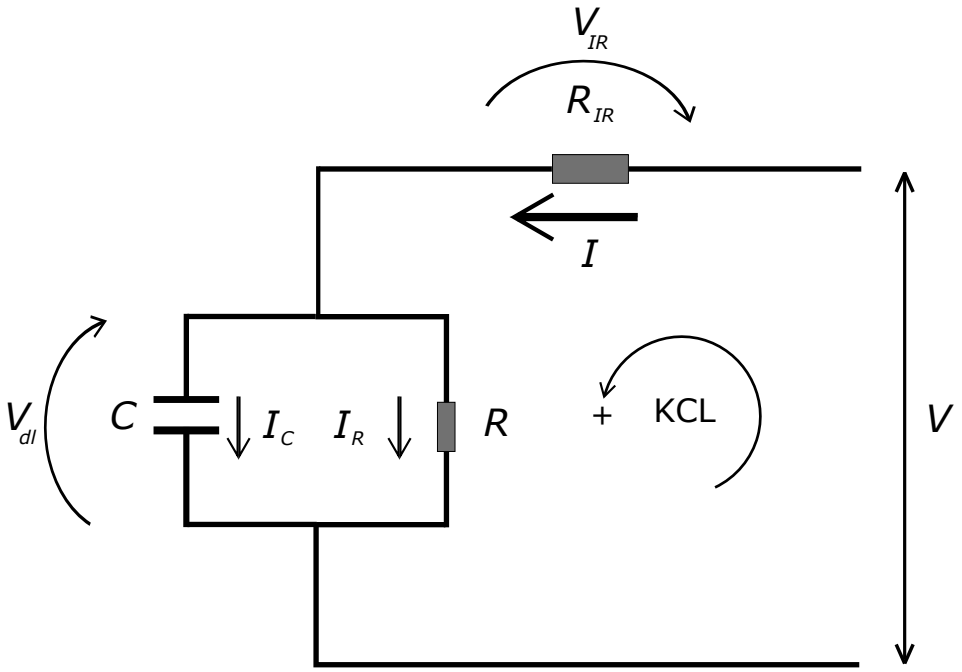

Figure 2.5: The Randles circuit. R_{IR} is defined in Eq. (2.16). R represents the leakage effect of the stored energy in the double layer (capacitor, C). V is the voltage over of the circuit and the Is are the currents [22]. KCL is Kirchhoff's Circuit Law. V_{dl} and V_{IR} are the overpotentials caused respectively by the double layer and IR.

As described in section 2.4, a cell behaves as a double-layer capacitor. The typical representation of an equivalent circuit for an electrochemical cell is called the Randles circuit, and is illustrated in Fig. 2.5 [22].

The equivalent circuit in Fig. (2.5) can be recognized as a first order parallel RC-circuit. By defining a positive direction and applying Kirchhoff's circuit law (KCL) to the circuit in Fig. 2.5, expression (2.21) is obtained.

$$I = I_C + I_R \tag{2.21}$$

I_C is the current through the electric double-layer capacitor and I_R the leak current through the double layer. In this paper, relaxation refers to the time from the circuit is opened (after IR) until the redox reactions are in equilibrium, and the cell voltage is fully relaxed (V_{rlx} = OCV). During an OCV-relaxation, I in Eq. 2.21 is zero. By using Ohm's law (Eq. (2.15)) and equation (2.18) the

expression in Eq.(2.21) can be rearranged to:

$$\frac{dV}{V} = -\frac{1}{RC}dt \tag{2.22}$$

By integrating both sides of Eq. (2.22) and solving for V, an expression for the voltage during relaxation is gained and shown in Eq. (2.23).

$$V(t) = V_i e^{-\frac{t}{RC}} \tag{2.23}$$

t is time and V_i is the initial (t = 0s, after IR-drop) voltage of the relaxation (overpotential from the DL). RC in Eq. (2.23) is known as the time constant τ. The time constant is defined in Eq. (2.24) and determines the rate of which the capacitor in Fig. 2.5 discharge over a resistance, R.

$$\tau = RC \tag{2.24}$$

When $t = \tau$, the capacitor has released 63 % of its initial stored energy [24].
$V(t \to \infty) = V_{rlx} = 0$ V means that the potential reference is set at OCV.

2.5.4 Capacity

The capacity is the amount of charge (Q) stored in the cell or battery. The capacity can be found by integrating the current, as shown in Eq. (2.25).

$$Q = \int_{t_0}^{t} \frac{dI}{dt} \tag{2.25}$$

t_0 is the time when the current is turned on, t the cut-off time. On a battery package, the rated capacity is given as Ah, and indicates the battery's capacity when fully charged [9].

2.5.5 Battery Life

The number of cycles before a battery ceases to provide the satisfying capacity, is called the cycle life of the battery. The cycle life of the battery depends on the structure and type of battery, but also on how heavily it performed during operation, on temperature, and on other factors [10][20].

Shelf life is a measure of how long a battery can be stored without losing its capacity. It is heavily dependent on the cell's chemistry, temperature, humidity and other conditions [20].

2.5.6 Coulombic Efficiency

The coulombic efficiency (η) is defined as:

$$\eta = \frac{Q_{out}}{Q_{in}} \tag{2.26}$$

where Q_{out} and Q_{in} are the amount of charges out of and into the cell, respectively. It essentially indicates how much of the infused charge (capacity) during the charging process of the battery will be retrieved when discharged. It is mostly determined by the cell's ionic- and electric resistance [20].

2.5.7 Temperature

Impedance, voltage, polarization, rated capacity and many other parameters of the cell are all material dependent and thus sensitive to temperature. The degree to which the battery's parameters are affected by changes in temperature is related to the cell's composition and chemistry. An electrode's chemical reaction potential was expressed in Nernst equation (2.9), where temperature has an influence on a cell's potential [13].

2.6 Li-ion battery

Lithium is an attractive candidate for battery technology. One obvious reason is the fact that it is the lightest metal in the periodic table, thus it has a specific capacity of 3.86 Ah/g. In comparison to a commonly used negative electrode (anode) material (like zinc with 0.82 Ah/g), lithium has a very high specific capacity [9]. Another reason why it is an attractive anode material is because of its high electrochemical reduction potential of -3.04 V vs. standard hydrogen electrode (SHE). The lithium redox-reaction is expressed in (2.27) [25].

$$Li^+ + e^- \longleftrightarrow Li \tag{2.27}$$

Lithium (Li) batteries were first made as a primary battery in the late 1970s to early 1980s by Exxon Company and Moli Energy. The formation of a solid electrolyte interface (SEI) layer on the anode (lithium-metal), prevented the charge process because of irregularities on the SEI surface that lead to lithium deposition in the electrolyte - causing an internal short circuit [2]. This was a problem, and it was not before 1991 that Sony demonstrated a working Li-ion battery. Before Sony, lithium batteries had one intercalation electrode (the cathode), but Sony realized that the

high cell potential allowed a second intercalation electrode. This made sure that lithium did not react as much with the electrolyte (forming a stable SEI) and made the battery reversible [9]. Intercalation is a process where Li-ions are inserted and extracted into a mechanically stable host. An example of how a rechargeable Li-ion battery work is illustrated in Fig. 2.6, with the electrode reactions (2.28) and (2.29) [20].

Negative:

$$C + xLi^+ + xe^- \underset{\text{dicharge}}{\overset{\text{charge}}{\rightleftharpoons}} Li_xC \tag{2.28}$$

Positive:

$$LiMO_2 \underset{\text{dicharge}}{\overset{\text{charge}}{\rightleftharpoons}} Li_{1-x}MO_2 + xLi^+ + xe^- \tag{2.29}$$

The M in reaction (2.29) stands for metal, C is graphite, x is between 0 and 1, O_2 is oxygen and e^- is the electron taking part in the reactions. When charging, the arrow in reaction (2.28) is pointing to the right, and Li-ions are in this case inserted into the graphite layers of the anode (as seen in Fig. 2.6). The process of inserting Li-ions into an electrode will be referred to as "lithiation" in this paper. On the positive electrode, the reaction arrow is also pointing to the right, and Li-ions are extracted from the host. This process will be referred to as "delithiation". The overall reaction is described in (2.30) [20].

$$LiMO_2 + C \underset{\text{discharge}}{\overset{\text{charge}}{\rightleftharpoons}} Li_xC + Li_{1-x}MO_2 \tag{2.30}$$

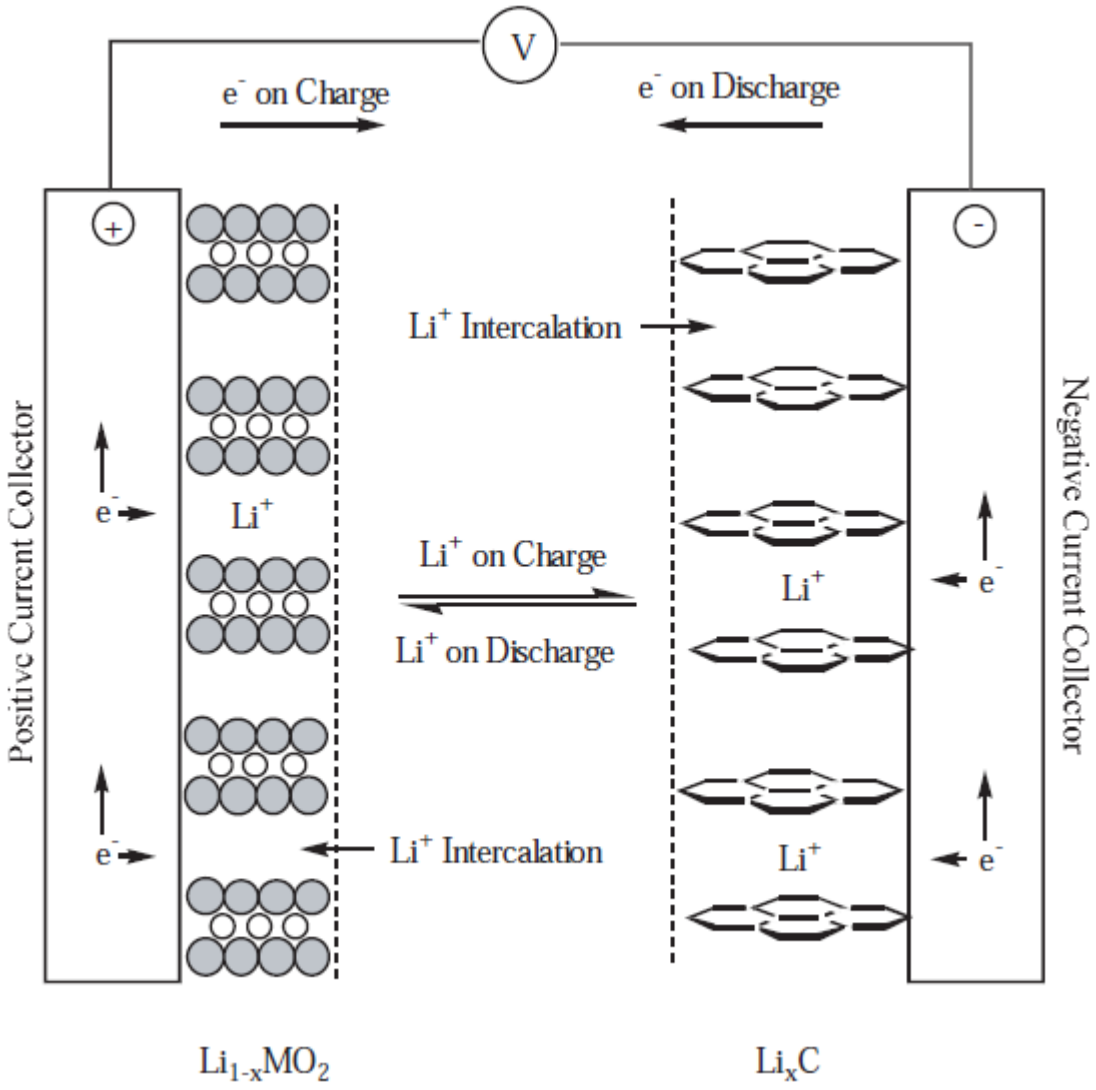

Figure 2.6: Intercalation of lithium-ions on both electrodes. Illustrating a working commercial Li-ion battery with two intercalation electrodes during charge and discharge. Reactions are described in (2.28) and (2.29) [20].

2.6.1 Solid Electrolyte Interface (SEI)

During the initial cycles of a Li-ion battery, the electrolyte solution is unstable and will begin to degrade onto the surface of the anode. The deposition of organic and inorganic products from the degradation of the electrolyte forms a layer at the electrode called “solid electrolyte interphase” (SEI). The formation of SEI depends on the composition of the electrolyte, the presence of additives in the electrolyte, the rate of process, etc. [26]. The formation is an irreversible process and thus is considered to be a loss of capacity. The amount of loss depends on the choice of electrolyte and electrode - since the formation happens at the surface, an electrode material with low surface area will give a lower loss of capacity [20]. For a Li-ion cell to work well, a stable SEI has to be made early in the cycle process [26].

It is desirable to achieve a thin and stable SEI which has a satisfying ion mobility and ensures no degradations of the electrode caused by chemical reactions with the electrolyte. To ensure a good SEI, it is common to include additives in the electrolyte [20].

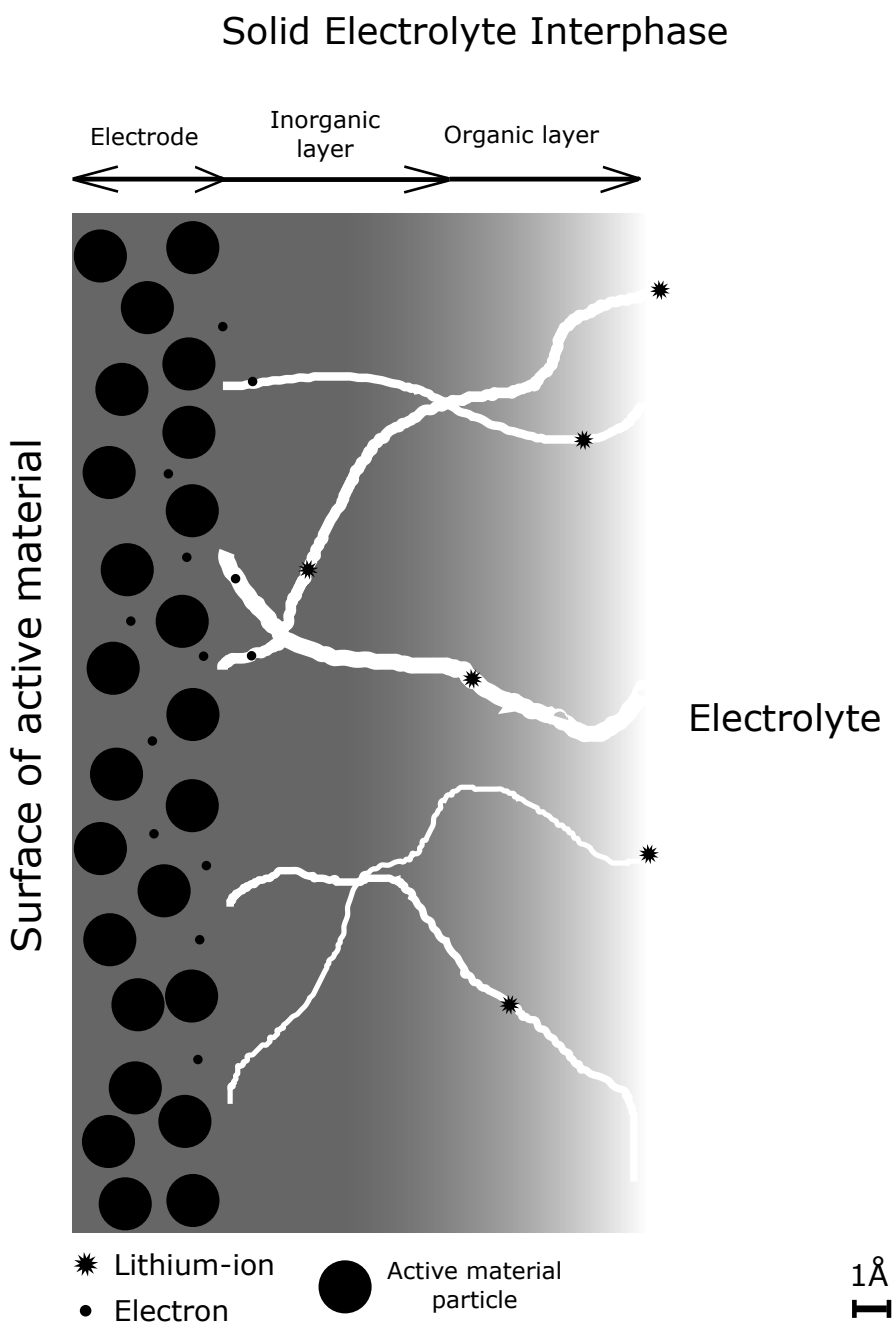

Figure 2.7: Generalized illustration of a solid electrode interphase (SEI) based on the models described in [26]. In this representation, the SEI-layer overlaps with both the electrode and the electrolyte, and is very thin (a few Å). The inorganic layer can be considered denser than the organic layer. The figure is not in proportion, and the scale is merely to indicate the SEI's thickness.

Fig. 2.7 illustrate how the SEI layer looks like at the interface between the electrolyte and active material of the electrode. Furthermore, Fig. 2.7 is partly illustrating that the thickness of SEI is

not well defined, as it overlaps with both the electrode and electrolyte in the range of a few Å or hundreds of Å. The white channels represent defects enabling Li-ions to move through the layer and recombine with an electron at the electrode surface. Most models of the SEI on a graphite anode propose a dense inorganic layer close to the graphite surface and a more porous organic layer closer to the electrolyte. If the active material in Fig. 2.7 were graphite, the particles would have a more layered structure, and there would be more space for Li-ions to move further into the electrode [26][28].

2.7 Components in a Li-ion Cell and their Characterizations

A lithium-ion (Li-ion) cell operates in the same way as most other battery cells, yet faces some particular challenges i.e., reactivity towards water and high cell voltage. This section will cover some component requirements for a Li-ion half-cell.

2.7.1 Negative Electrode Materials

To achieve a high cell voltage (V_{cell}), the negative intercalation electrode should have a redox potential that is close as possible to 0 V in Fig. 2.8 [4]. Another important quality for the choice of anode material is that it forms a stable SEI with the chosen electrolyte, preferably in the initial cycles [26]. The lithium-metal would theoretically yield the greatest cell voltage in a Li-ion cell, but as mentioned in section 2.6, lithium-metal does not enable the lithium battery to be rechargeable.

Commercially available Li-ion batteries generally use graphite as their active anode material, mostly because it has a very low cell voltage of about 0.1 V vs. Li/Li^+ (Fig. 2.8), high electronic/ionic conductivity, mechanical stability and has a low cost. Most common graphite anodes can store 1 lithium atom per every 6 carbon (LiC_6) [1].

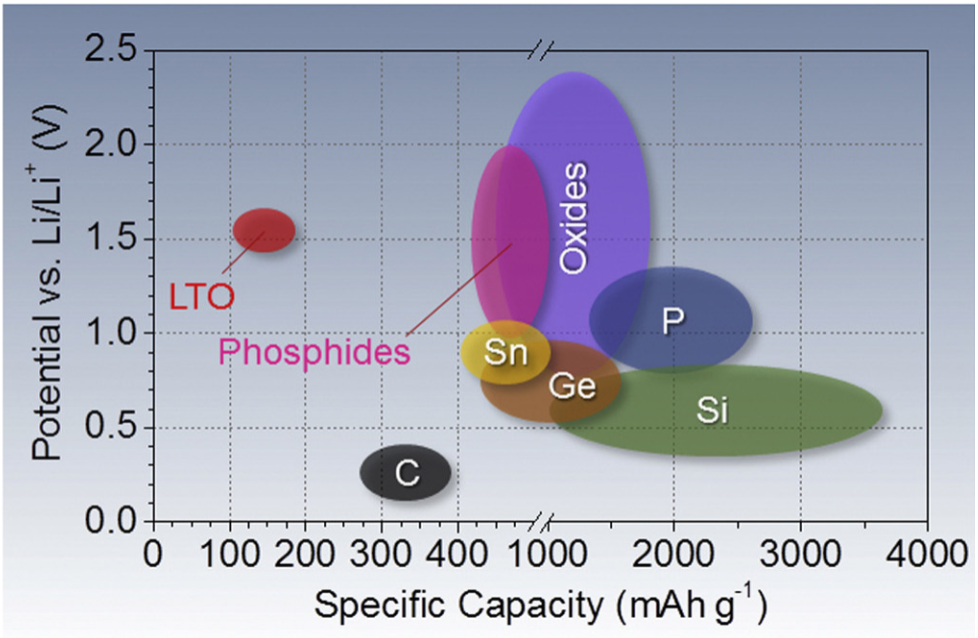

Figure 2.8: Common types of anode materials with their voltage vs. Li/Li^+ and their specific capacity. The chart is from [4].

Looking at Fig. 2.8, there are many potential anode material candidates for a Li-ion cell - silicon (Si) is one of them. Si is not as close to 0 V as carbon, but its specific capacity is 10 times carbon's capacity. With the combination of a high voltage cathode and the Si on the anode, a high voltage and capacity Li-ion battery should be possible to achieve. As mentioned before, graphite is a popular choice because of i.a., its mechanical stability when lithiated and delithiated, and its ability to make a stable SEI. Si however, has a very large volume expansion, which reduces the cell's cycle life [4].

2.7.2 Silicon as Anode Material

In recent years there has been a growing focus on experimenting with silicon (Si) as active anode material, because of the material's great ability to host lithium. Compared to the common graphite anode - with its specific capacity of 372 mAh/g_C at the lithiated state of LiC_6 - Si have a very high theoretical specific capacity. The specific capacity of silicon-based anode in fully lithiated state of the alloy $Li_{15}S_4$ is 3579 mAh/g_Si [3]. The lithium-silicon alloy has a low average delithiation potential of about 0.4 V vs. Li/Li^+ [1].

Silicon's surface is important to focus on, as it affects the charge density and reaction rate in a cell. This paper will not go deep into the details regarding silicon's surface structure, as this

is a field of study on its own. To simplify, it is sufficient to know that silicon is in group IV in the periodic table. Elements in group IV are known to crystallize together and make a so-called "zincblende structure". The octet rule of thumb suggests that there are in average four valence electrons per silicon in a crystalline silicon (c-Si). There are no more silicon atoms on the c-Si surface, but four nonbonded electrons. These four electrons are referred to as "dangling bonds", and are illustrated in Fig. 2.9. Dangling bonds have also been observed in amorphous Si structure (a-Si)[30]. Recall that Fig. 2.3 illustrates the double layer formed at the interface between the electrode surface and electrolyte. Fig. 2.3 draws an example of the situation with a negatively charged electrode surface. This situation can be considered valid in the case of silicon as anode material, because the dangling bonds at the silicon surface are assumed to make the electrode surface negatively charged.

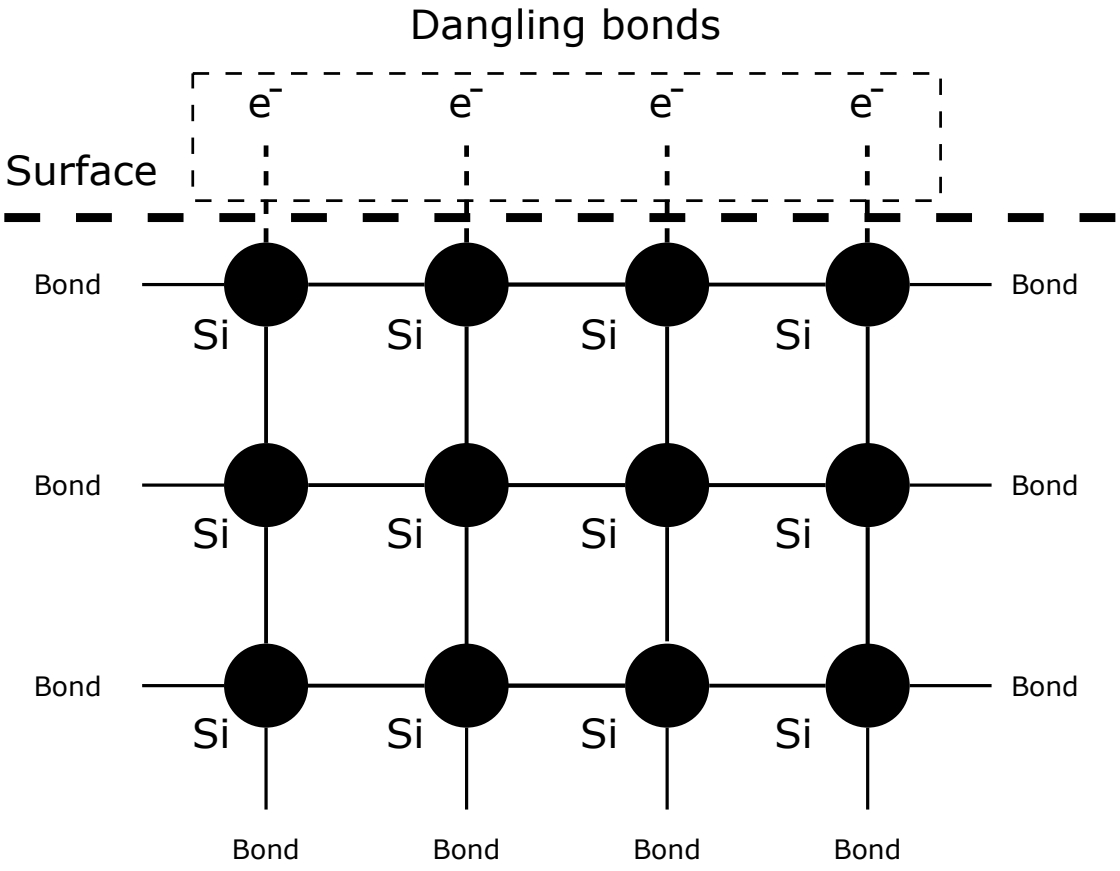

Figure 2.9: Dangling bonds of c-Si [31].

As mentioned in the subsection above, silicon tends to expand dramatically when lithiated - 290% of the alloy $Li_{15}S_4$ [5]. With such a high change in volume during the first lithiation, c-Si cracks and an a-Si structure is formed during the first cycling. It seems that the lithiation redox potential shifts when Si is enclosed by lithium (~ 2.3 Li per Si). The formation of an amorphous structure is caused by a shell of $a-Li_{2.5}Si$ which migrates into the core of the silicon as it is lithiated. After the whole c-Si structure is turned into a-Si, lithiation continues until the $a-Li_{3.75}Si$ (that is $a-Li_{15}Si_4$) alloy is constructed. Some research report cracking of c-Si when the particles have a diameter > 150 nm and a-Si > 870 nm. Thus a-Si is more stable with cycling than c-Si [3]. Other studies observed a crystalline-to-amorphous transition at $Li_{0.3}Si$, and confirm that the breaking of c-Si appear during the first lithiation [32].

Zhang et al. have performed a first-principle (no adjustable parameters) simulation of lithium insertion into silicon - based on density-functional theory [32]. They found the rate at which lithium diffuse into c-Si and a-Si at room temperature by extrapolation. The diffusivity values for lithium into c-Si and a-Si was estimated to be:
$D_{Li_{c-Si}} = 1.67\times10^{-10} \sim 4.88 \times 10^{-9} cm^2 s^{-1}$ and $D_{Li_{a-Si}} = 1.25 \times 10^{-9} \sim 3.69 \times 10^{-8} cm^2 s^{-1}$

An example of the performance of a Si-based negative half-cell electrode is illustrated by Oumellal et al. [6]. Their electrode had a thickness of ~20μm, and was prepared with a 1 M $LiPF_6$ electrolyte solution in 1 : 1 DEC/EC and 1 cm^2 Li metal as the electrode. They reported that the electrode did not achieve $Li_{15}Si_4$, but had up to $Li_{1.25}Si$ on discharge and $Li_{0.2}Si$ on charge. Discharge and charge here are lithiation and delithiation, respectively, because they were using a Li-metal reference electrode. Table 2.1 shows how the cell's cycle life and capacity loss was affected by different electrode compositions [6].

Table 2.1: Cycle characteristics of Si-based anodes in different situations and preparations. The mixing method was either ball milling (B.M.) or magnetic stirring (M.S.) [6].

	Si (wt%)	C type	C (wt%)	CMC (wt%)	Mixing method	First cycle irreversible loss (mAh g^{-1})	Slope of cumulative irreversible loss (mAh g^{-1} per cycle)	Cycle life (number of cycles)
A	80	SP	12	8	B.M.	260 ± 40	35 ± 10	100 ± 15
B	72	SP	20	8	B.M.	290 ± 40	32 ± 10	95 ± 15
C	80	SP	12	8	M.S.	275 ± 40	37 ± 10	105 ± 15
D	80	VGCF	12	8	B.M.	250 ± 40	35 ± 10	102 ± 15

6202 | *J. Mater. Chem.*, 2011, **21**, 6201–6208 This journal is © The Royal Society of Chemistry 2011

Oumellal et al. made some first approximations (qualified guesses) and calculated the diffusion time for Li-ion into the composite electrode with the Eq. (2.17). They calculated (with rough values) a diffusion time into the electrode of 1-10 seconds. They also observed a slower diffusion rate into the liquid electrolyte at the first cycle, compared to 10th cycle and beyond. The diffusion rate into the electrolyte was about 1s at first cycle and 0.1s at the 10th cycle. The charge transfer process was 10^{-4}s after cycle 10 and the corresponding RC-resistance and capacitance were respectively increasing and decreasing. They concluded that the main reason for a capacity fade in silicon-based anode material was because of a growing SEI-layer, caused by degradation of the electrolyte. The increased of SEI thickness prevented lithium from moving into the electrode [6].

2.7.3 Liquid Electrolyte

The main disadvantage of using lithium is that this material is highly reactive towards water. A non-aqueous electrolyte must be used, otherwise lithium-ions will react with oxygen in water and leave hydrogen for themselves. The hydrogen ions form hydrogen-gas - which is flammable and causes an increase of pressure in the battery [9]. The electrolyte needs to be able to transport the Li-ions from one electrode to the other. For liquid electrolytes, the Li-ion conductivity should be more than $3 \cdot 10^{-3}$ S/cm and stay liquid in a wide temperature range (-40 to 70 °C). As well as being thermally stable, the liquid electrolyte has to be able to withstand the high electrical potential of a Li-ion battery, and solvate the Li-ion particles. Evidently, the chemical components of the electrolyte cannot be toxic, flammable or in any way a hazard to the surroundings [29].

Nowadays liquid electrolyte is usually formed by a solution of lithium salt in a carbonate organic solvent (e.g., propylene carbonate (PC), ethylene carbonate (EC) or a mix). The most common salt used in a liquid electrolyte is $LiPF_6$. When dissolved by a solvent, it makes a safe solution

with a high conductivity. However the LiPF6 salt has a high cost, is hygroscopic (attracts water from the air) and produces hydrofluoric acid (HF) - HF acid is highly corrosive towards oxides (i.e. silicon oxide) and toxic for both humans and the environment [20][33]. Therefore $LiPF_6$ must be handled in a dry environment.

When it comes to the choice of organic solvent, it is important to pick one which will improve the ion-conductivity of the electrolyte. Organic solvents should therefore have a strong dipole, to dissolve the salt easily and yield a solvate compound with the solute. An illustration of solvate compounds is shown in Fig. 2.3 as the package of gray solvents surrounding an ion. Factors like melting point (MP) and boiling point (BP) must be considered, as they may limit the temperature range of the operating battery. The organic solvents density and viscosity also play a role in the electrolyte's conductivity [9]. Additionally, it is a perquisite that the solvents do not interfere with the solid electrolyte interphase (SEI) layer (see subsection 2.6.1).

Chapter 3

Method

This chapter presents the methods used to answer the fundamental problem outlined in subsection 1.1.1. The first section introduces the cells and how they were assembled. In the following section, a cell model is proposed with the reasoning behind the assumptions made. Lastly, the equipments and tools used for the cell cycling and fitting of the parameters are elaborated.

3.1 Making a Cell

The cells which were made in this thesis are coin cells of type CR2032. The cells were assembled in the way that is shown in Fig. 3.1. The gasket in the top cap is there to prevent current from leaking through the edges of the layers. The spring forces contact between the components in the coin cell, while the spacer is used as stuffing. The slurry of Elkem crystalline silicon was casted onto a copper foil by a proprietary method. The copper foil with the active material was placed in the bottom can. Some electrolyte was also added to the bottom cap to improve the anode stick. The separator was soaked in electrolyte. The cell assembly was performed in an Ar gas-filled glove box.

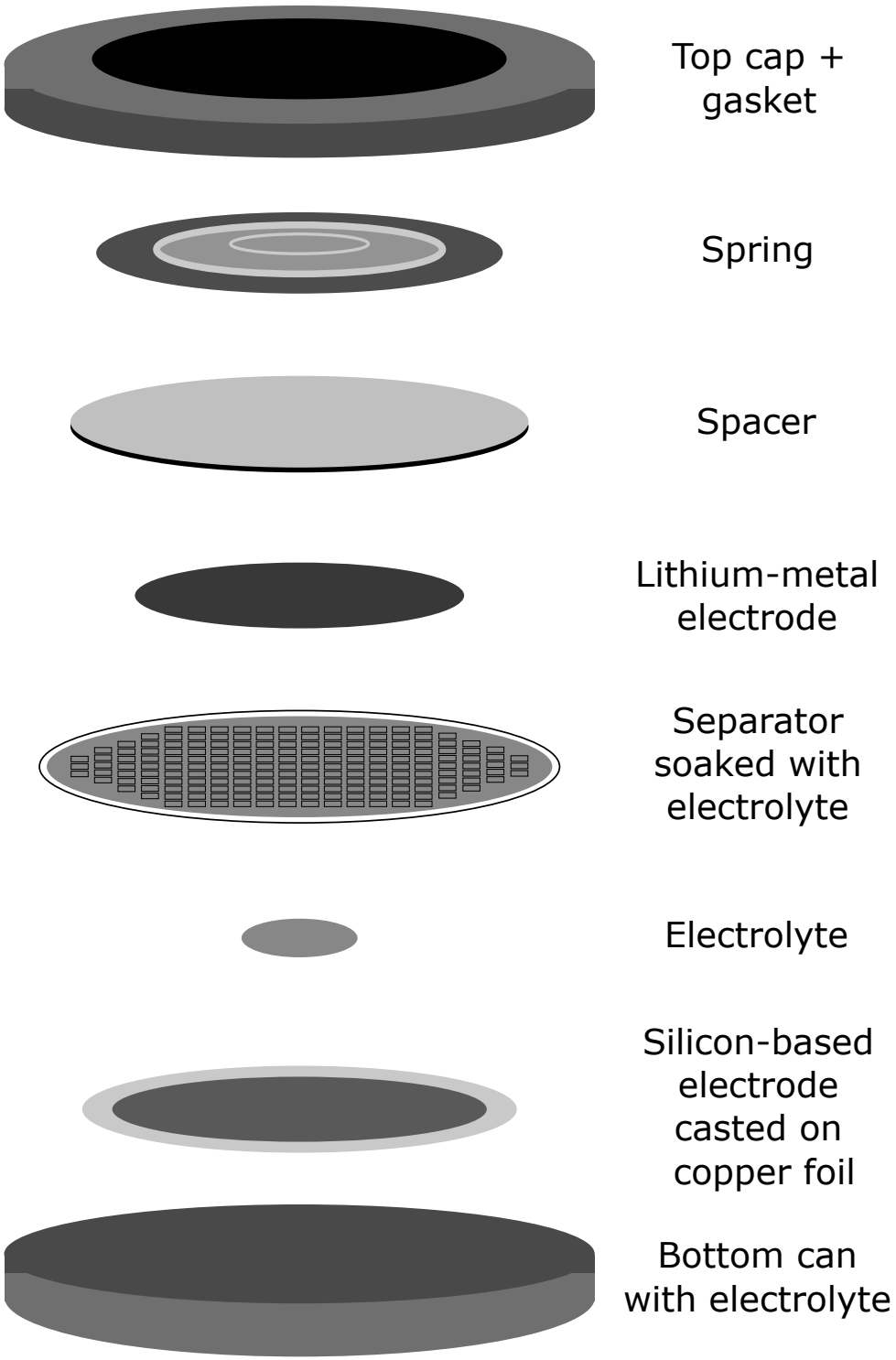

Figure 3.1: The composition of a coin cell assembled in the laboratory at IFE [34].

When making the coin cell, disks with a diameter of 15 mm were first punched out and weighted. The disk puncher and scale used are shown in Fig. 3.2. The disks of slurry and copper were weighted on the scale shown in Fig. 3.2b with an accuracy of ±0.01 mg. Coin cells dimensions and mass are shown in table 3.1. The electrode mass with copper and mass of the active materials, without copper, are shown in table 3.2.

Table 3.1: Coin cells assembly.

Elements	Mass (mg)	Thickness	Diameter (mm)
Coin cell	28.72 ±0.03 %	32 mm	20
Electrode	In table 3.2	5.2 μm ±2%	15
Copper	27.72 ±0.2%	N/A	15
Separator (celgard K2045)	N/A	20 μm ±5%	15

(a) Disk puncher used to make cell disks with a 15 mm diameter.

(b) Weight scale. Has an uncertainty of ±0.01 mg.

Figure 3.2: Equipment used for making disk and weighting.

The electrolyte was made with and without additives, with the weight distribution and chemical compounds shown in table 3.3. The additive specifications are proprietary. In table 3.2, "A" in a cell's name indicates that the electrolyte solution includes additives. All cells were cycled with routines described in table 3.5. "S" indicates that the cell was stored for a longer period (1 month) compared to the other cells (less than 24 hours), before initial lithiation. Additionally was the S cell's anode composed of a thinner copper foil than the other cells. The S cell's expected capacity was higher than the other cells, mostly because of its different copper foil. The expected capacity was calculated with the active material's mass and theoretical specific capacity, 3.579 mAh/mg, from subsection 2.7.2. Cell EA was not made for OCV fitting, but to perform an EIS study that could be used to compare with the fitted results.

Table 3.2: Specifications of the cells. Cell names with "A" contained additives in their electrolyte. E cell was made for EIS. The S cell was stored for a longer period of time than the cells, and used a thinner copper foil (thus the lower electrode mass). The expected capacity was calculated with theoretical value of 3.579 mAh/mg.

Cell name	Mass of electrode (mg)	Silicon (%)	Active Material (mg)	Expected capacity (mAh)
	(±0.01 mg)		(±0.2 %)	(±0.2 %)
A1	29.45	52.20 %	0.3810	1.364
A2	29.44	52.20 %	0.3758	1.345
1	29.41	52.20 %	0.4176	1.495
2	29.42	52.20 %	0.3602	1.289
3	29.51	52.20 %	0.3549	1.270
S	28.78	53.27 %	0.8635	3.090
EA	29.45	52.20 %	0.3800	1.364

Table 3.3: Electrolyte composition of the cells. The right column is without additives. The electrolyte contained 9 ppm and 26.9 ppm of water and HF, respectively. The additives had a volume ratio of 1:1:3. Solvents: EC = ethylene carbonate, PC = propylene carbonate, DMC = dimethyl carbonate.

Role	Electrolyte	wt.%	wt.%
Salt	LiPF6	11.56	11.56
Solvents	EC	16.49	17.81
	PC	16.49	17.81
	DMC	49.46	52.90
Additives	1	1.000	
	2	5.000	

3.2 Cell Model

To ensure a decent fit of the relaxation voltage at open circuit (OCV), a reasonable model of the cell was needed. This section explains how the model was deduced, based on the theory and assumed behavior of a cell.

In order to find a representable model for the cell, it was necessary to understand how the cell functions and what data was available. The Arbin instrument has contact points at the cell's positive and negative terminals, and measures the cell voltage (V_{cell}) between those two points. V_{cell} includes all polarization potentials inside the cell, and is important in the model because it contains a lot of information and is easily measured [21]. The subsections 2.5.1 and 2.5.2 describe the behaviors of the different polarizations. Polarizations from i.e., the double layer and internal resistance (IR) were recognized as analog to the Randles circuit's elements in Fig. 2.5. The Randles cell was therefore used as a underlying model.

3.2.1 Reaction Rates

The rate of a polarization process was essential to estimate in order to make reasonable assumptions when proposing a cell model. In subsection 2.7.2, some previous research about silicon in a cell and diffusivity of lithium in a Si-based electrode were introduced. In table 3.4, the time below "no Eq." was estimated by using diffusion values from subsection 2.7.2. "With Eq." refer to Eq. (2.17). The thickness used in the calculations was 5 μm. The porosity was assumed to be $\epsilon = 0.6$ and the tortuosity, $\alpha = 4$ [6].

Table 3.4: Estimated time of processes. "Eq." refer to Eq. (2.17). It was assumed that $\epsilon = 0.65$ and $\alpha = 4$ in Eq. (2.17). The rate of charge transfer and electrolyte was found with EIS on a 20μm thick electrode with 70-80 wt.% silicon [6].

Process	**Time**	**Square of electrode thickness**	**Diffusivity**
No Eq.	(s)	(cm^2)	(cm^2/s)
Lithium in c-Si	1619 - 55	2.7×10^{-7}	$1.67 - 48.8 \times 10^{-10}$
Lithium in a-Si	216-7	2.7×10^{-7}	$1.25 - 36.9 \times 10^{-9}$
With Eq.			
Lithium in a-Si	0.1-0.3	2.7×10^{-7}	
EIS values			
Charge transfer	0.0001		
Li in electrolyte	0.1 - 1		1.50×10^{-6}

Although table 3.4 are only rough estimates of the time for a process to occur, it gives an idea of what processes to model. The calculated times with and without Eq. (2.17) are not the same for lithium in a-Si. The aim was to point out that the lithium diffusion is indeed longer than the charge transfer. The lithium diffusion in electrolyte has about the same time as diffusion into Si (with Eq. (2.17)), thus this process was considered the same as diffusion into Si, as it would be difficult to distinguish their fitted time constant. The charge transfer on the other hand should be included as a different process, since it happens 1000 times faster than the other processes. As for the lithium-metal cathode, the diffusion of lithium into more lithium would not be registered as a change in voltage, and as a result it was assumed that the charge transfer process was the only process affecting the observed cell potential. This mean that most of the polarizations in the measured relaxation voltage came from the Si-based anode.

In commercially available Li-ion batteries, the charge transfer process is known to happen much faster than the lithium diffusion process. For instance, in a $LiMn_2O_4$/graphite cell with capacity of 6 Ah, the charge transfer during OCV-relaxation could occur in less than 1 minute, and the diffusion process for more than several hours [35]. This supports the assumptions made in the paragraph above. Previous studies show that the IR-drop immediately disappeared when the circuit was opened [35]. The IR-drop was included in the model, but not fitted because it is a linear voltage drop and can be easily calculated with Ohm's law in Eq. (2.16).

3.2.2 Equivalent Circuit

Previous research and assumptions made in subsection 3.2.1 promoted usage of the Randles circuit from Fig. 2.5 to make an equivalent circuit for the OCV-relaxation situation [22][35]. The equivalent cell circuit is shown in Fig. 3.3, and was used as the cell model in this thesis.

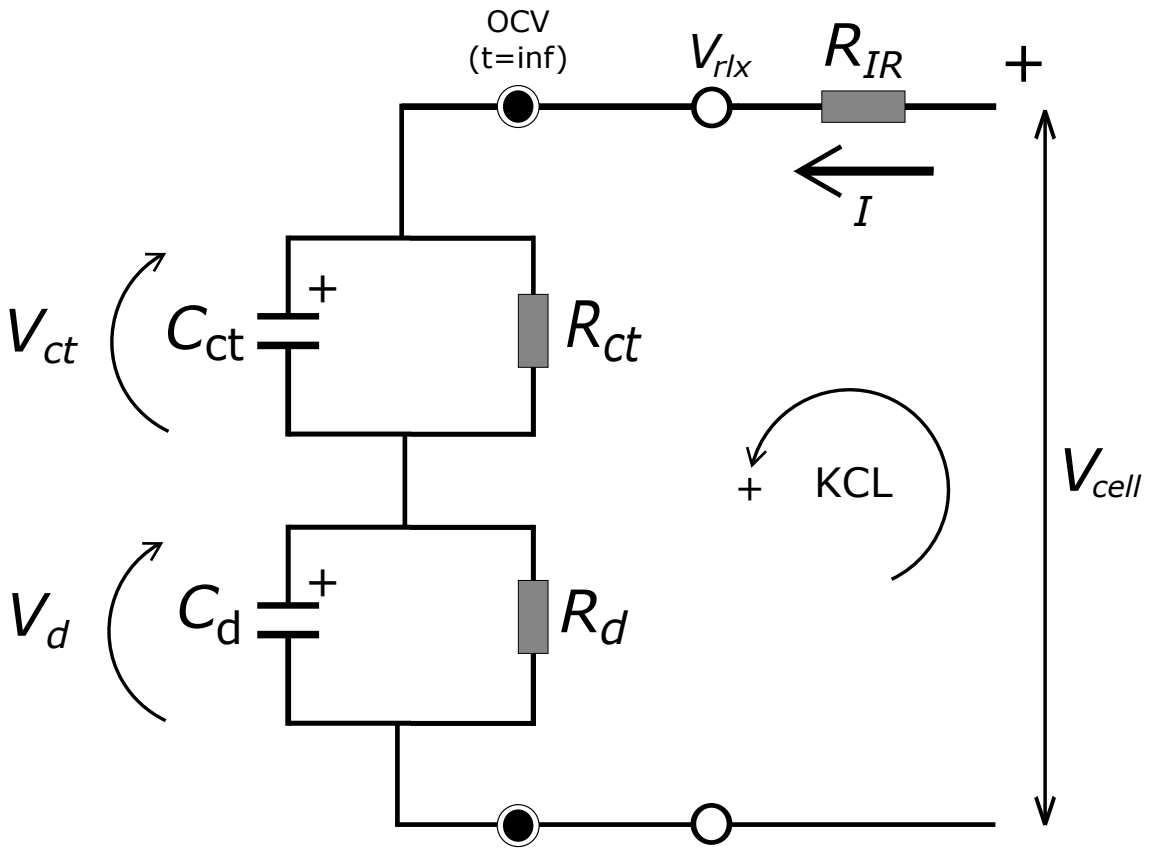

Figure 3.3: Equivalent circuit model of the cell. Based on a Randles circuit [22]. d stands for diffusion, ct, for charge transfer and IR for internal resistance. V_{cell} and V_{rlx} are the relaxation voltages respectively before and after IR-drop. KCL is the abbreviation for Kirchoff's Current Law. The OCV is the cell voltage when fully relaxed with respect to the reference Li/Li^+. Note that $V_{rlx} \rightarrow OCV$ when $t \rightarrow \infty$. I is the current through the cell during charge/discharge and is zero the moment the circuit is open.

The V_d and V_{ct} indicate the overpotentials for diffusion- and charge transfer process, respectively. The sum of the potentials over the Rs are the total overpotential of the cell (ΣV_{over_pot} from Eq. (2.13)). Equation (3.1) expresses the sum of all the potentials in the circuit shown in Fig. 3.3.

$$V_{cell} - V_{IR} - V_{ct} - V_d = 0 \tag{3.1}$$

Where $V_{cell} - V_{IR} = V_{rlx}$ and $V_{IR} = R_{IR}/I$ is the overpotential caused by internal resistance from the electrolyte. In V_{ct} and V_d can be substituted with the expressions in Eq. (2.23), gained from using Kirchoff's Current Law (KCL) on a simple Randles cell. This transforms Eq. (3.1) to equation (3.2)

$$V_{rlx} = V_{0ct}e^{-\frac{t}{\tau_{ct}}} + V_{0d}e^{-\frac{t}{\tau_d}} \tag{3.2}$$

V_{0ct} and V_{0d} are the initial overpotentials for respectively the charge transfer and diffusion. t is the time, $\tau_{ct} = R_{ct}C_{ct}$ and $\tau_d = R_dC_d$ are the time constants for the charge transfer and diffusion process (explained in the theory, page 20). OCV in Fig. 3.3 has been defined when time equal infinity. When time in Eq. (3.2) increase to infinity, $V_{rlx} = OCV = 0$. This means that Eq. (3.2) has OCV as a reference point, and not Li/Li^+. To change the reference for Eq. (3.2), OCV had to be added to the equation. The model's final expression for V_{rlx} is declared in Eq. (3.3).

$$V_{rlx} = V_{0ct}e^{-\frac{t}{\tau_{ct}}} + V_{0d}e^{-\frac{t}{\tau_d}} + OCV \tag{3.3}$$

It was assumed that C_{ct} and C_d had been fully charged the instant before the circuit was opened (before IR). At this point, the current only flow through the resistor-equivalent, and the capacitor-equivalent was presumed to induce a potential equal to the apparent overpotential. By fitting the initial voltages (overpotentials, V_{ct} and V_d) of the RC-circuits and the corresponding time constants (τ_{ct} and τ_d), the apparent resistances and capacitances can be calculated with Ohm's law (Eq. (2.15)) and Eq. (2.24). Equation (3.3) was therefore used in fitting of the cells OCV-relaxation to determine the apparent resistances and capacitances of the polarization processes.

3.3 Equipments

Arbin Instruments- and Bio-Logic's battery testers were used for the cycling of cells and the obtention of experimental data.

3.3.1 Arbin BT2000

Arbin BT2000 is a battery testing equipment made for life cycle and quality control testing on coin cells. Arbin's MITS Pro 4.0 software enabled easy programming of cycle routines. Arbin BT2000 type B was used in this research. Type B can hold two modules with 16 cells in each module, making it possible to connect 32 cells in total. The channels holding the cells were in a temperature controlled environment of 30 °C, and are shown in Fig. 3.4.

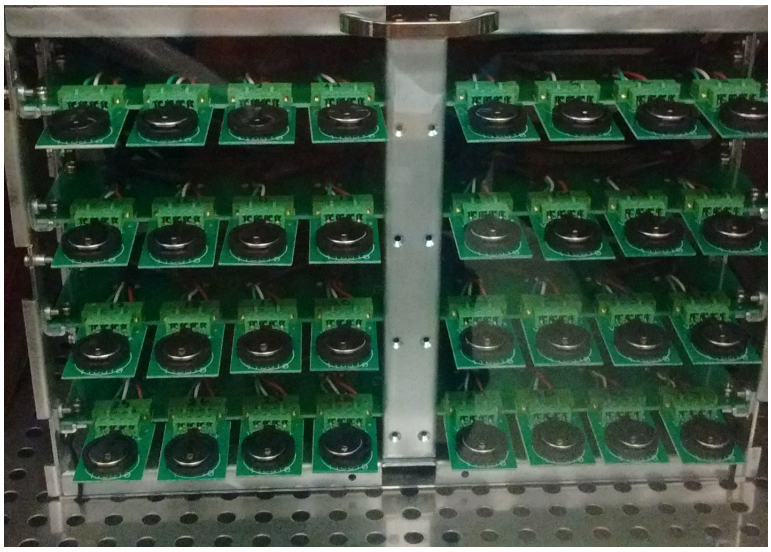

Figure 3.4: Arbin BT2000 type B instrument's channels in a temperature controlled environment of 30 °C. The image shows two modules with 16 channels each.

BT2000 type B's accuracy was ±0.1 % of full scale range for both the current and voltage output ([36]). Figure 3.5 shows the full scale range for the instrument. The expected capacity was displayed in table 3.2. The maximum C-rate used for cycling was 1/10C, which gave a maximum current of:

$$I = \frac{\text{max expected capacity}}{10\text{ h}}$$

$$I = \frac{3.09\text{ mAh}}{10\text{ h}} = 0.309\text{ mA}$$

Thus the medium current rate of ±10 mA in Fig. 3.5 was chosen as the full scale range. The instrument's voltage range was ±10 V.

Channel #	High	Medium	Low	Voltage	Ext. Ch./Load
1-32	±500mA	±10mA	±100uA	±10V	

Figure 3.5: Range specification plate for the instrument used.

3.3.2 Electrochemical Impedance Spectroscopy (EIS)

The "EA" cell in table 3.2 was cycled with the Bio-Logic VSP product shown in Fig. 3.6. The purpose of using Bio-Logic was to perform EIS and compare the impedance with the fitted impedance. EA cell's cycle routine is shown in table 3.6.

Figure 3.6: The Bio-Logic Science Instruments' product used for cycling cell EA. The main purpose was to perform an EIS study on the cell.

The Bio-Logic instrument applied a 10 μA sinusoidal AC current through the cell, and measured the voltage response. The current signal applied by Bio-Logic is expressed in Eq. (3.4) and the voltage response is shown in Eq. (3.5) [37].

$$I_a(t) = I_0 \sin(\omega t) \tag{3.4}$$

$$V(t) = V_0 \sin(\omega t + \phi) \tag{3.5}$$

Where $I_a(t)$ is the applied AC current as a function of time, I_0 the amplitude of sinusoidal current (10 μA). $V(t)$ is the voltage as a function of time, V_0 the amplitude of the potential response, ω the radial frequency and ϕ is the phase shift. Equation (3.4) and (3.5) can be used to obtain the cell's impedance derived from Ohm's law (Eq. (2.15)), expressed in Eq. (3.6).

$$Z = \frac{V(t)}{I_a(t)} = Z_0 \frac{\sin(\omega t + \phi)}{\sin(\omega t)} \tag{3.6}$$

The impedance (Z) is a function of its magnitude ($Z_0 = V_0/I_0$), its phase shift and the radial frequency. The radial frequency is expressed as: $\omega = 2\pi f$ where f is the frequency in Hz. With Euler's formula, Eq. (3.6) can be expressed as a complex function defined in Eq. (3.7)

$$Z(\omega) = Z_0 e^{(j\phi)} = Z_0(\cos(\phi) + j\sin(\phi)) \tag{3.7}$$

j is the complex number $j = -\sqrt{-1}$. The impedance's real part and its imaginary part can be plotted on the x- and y-axis, respectively, in what is called a Nyquist plot. In the theory part was given the explanation of how a cell behaves similarly to components in an electric circuit. By using a equivalent circuit model for a cell, like the Randles cell in Fig. 2.5, it was possible to make a Nyquist plot with the capacitive impedance (Eq. (2.20)) on the y-axis and the real part (Eq. (2.15)) on the x-axis.

Equivalent circuit models are used to find the resistance and capacitance of an electrochemical cell, by fitting the model to the measured impedance acquired from an EIS analysis. When equation (3.7) and the Randles cell in Fig. 2.5 are plotted as a Nyquist plot, they yield the shape of a semicircle, like the one displayed in Fig. 3.7. Fig. 3.7 illustrates how to read a Nyquist plot from an EIS analysis. The y-axis increases in negative direction, because the voltage is phase-shifted 90°behind the current.

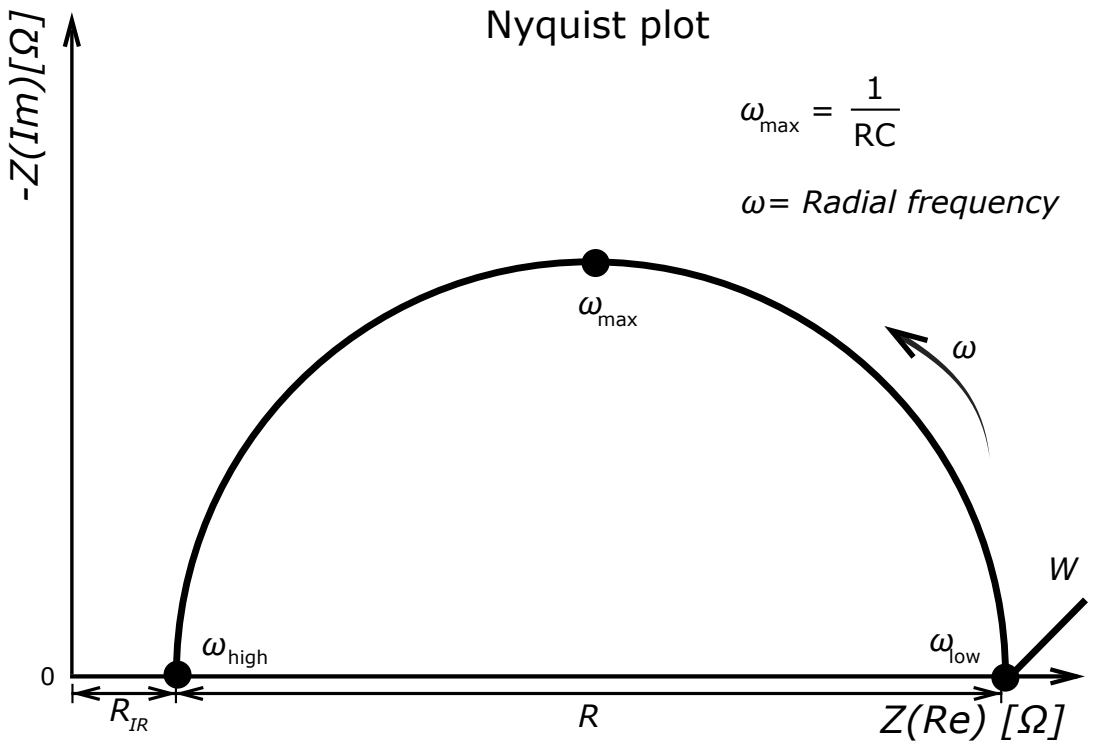

Figure 3.7: A typical Nyquist plot for a Randles cell like the one in Fig. 2.5. The negative impedance value means that the voltage is phase-shifted 90°behind the applied current. The resistance R can be found as the diameter of the semicircle. The capacitance can be calculated through Eq. (3.8). The arrow indicates which direction the radial frequency ($\omega = 2\pi f$) increases [22][38].

The real values (R_{IR} and R) in Fig. 3.7 can be simply read of the x-axis. Equation (3.8) expresses the relationship between the semicircles diameter (R), maximum frequency (ω_{max}) and EDLC(C). A semicircle in a Nyquist plot describes one time constant ($tau = RC$) [38].

$$\omega_{max} = \frac{1}{RC} \tag{3.8}$$

The Warburg impedance (W) is commonly observed in a Nyquist plot as a diagonal line with a slope of 45°. It usually occurs at low frequencies because it is a function of the reactants diffusion length. As it is not easy to model, the Warburg impedance was not included in the cell model [39].

3.4 Cycling of cells

Before cycling the cells, the routine in table 3.5 had to be specified and programmed in Arbin's software, Mits Pro. Table 3.6 was set up in Bio-Logic's EC-lab software. The initial cycling process was programmed to have a lower current in order to form a stable SEI. Arbin cycled three times before changing the current, while Bio-Logic only lithiated once. To obtain sufficient data for the fitting of OCV, the Arbin sampled 2 hours of OCV after lithiation and delithiation. Arbin sampled whenever the voltage changed with more than 0.001 V, and every 10 seconds. For the Bio-Logic instrument, the EIS after OCV was the most important part, thus did it not need to record as many OCV points and for as long a time. It was assumed that an amplitude of 10 μA was sufficient to observe the impedance from relevant processes.

When Arbin first started the cycling of the cells, the cells were discharged (lithiated). Technically, the Si-based electrode would be referred to as the cathode because it has the highest potential vs. Li/Li^+ of both electrodes in this case. However, a silicon-based electrode would have a lower potential than the counter electrode in a commercial Li-ion battery, and therefore it would be the anode. To clarify, this paper will continue referring to Si-based electrode as the cell's anode, even though it is technically a cathode in these cells.

Table 3.5: Arbin's programmed cycle routine.

Process	Stage	C-rate	Duration (h)	Step in time (s)	Step for change in voltage (V)	Cut - off voltage (V)	Repetitions
Initial cycles:							
	Rest	0	24	60	0.005		1
	Lithiation	1/20	480	120	0.005	0.05	3
	OCV-lithiation	0	2	10	0.001		3
	Delithiation	1/20		120	0.005	1	3
	OCV-delithiation	0	2	10	0.001		3
Cycling:							
	Lithiating	1/10		120	0.005	0.05	100
	OCV-lithiation	0	2	10	0.001		100
	Delithiation	1/10		120	0.005	1	100
	OCV-delithiation	0	2	10	0.001		100

Table 3.6: Bio-Logic cycle routines. Current amplitude during EIS was 10 μA.

Process Bio-Logic	Repetitions	Cut - off voltage (V)	Stage	C-rate	Duration	Step in time (s)	Step for change in voltage (mV)
Initial lithiation:	1	0.05					
			Rest	0	3 % change in SOC	10	0.5
			Lithiation	1/20	Until cut-off	120	1
			EIS	0	10 kHz - 10 mHz		
Cycling	9						
Delithiation cycling:	1		Delithiation	0	3% change in SOC	10	0.5
	Until cut-off	0.05	OCV	0	30 min	120	1
			EIS	0	10 kHz - 10 mHz		
			Delithiation	1/10	5 % change in SOC	120	1
Lithiation cycling:	1		Lithiation	0	3 % change in SOC	10	0.5
	Until cut-off	0.05	OCV	0	30 min	120	1
			EIS	0	10 kHz - 10 mHz		
			Lithiation	1/10	5% change in SOC	120	1

3.5 Programming Tools

One of the main approaches in this thesis was to develop a program, using Python 2.7, that would make it easier for scientists to analyze the processes which occur inside a cell or battery. In order to make a user-friendly and flexible program, it had:

- Use a powerful mathematical optimization algorithm
- Handle different battery models
- Require little programming skills
- Have good documentation

The program developed in this thesis is a utility tool in the Python package, `cellpy` [40]. The mathematical approach that was used in the program for fitting of parameters was the Levenberg-Marquardt's (LM) method of non-linear least square minimization. Python offers many packages which make it easier to implement LM's mathematical method.

3.5.1 Python 2.7

Python is an open, readable and powerful programming language. It was used in this thesis because of its open source and its many useful packages. It was necessary to install a 32-bit version of Python because the cycle data was stored in a 32-bit Microsoft Access database system. The Anaconda platform distributes Python with many popular packages (i.e., `Pandas`), and was used to install Python 2.7.

A popular Python package, called `SciPy`, provides useful optimization methods that could be convenient for the purpose of this thesis. For instance, it has an optimization package with a function called `curve_fit`. It uses a non-linear least square (NLLS) analysis to iterate the parameters of a model until the model fits the measured data [41]. Nevertheless, `curve_fit` only returns an array of the best fitted parameters and its covariance matrix. It did therefore require a lot of self-made functions to fully utilize its service. For instance, `curve_fit` does not allow a user to freeze one parameter while iterating the others. Luckily, there exists other packages that are already built on `SciPy`'s `optimize` package, and offer a wide range of methods.

`LMFIT` is a Python package that uses `SciPy`'s `optimize` method to perform a LM non-linear least-square minimization fit (`LMFIT`). `LMFIT` uses a `Parameter` object that tracks a parameters properties and can be constrained by an algebraic function of other parameters. `LMFIT`

also gives the user an opportunity to make a Python class of the model used to model the data. This model class has a function `fit` that runs NLLS with some predefined parameter hints, and iterates the best parameter values based on the model and measured data. The results from the model class can re-run the curve-fitting, using the best values from the previously fitted parameters as initial parameter guesses. The model's results offer many other methods as well, like plotting, printing parameters, reporting the statistics of the fit. It can also run a method which determines the confidential interval by exploring parameter space. The confidential interval is used for finding a better estimate of the standard deviation error, and is mostly useful when running a more advanced model with i.e., two or more exponential functions. To summarize, `LMFIT` provides many useful methods which make it easier to perform curve fitting, compared to using `SciPy`'s `curve_fit` [42]. Because of `LMFIT`'s many convenient methods, it was used as a basis for fitting OCV-relaxation with a cell model.

3.5.2 Git

When working in a software developing project, it is recommended to use a type of version control system, like Git. Git keeps track of changes, is fast, handles large projects and allows a non-linear work flow. It is advantageous for parallel work flows and is a powerful tool when working in a project with many different contributors [43]. Github was used as a host for the git repository (storehouse). Git itself is a command line system, but Github is a graphical interface which simplifies learning and usage Git. Github is also a social network where many programmers seek help or post ideas. SourceTree is a graphical interface program developed by Atlassian. SourceTree makes it even easier to visualize Git by showing the changes that were made and Git flowchart.

If two or more people are working on project, it is fundamental to agree on a git-flow. In 2010, Vincent Driessen posted "A successful Git branching model" as shown in Fig. 3.8 [44].

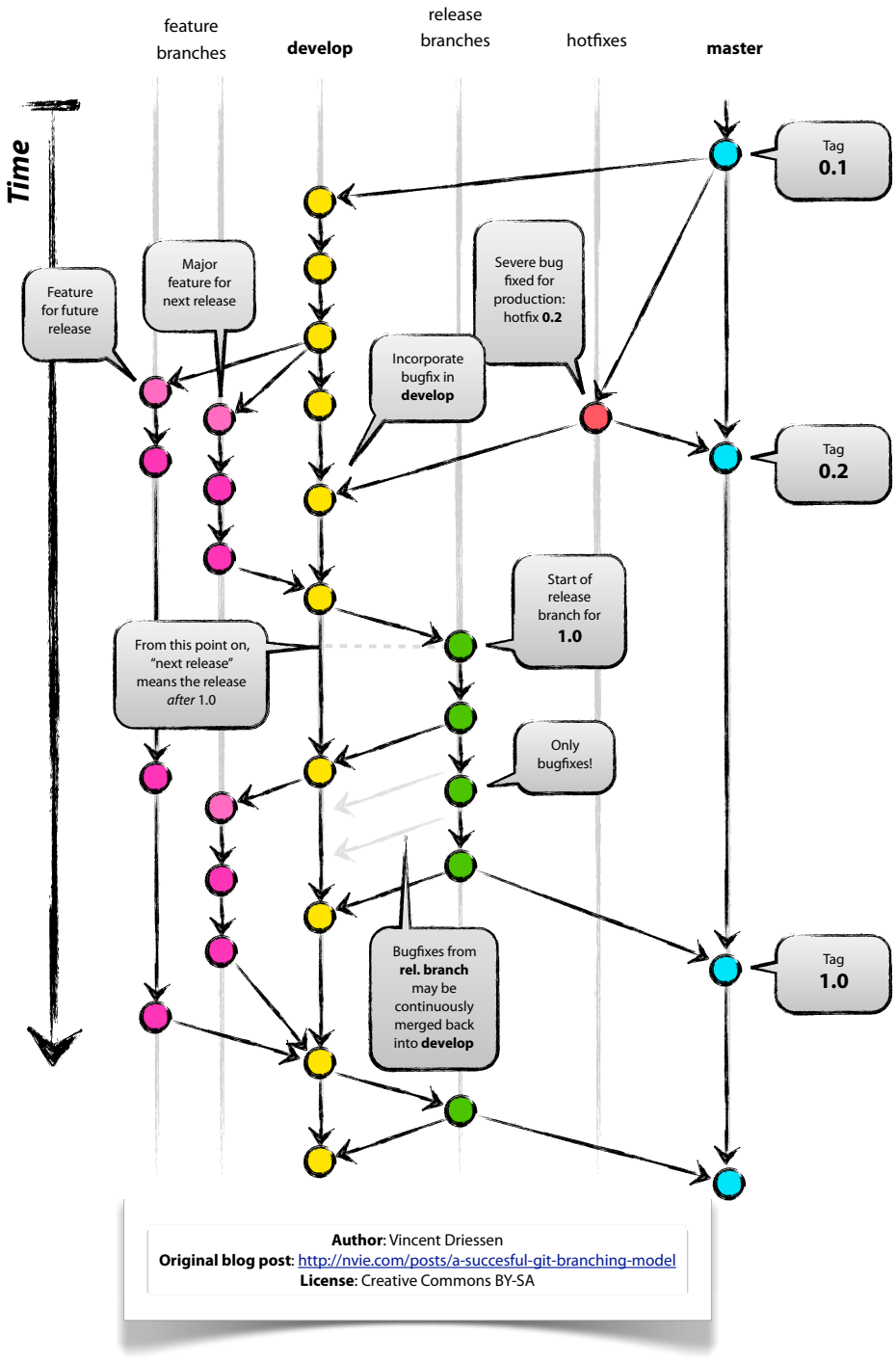

Figure 3.8: Vincent Driessen's suggested Git-flow branching model [44].

When using the Git-flow in Fig. 3.8, the master and develop branches are always parallel, and the develop will never directly merge into the master. This is convenient because it distinctly separates the released software from the developing process. Anyone who would like to contribute can connect with the developing branch and create a new `feature` branch where they can add code or change it [44].

Git, Github, SourceTree and Driessen's git-flow were all used to further develop `cellpy` in an easy and efficient way.

3.6 Programming

The program developed is a utility tool within the Python package, `cellpy`. The program was built around the benefits from `LMFIT`. The core functions of the program are performed in the `cell_ocv`-script, and the most important lines are listed in 3.1. The first line represents Eq. (3.2) and the second one is Eq. (3.3). The full `cell_ocv` code is listed in appendix A.1. The blue texts are Python statements.

```
from numpy import exp

v0 * exp(-time / tau) + ocv
```

Listing 3.1: Equation (3.3) in the `cell_ocv` script. Returns the relaxation voltage. Numpy is a Python package. It was used for handling 1-dimensional arrays. v0 = initial voltage for rc-circuit, time = numpy array of measured points in time, tau = time constant of current rc-circuit, ocv = open circuit voltage.

The `fitting_cell_ocv` script was designed to run `cell_ocv` (code A.1) (see appendix for extended the code of `fitting_cell_ocv`). The `lmfit` codes shown in 3.2 are the main lines in `fitting_cell_ocv`. Code 3.2 used `lmfit`'s `Model` class and made an object of the function `relax_model`. `relax_model` used the line in listing 3.1. The `Model`-object had all of `LMFIT`'s methods and the last line in listing 3.2 executes `LMFIT`'s fitting method with `model.fit()`. `model.fit()` performs a LM least square minimization on the model and return an useful object that was created by `LMFIT`. The returned object is called `ModelResults` and contains the best parameters, covariance matrix and additional information about the fitting. In the listing below, the `ModelResults` object has the alias `result`. The blue texts are Python statements and the purple text is a comment.

```
import lmfit
model = lmfit.Model(relax_model)

# result is a lmfit.ModelRestults object containing results from the fitting
   process.
result = model.fit(meassured_voltage, params=parameters, t=time)
```

Listing 3.2: Starts the fitting of the parameters with lmfit. Code-lines are from `fitting_cell_ocv`. lmfit first defined a model based on a function (`relax_model`) that calls the code in listing 3.1. The next line performed the actual parameter iterations. Purple text is comments.

The `fitting_cell_ocv` script saves the `result` variable for each cycle in a list and uses it to calculate the processes' (rc-circuits) resistances (R) and capacitances (C). R was calculated with Ohm's law in Eq. (2.15), where I was the current through the cell during cycling and V was the fitted initial voltage (overpotential) over the rc-circuit. The relationship between the time constant (τ), C and R from Eq. (2.24) was used to find C with the fitted time constant, stored in `result` (see subsection 3.2.2). R and C for each cycle were stored in a separate list than `result`. At the end of `fitting_cell_ocv`, the lists including fitted results and calculated RC-parameters were returned to the user.

Chapter 4

Results and Discussion

In the first section of this chapter, cell characterizing graphs are displayed and discussed. In the following sections, the model was fitted to a selection of cells' open circuit voltages (OCV) relaxation data. The fit was achieved from the program develop during this thesis. The model used for fitting of OCV-relaxation was presented in subsection 3.2.2. An electrochemical impedance spectroscopy (EIS) was performed on the cell EA to validate the fitted results achieved from the program and cell model.

4.1 Arbin Data

The cells S, 2, A1 and A2 were mostly displayed in the following section. The cell 2 was chosen for comparison because its mass was the closest to the cell A1. The cells 1 and 3 were not included because they would be redundant, since their behaviors were similar to the cell 2's. The S cell was stored for a longer period than the others, before initial lithiation. It was included to compare its performance to the younger cells.

4.1.1 Capacity

Arbin and its software provide several data elements about a cell's condition, one of them being the cell's capacity. The charge capacity (delithiation) and the discharge capacity (lithiation) in Fig. 4.1 are Q_{out} and Q_{in} from Eq. (2.26), respectively. They were both calculated by Arbin with Eq. (2.25), which is a function of current and time. Arbin's current accuracy was specified as 0.1 % of full scale range (±10 mA). The S cell was assembled a long time before it was cycled, compared to the other cells. "A" in a cell name indicates that the cell has additives in the electrolyte. Specifications for the cells are shown in table 3.2.

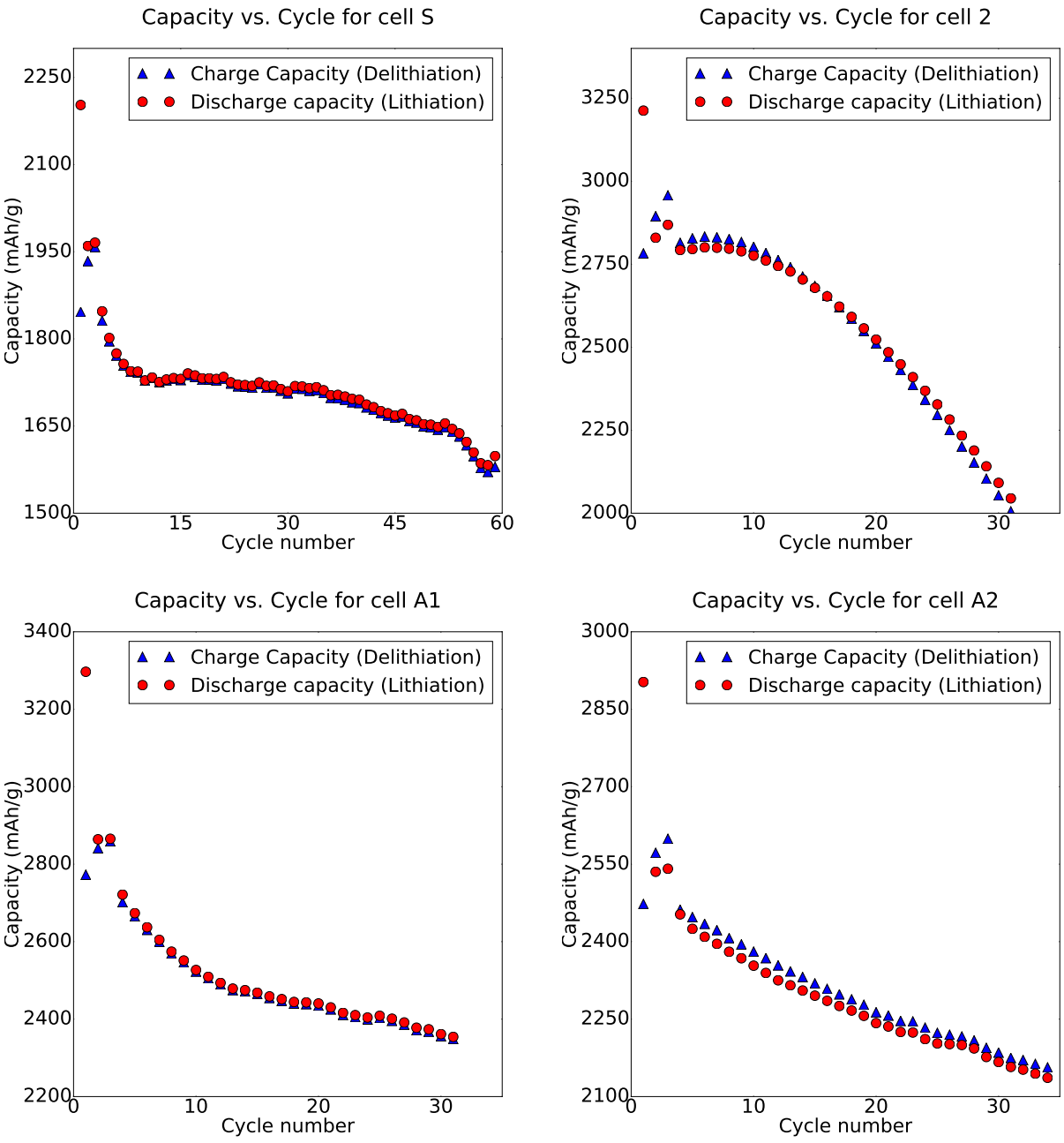

Figure 4.1: Specific capacity vs. cycles for a selection of cells. The capacities are per gram silicon. Cells with A in their name had additives in the electrolyte. Current accuracy was stated in Arbin's user manual as 0.1 % of full scale range.

In Fig. 4.1, all the cells have a bigger gap between the specific capacity in the first cycle than in the rest of the cycles. This indicates that the silicon (Si) anode was a better host to lithium (Li) in the first cycle than the later ones. It makes sense that the Si anode accepted more Li atoms during the first lithiation because it was mostly pure silicon. In addition, a solid electro-

lyte interphase (SEI) was not present at the electrode before the first lithiation. After the first lithiation, a SEI was formed and the lithium had more resistance on the way out from the Si electrode than on the way in. Thus a lower specific capacity of the cells was observed after delithiation in the first cycle. Furthermore, the Si had a crystalline structure before first lithiation, yet studies show that the crystalline structure tends to break and to become amorphous during the first lithiation (see subsection 2.7.2), which could also contribute to a drop of delithiation capacity. These factors are most likely the reason why the coulombic efficiency (Eq. (2.26)) was less than 90 % for all cells in the initial cycle.

In some cycles the delithiation capacity was higher than the lithiation capacity for the cells 1-3 and A2, indicating a coulombic efficiency higher than 100%. A possible explanation could be that some of the lithium from the first lithiation was not extracted after the first delithiation, but in later cycles. In this case, it would be possible to obtain a coulombic efficiency higher than 100 %. However, it is more likely that the channels these cells were cycled in, were not properly calibrated.

The S celll had a lower specific capacity than the rest of the cells. This was probably because S was stored longer before initial lithiation, compared to the rest of the cells. To evaluate the effect of storing a cell before lithiation, the total capacity of the cell had to be compared with the expected value. By using the mass of the active material, presented in table 3.2, the total capacity of the cells S, A1, A2 and 2 were calculated, and are displayed together with expected capacity from table 3.2, in table 4.1. The specific capacities in table 4.1 are all from cycle number 9, after lithiation. Cycle number 9 was chosen because it looked the most stable for the cells A1 and 2 in Fig. 4.1, and the cell A1 showed some degree of stability after cycles 9-12. The deviation in table 4.1 was calculated from the capacity and expected capacity - where the capacity was calculated with measured specific capacity (from Fig. 4.1) and expected capacity with the theoretical value, 3.579 mAh/mg. The uncertainty of the capacity is calculated based on the current output accuracy stated by Arbin (0.1 % of full scale range ($\pm$10mA)). The other uncertainties were calculated with the standard deviation of the mass and Arbin's measurement accuracy.

Table 4.1: The capacity of a selection of the cells, compared to the theoretical capacity. The measured specific capacities are all at cycle 9 (lithiation) from Fig. 4.1. The masses of the active material are from table 3.2. The deviation is the capacity based on measured specific capacity and expected capacity (calculated with theoretical capacity of 3.579 mAh/mg).

Cell name	Active material (mg)	Measured specific capacity (mAh/mg)	Capacity (mAh)	Expected capacity (mAh)	Deviation
A1	0.3810 ±0.001	2.552 ±0.030	0.9724 ±0.009	1.364 ±0.003	-28.7% ±0.6%
A2	0.3758 ±0.001	2.586 ±0.028	0.8899 ±0.008	1.345 ±0.003	-33.8% ±0.7%
2	0.3602 ±0.001	2.705 ±0.034	1.005 ±0.010	1.289 ±0.003	-22.0% ±0.5%
S	0.8635 ±0.002	1.732 ±0.012	1.506 ±0.006	3.090 ±0.008	-51.3% ±0.5%

The deviation between capacity and expected capacity in table 4.1 points out that the S cell only managed to store half of predicted charge, while the cells A1, A2 and 2 store around 20-35 % less than expected. This confirms that storage of S for 1 month, reduced its capacity. Nonetheless, Fig. 4.1 points out that the cell S's capacity did not as heavily during the first 10 cycles, as with the other cells. The cell A1 dropped from ~2700 mAh/g to ~2500 mAh/g from cycle 4 to 10. This was a significant loss in capacity compared to the S cell, which only dropped from ~1850 mAh/g to ~1700 mAh/g from cycle 4 to 10. Additionally, the S cell was pretty stable during cycle 10-53, but died shortly after cycle 53.

A possible explanation for the lower capacity after storage could be that a SEI was formed during shelf time. Nonetheless it is likely that this SEI was differently composed than one formed during lithiation. Perhaps the SEI formed during storage was a stable SEI layer which increased the cell's cycle life, but reduced its storage capacity.

The increase of capacity during the first three cycles might be the result of a stable SEI-formation. The decline in capacity after the third cycle could be because of a higher current, causing more volume expansion and contraction of the Si anode, which leads to cracking of SEI and the Si-anode.

The observed reduction of capacity after cycle three in Fig. 4.1 is perhaps the result of an increased SEI-layer, blocking the lithium on its way into the electrode. Available surface area of active material would decrease, and thus the charge transfer resistance would increase, inducing a loss of capacity.

4.1.2 Capacity and Voltage

Figure 4.2 presents the specific capacity of the same four cells as in Fig. 4.1, but with voltage instead of cycles. The plots include both lithiation (lower lines), open circuit and delithiation (upper lines). Open circuit after lithiation can be observed at the very right, where the capacity was constant and voltage was increasing. Open circuit after delithiation is on the left of plot. Figure 4.2 does not include the resting period of the cell before cycling. The blue graph (first cycle) has an initial potential at about 2.8-3.1 V after a 24-hour rest period.

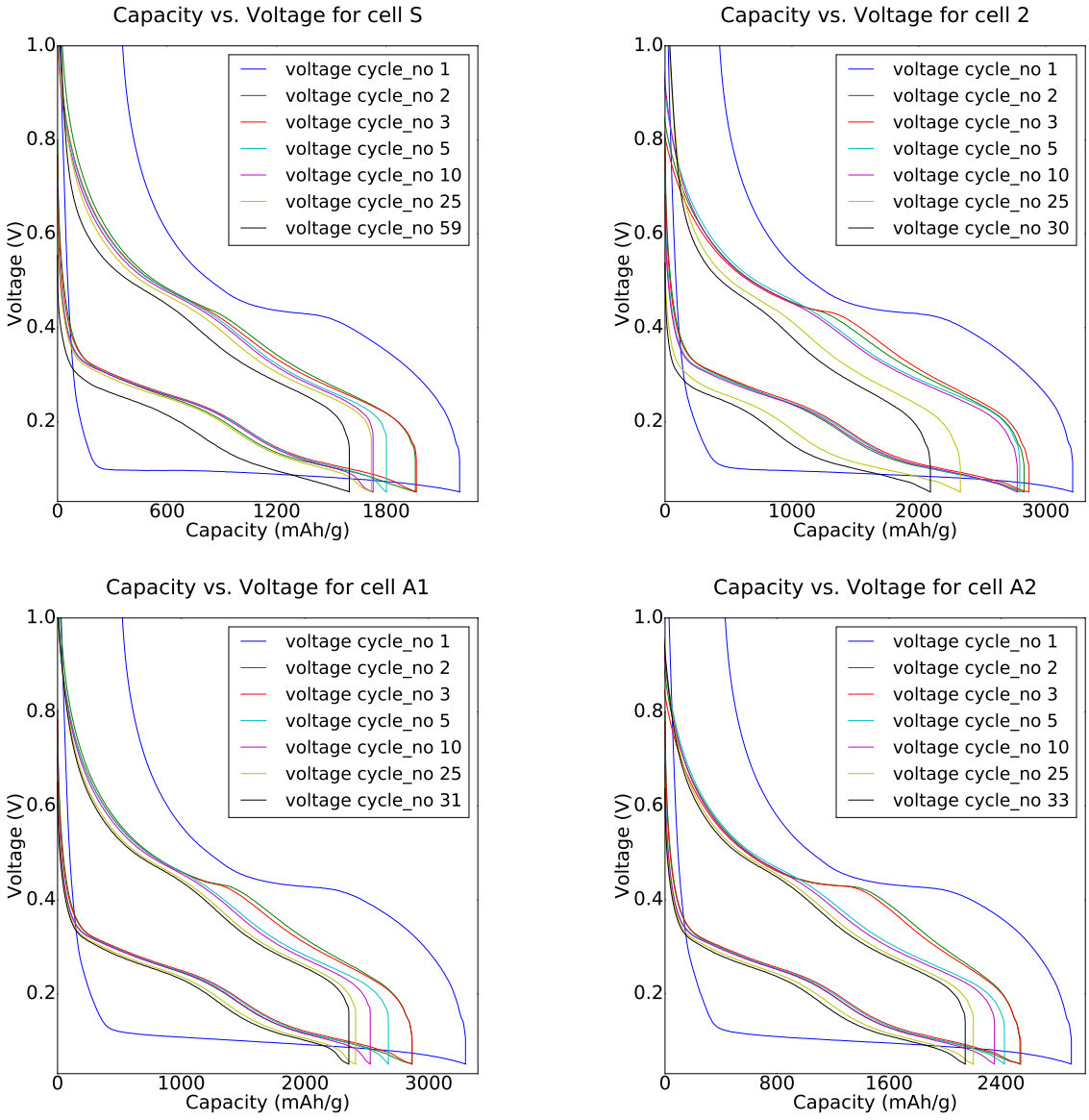

Figure 4.2: Specific capacity plotted with voltage for a selection of cells. The capacities are per gram active material. Cells with A in their name have additives in the electrolyte.

When the initial lithiation current was applied, the voltage went down to ~0.08 V for all the cells, and stayed constant until it reached cut-off voltage. After the first cycle, the voltage dropped to about 0.4 V for all the cells, and slowly decreased during lithiation until cut-off. The reason why the first cycle dropped almost instantly to 0.08 V, and not 0.4 V - 0.5 V, was that the anode was mostly silicon before the first lithiation process. After first lithiation, the anode phase-shifted from crystalline to amorphous Li-Si alloy. Subsection 2.7.2 in the Theory section mentions that a Li-Si alloy has a delithiation potential around 0.4 V vs. Li/Li^+, which can be observed in 4.2.

4.1.3 Measured Relaxation Voltage

After Lithiation

The open circuit relaxation situations after lithiation are shown in Fig. 4.3. The cells relaxed for 2 hours after lithiation. The first three cycles for all cells had a 1/20 C-rate and are graphed for all cells i Fig. 4.3. The data was collected with the same sampling rate as described in table 3.5: every 10 seconds, or when the voltage changed more than 0.001 V. The voltage fits for the cells S and A2 were plotted for every 30 points and the cells A1 and 2 every 10 points. The voltage range was ±10 V and the measurement accuracy was stated by Arbin as 0.1 % of full scale range.

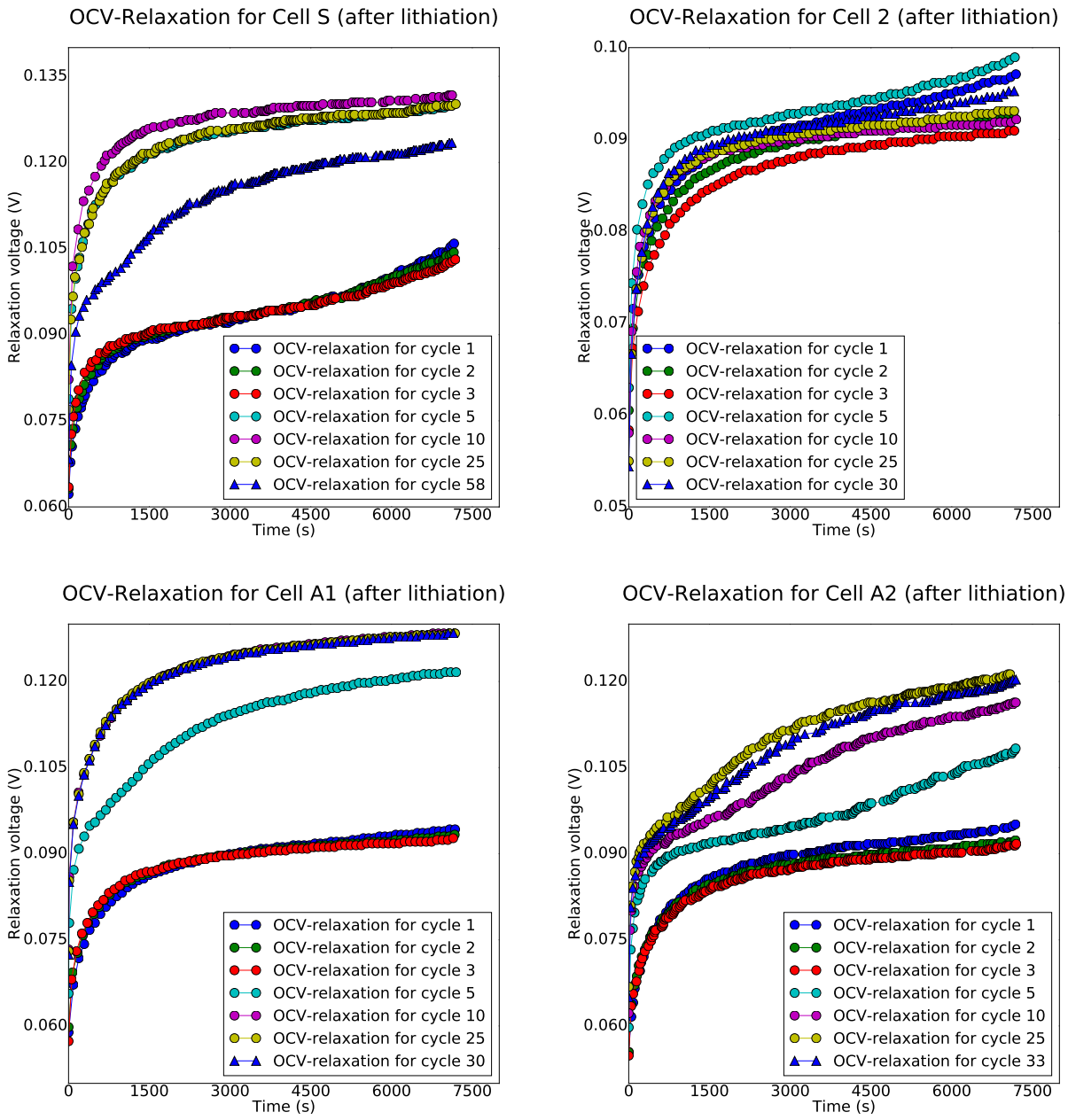

Figure 4.3: Open circuit voltage relaxation after lithiation for a selection of cells. The voltage fit for the cells S and A2 are a plot for every 30 measured points, the cells A1 and 2 every 10 points. The IR-drop was excluded.

All the graphs in Fig. 4.3 behaved partly like a capacitor, caused by the electric double layer. The voltage relaxed towards an equilibrium (OCV), but there were some exceptions. The cell S's cycles 1-3, and cycles 1 and 5 in the cell 2 all started as an exponential decay, but ended up accelerating near the end. Furthermore, all but the three initial cycles of the cell A2 behaved in an unforeseen manner. It looked as if some unknown reactions started when the measured

relaxation voltage reached about 0.09 V. In fact, when examining the OCV-relaxation after lithiation for all the cells - including the cells 1 and 3 in Fig. 4.4 - it was apparent that something had happened around a relaxation potential of 0.09 V vs. Li/Li^+.

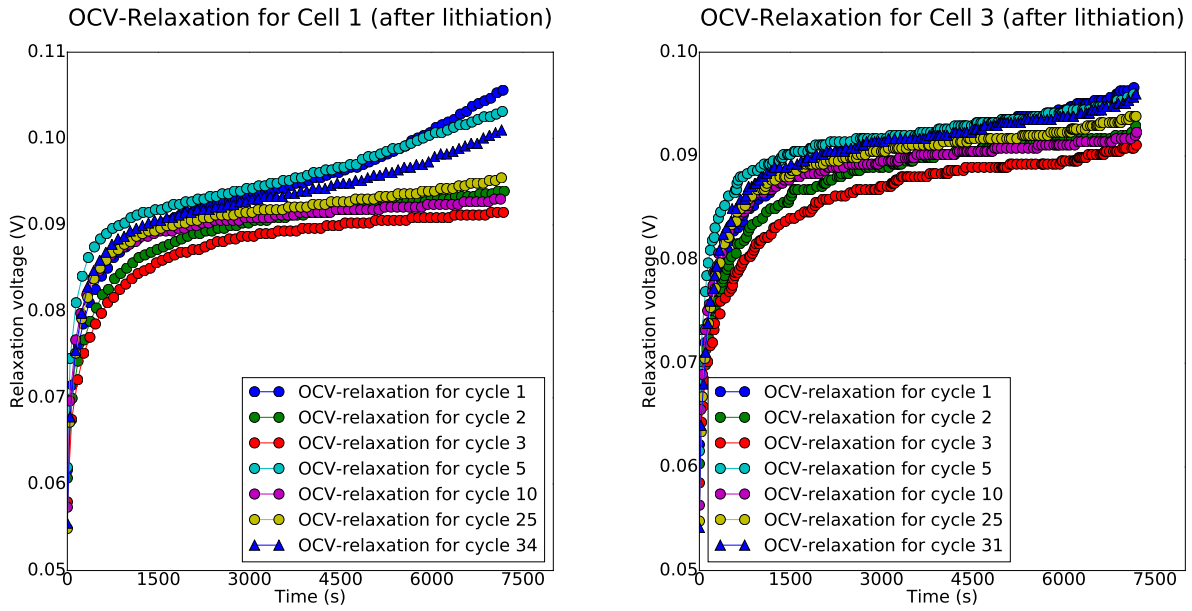

Figure 4.4: Open circuit voltage relaxation after lithiation for the cells 1 and 3. Graphs 1 and 3 were plotted for every 10 points. The IR-drop was excluded.

A proposed illustration for why the cell voltage increases after lithiation is displayed in Fig. 4.5. Hypothetical voltage measurement points are illustrated with black sticks in the figure. The voltage (V) was increasing with time (t), and the model is divided into three time phases: the charge transfer (the fastest increase of voltage in Fig. 4.3), the diffusion and the equilibrium (OCV). x, y and z are the amounts of lithium (Li) in one silicon (Si) particle. e^- represents an electron. $t = 0$ was right after the IR-drop.

The model in Fig. 4.5 is based on the Theory section 2.5.2. The surface of the cell caps was the points which were monitored by Arbin's voltmeter. The cell components, beside the anode, cathode and electrolyte, were assumed to function perfectly. Therefore it was assumed that the measured voltage was the activities on the electrode surfaces instead of the surface of the cell caps.

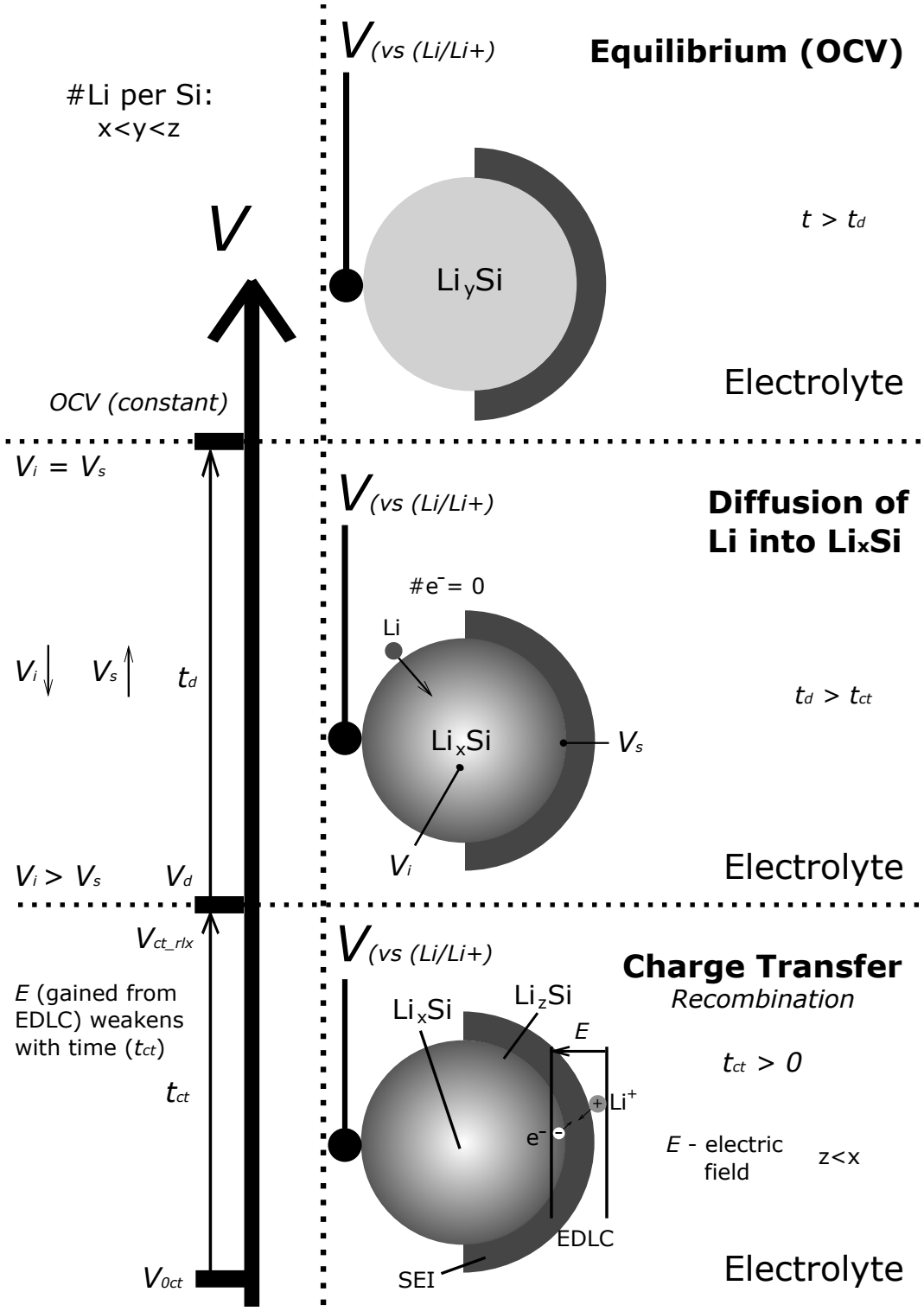

Figure 4.5: Sketched explanation for the increase in relaxation voltage after lithiation. The process is divided into three time phases. The charge transfer and diffusion into the electrode are assumed to be the dominating processes during relaxation. The IR-drop was excluded. V's are voltage and the stick attached to them symbolizes measurement points. x, y and z are the amounts of Li per Si particle. Time increases from bottom to top.

The model suggests that electrons and lithium ions were recombining at the surface during charge transfer. The recombination was partly due to the electric double layer's capacitance (ELDC) formed at the interface between the electrolyte and electrode (see section 2.4). EDLC induced an electric field (E) that applied a force on positively charged Li-ions, causing them to move towards the anode surface. The direction of E was pointing inwards, because it was assumed that dangling bonds at the Si-surface and positive charges in the electrolyte had formed a double layer as seen in Fig. 2.3. A recombination of Li-ions and electrons caused a loss of free electrons at the silicon surface, and thus an increase in potential vs. Li^+/Li. The charge transfer process could be considered over when all the electrons at the surface were consumed and there were no Li-ions remaining, because the electric field (E) was too weak to transfer more Li-ions.

A total increase of voltage was seen in Fig. 4.3, because of a high charge transfer rate and diffusion of lithium into the lithium-silicon alloy. When the charge transfer was over, the diffusion of Li into the lithium-silicon alloy continued, and this was most likely the cause of the slower increase in voltage. If it were possible to record the voltage inside the electrode and at its surface, the inside voltage would be higher than the surface's (with reference to Li^+/Li). The potential at the surface would be lower than inside because there were more lithium atoms at the surface. The voltage measured at the surface, during the diffusion process, increased as the lithium moved away form the surface and into the electrode. When all this accumulated lithium from the charge transfer process was distributed evenly in the electrode, the cell voltage would be fully relaxed at OCV. x number of lithium particles in one silicon particle would increase towards y number of Li during the diffusion process, and z at the surface would decrease to y.

After Delithiation

Relaxation voltage for the cells S, 2, A1 and A2 after delithiation are plotted in Fig. 4.6. The data-sampling was the same as for OCV-relaxation after lithiation, following the schedule described in table 3.5. For a better visualization of the results, every 30 measured points for the cells S and A2 and every 10 points for the cells A1 and 2 were plotted in Fig. 4.6.

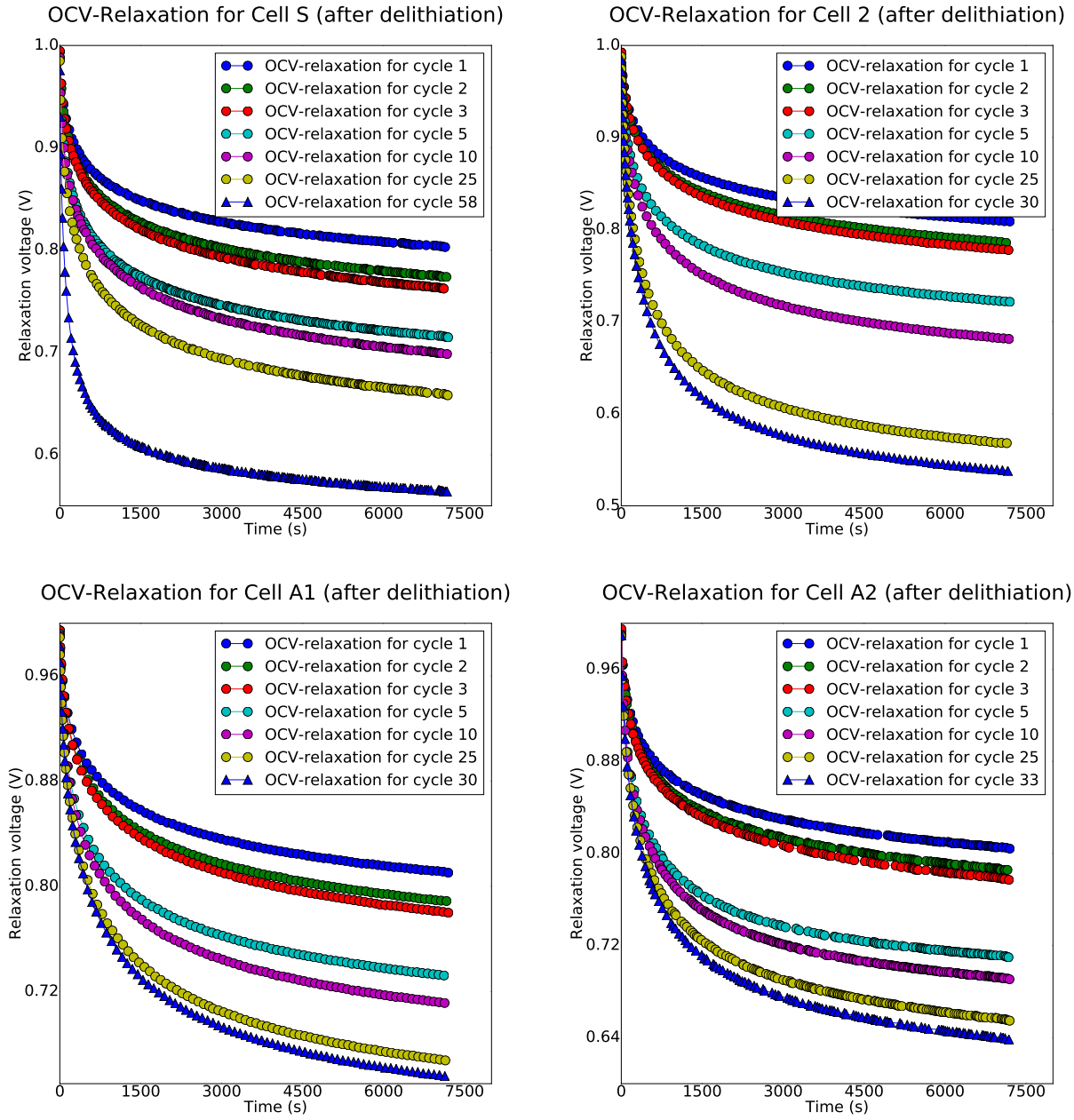

Figure 4.6: Open circuit voltage relaxation after delithiation for a selection of cells. The cells S and 2 were plotted at every 30 points, the cells A1 and 2 at every 10 points. The IR-drop was excluded.

The reason behind a decrease of voltage after delithiation was probably similar to what was explained in Fig. 4.5. The difference from after lithiation was that the electric field E was likely facing the opposite way in the situation after delithiation, compared to after lithiation. An other interesting observation is that the overpotential after delithiation is considerably greater (~2~ 4 times) than after lithiation. Recall from subsection 2.7.2 that a $Li_{15}Si_4$ alloy had a typical delithiation potential of about 0.4 V vs. Li/Li^+. The cut-off voltage after delithiation was 1 V, which is a higher than what was necessary for delithiation to occur on the anode. This is probably the reason why the overpotential after delithiation was greater than the overpotential after lithiation. The relaxation process after delithiation is illustrated in Fig. 4.7.

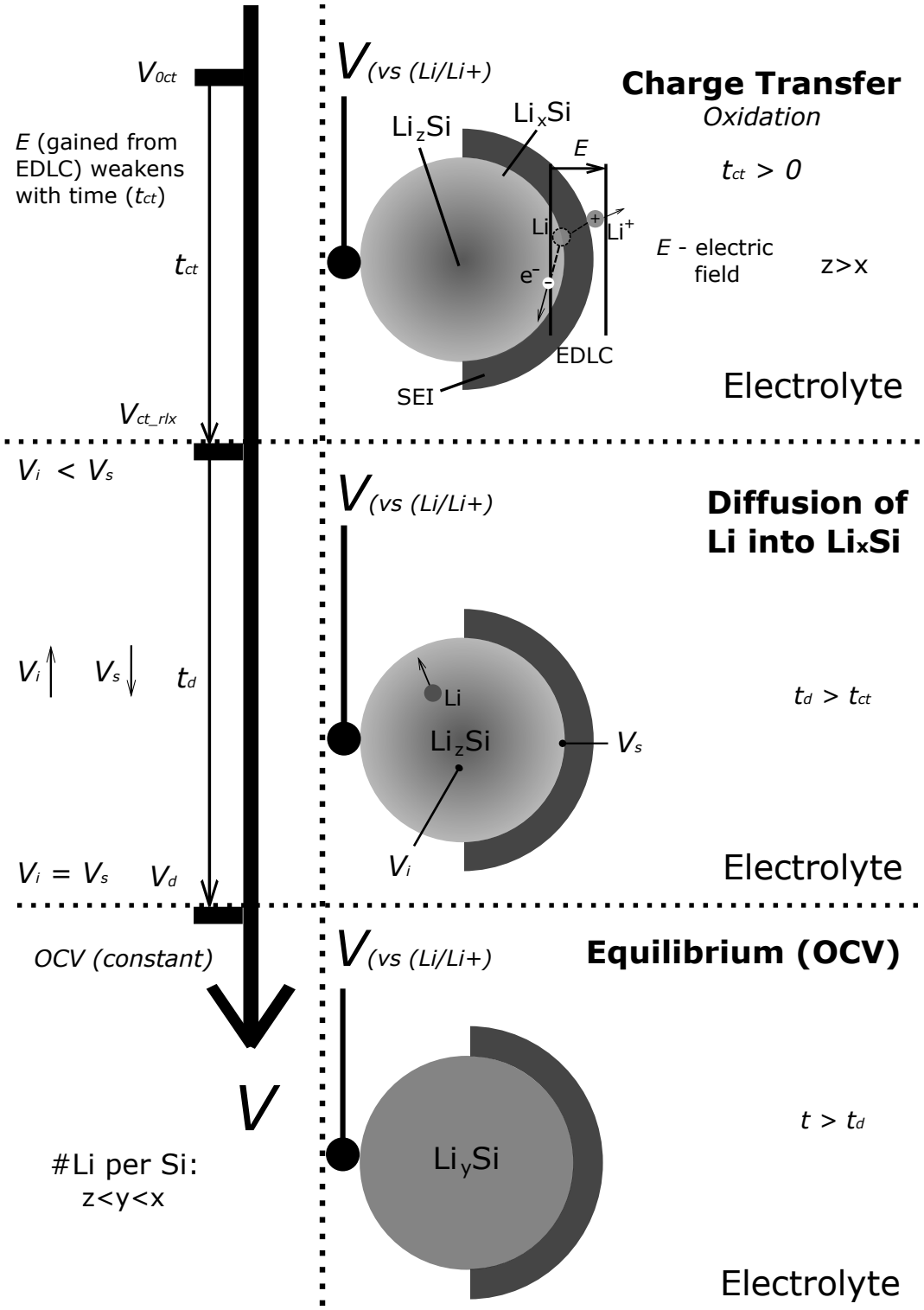

Figure 4.7: Proposed illustration of anode activity after delithiation. The illustration is divided into three time phases: charge transfer, diffusion and equilibrium (OCV). The situation was similar to what was shown in Fig. 4.5, but with some important differences - x and z have swapped positions and as a result, the voltage was decreasing with time. x, y and z are amounts of Li per Si particle. IR-drop was excluded. Time decreased from top to bottom.

During the charge transfer process in Fig. 4.7, the EDLC was strong enough to induce an oxidization of a lithium atom into a Li-ion/electron pair, and transfer the Li-ion away from the surface into the electrolyte. The measured cell voltage at the surface of the Li-Si alloy would then decrease, since more free electrons were detected. When looking at Fig. 4.3, the charge transfer period after lithiation showed a smaller overpotential than after delithiation. To interpret this observation with Fig. 4.7, the electric field (E) induced by the electric double layer had to be a larger than the one in Fig. 4.5. The charge transfer process was considered done when E was too weak to oxidize lithium and move the ions away from the surface. Note that in Fig. 4.7 and 4.5 that the EDLC does not have clear boundaries. It was displayed this way because the SEI layer is in both solid and liquid phases, thereof the name Solid Electrolyte Interphase.

The model represented in Fig. 4.7 shows a lesser amount of lithium atoms at the electrode surface than at the core ($z > x$). The potential measured at the surface would therefore be larger than what would hypothetically be measured inside the electrode. Lithium atoms replenished at the surface because of a concentration gradient between the core and the electrode surface. The addition of Li-atoms to the surface would lead to a further decrease in voltage. This has been proposed as the explanation for the slower decrease in voltage at the end of relaxation observed in Fig. 4.6. If lithium in the silicon was equally distributed in the Li-Si alloy, the cell would be in equilibrium.

4.2 Fitting of Relaxation Voltage

The following results are mostly based on the cell A1. The cell 2 had a coulombic efficiency higher than 100 % in some cycles. Despite this, the cell 2 was used to compare parameters with the cell A1. The cell 2 was chosen because its anode was composed of the same slurry as the cell A1. Additionally, it had almost the same mass of active material and was without additives in the electrolyte. The cells A1 and 2 were compared mostly in the OCV-relaxation after delithiation, because the cell 2's OCV-relaxation after lithiation reached 0.09 V at cycles 1 and 5. As seen in Fig. 4.3, the cells reaching 0.09 V during OCV-relaxation acted unpredictably, and were not well suited for a fitting of parameters with the model suggested in subsection 3.2.2. The first subsections present the fit after delithiation, and then follows lithiation.The fits for the rest of the cells are shown in appendix B.

4.2.1 After Delithiation

The following results were produced by `cellpy`'s `fitting_cell_ocv` (listing A.1 and A.2 in appendix). The fitted OCV-relaxation was displayed for cycle 4 and 30, because the cell 2 did not have more data after cycle 30. The cell A1's fit of cycle 4 and 30 after delithiation are shown in Fig. 4.8 and the cell 2's fit in Fig. 4.9. Every fit after cycle 1 used previously fitted parameters as initial guesses for new fittings. The initial guess for cycle 1's time constants were 50 s for charge transfer and 800 s for diffusion. The initial voltages were guessed as 20 % and 80 % of the relaxation overpotential (after IR-drop) for the charge transfer and diffusion process, respectively. The residual between fit and measured data are also displayed in the figures. The residual help uncover when the cell model did not compare with the measured data.

The best fit for the charge transfer and diffusion processes was graphed by using the best fitted parameters and Eq. (2.23). For the cells A1 and 2, cycles 4 and 30, the contribution from each process is graphed in Fig. 4.10. The rc-lines decay towards zero because the reference was OCV.

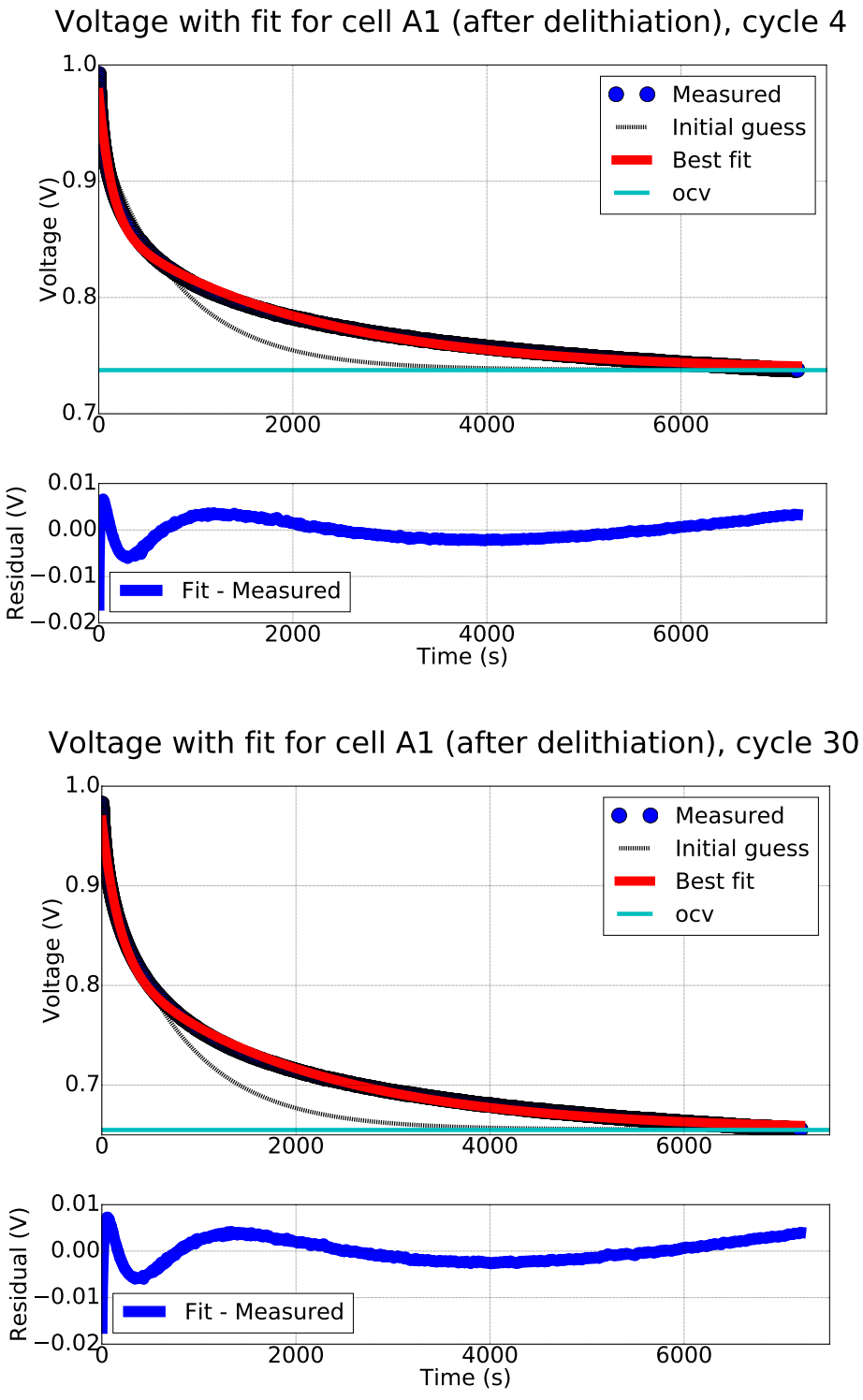

Figure 4.8: Fitted OCV-relaxation after delithiation for the cell A1, cycle 4 and 30. Generated with `cellpy`. The measurement accuracy was stated as 0.1 % of full scale range. Initial guess was plotted with Eq. (3.3). All initial guessed values were the best fitted parameters from the previous cycle. Delithiation current was 1/20 C-rate. IR-drop was excluded.

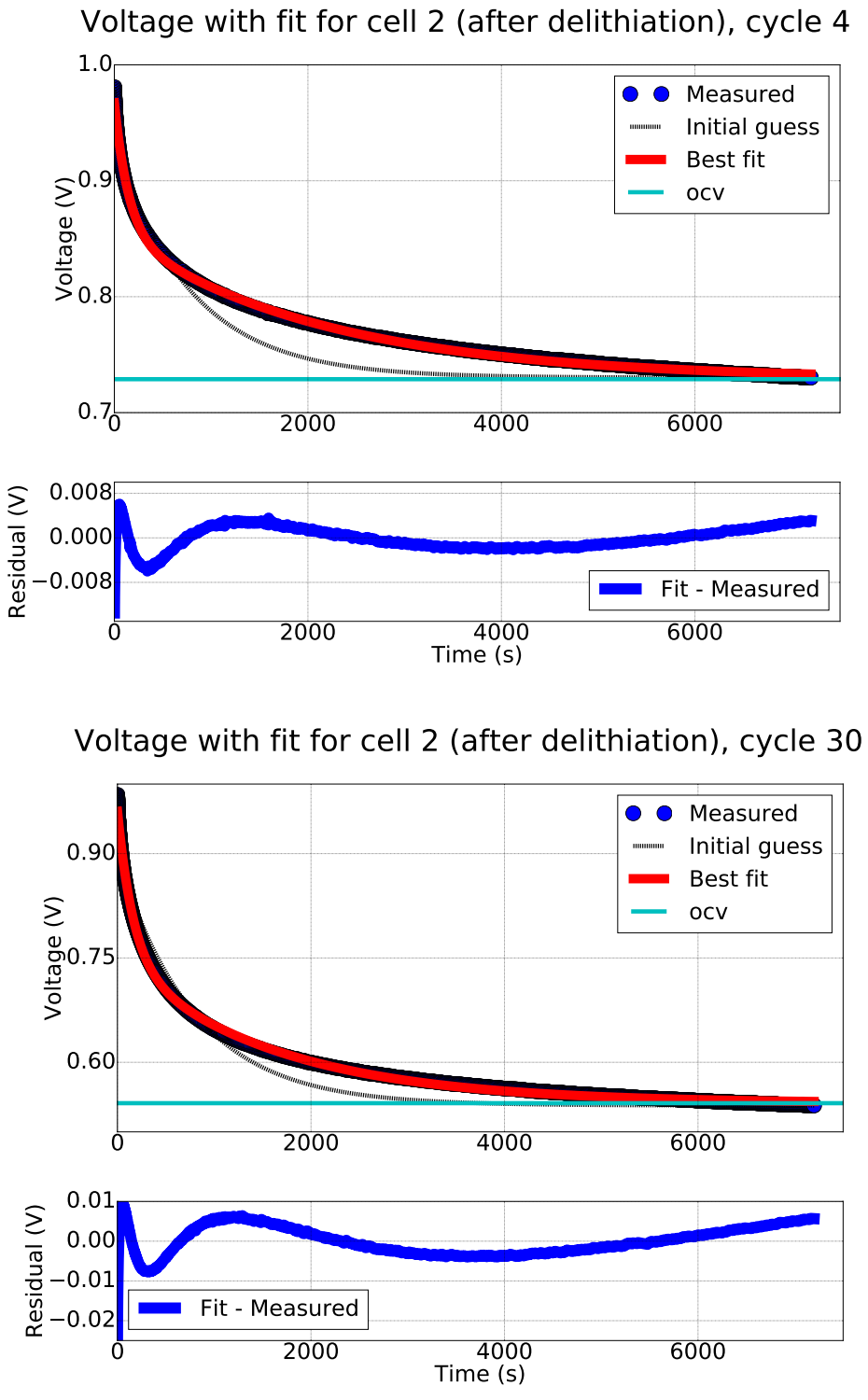

Figure 4.9: Fitted OCV-relaxation after delithiation for the cell 2, cycle 4 and 30. Generated with `cellpy`. The measurement accuracy was stated as 0.1 % of full scale range. Initial guess was plotted with Eq. (3.3). All initial guessed values were the best fitted parameters from the previous cycle. Delithiation current was 1/20 C-rate. IR-drop was excluded.

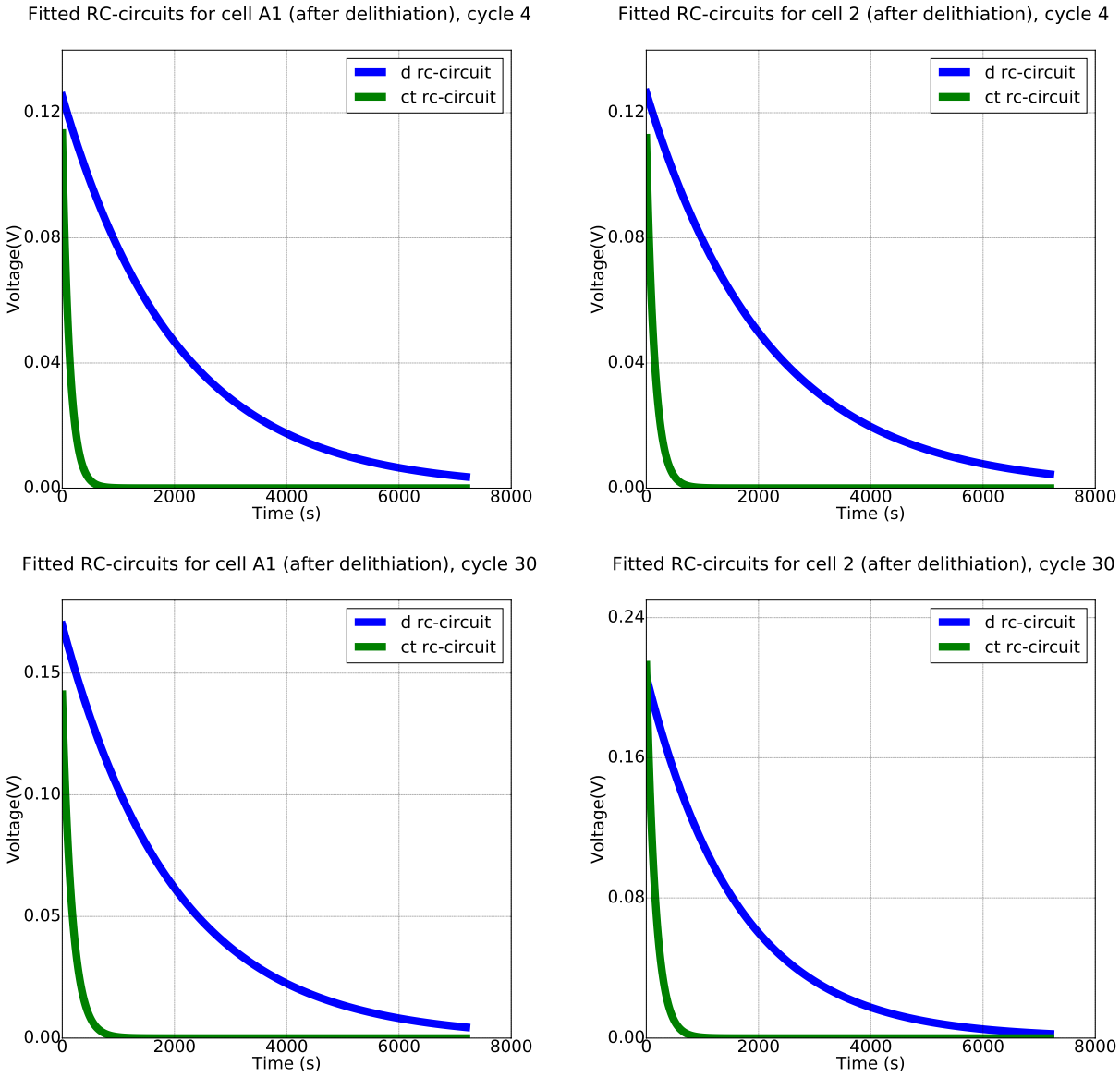

Figure 4.10: RC-circuits for the cells A1 and 2 after delithiation for cycle 4 and 30. d and ct RC-circuit stands for diffusion and charge transfer. Both graphs were plotted with the fitting results from `cellpy` and Eq. (2.23). ct- and d-RC-circuits are both decaying towards OCV. d and ct decay towards zero in this graph because OCV was the reference. Delithiation current was 1/20 C-rate.

How fitted parameters changed with cycles is interesting to examine because they could reveal the information about which parameters were affected the most. All fitted parameters for the cells A1 and 2 are respectively shown in Fig. 4.11 and 4.12.

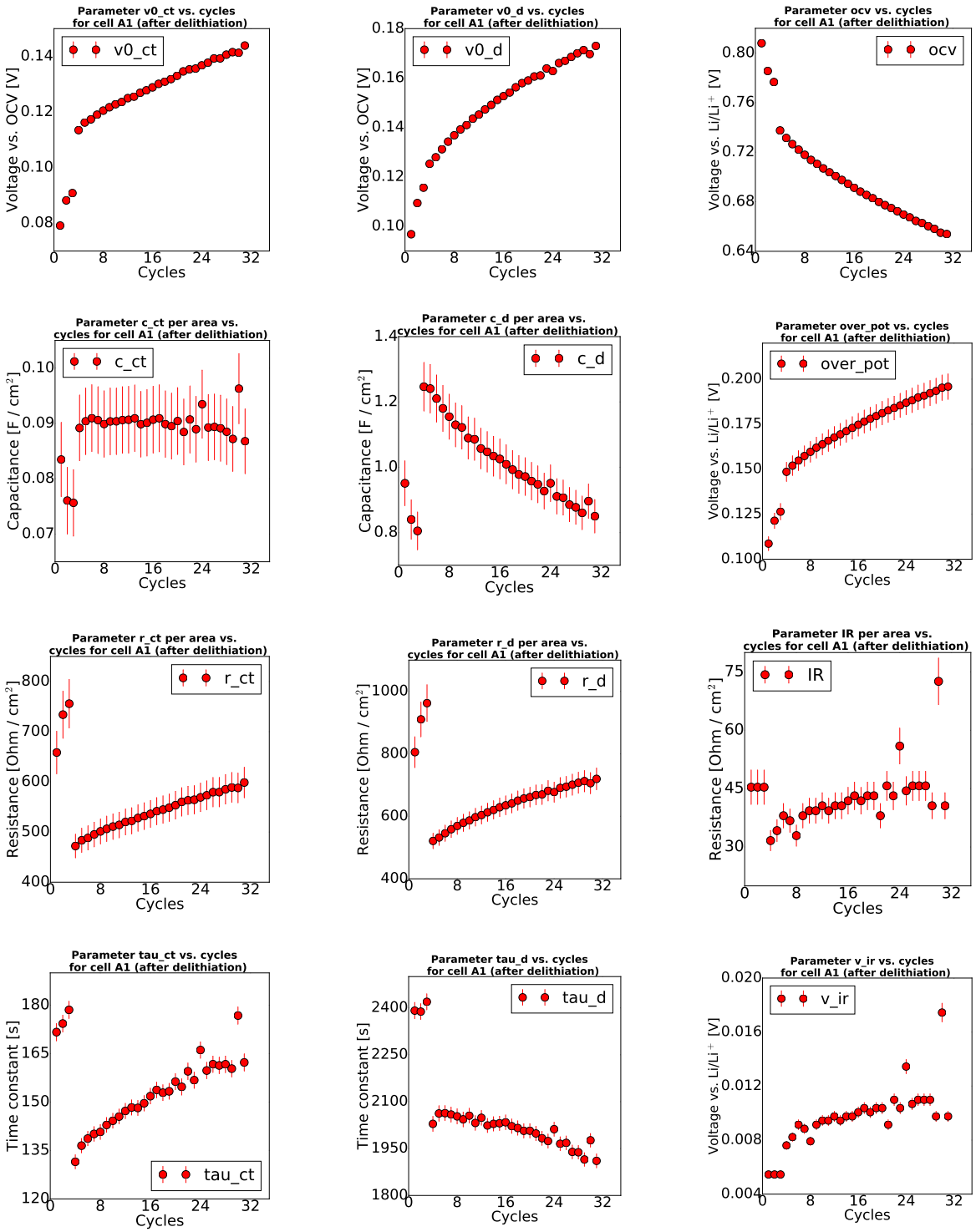

Figure 4.11: Fitted parameters vs. cycling for the cell A1 after delithiation. "tau_d", "tau_ct", "v0_d", "v0_ct" and "ocv" were fitted by with lmfit, and their error are the standard deviation, calculated by the least square minimization. "over_pot" is the magnitude of the total overpotential in the cell, calculated by subtracting "ocv" from the cut-off voltage. "ct" and "d" are charge transfer and diffusion. "tau" represents the time constant (τ). "r" and "c" are the resistance and capacitance, while "IR" is the internal resistance. Resistance, capacitance and IR are per area of the 1.5 cm diameter disk.

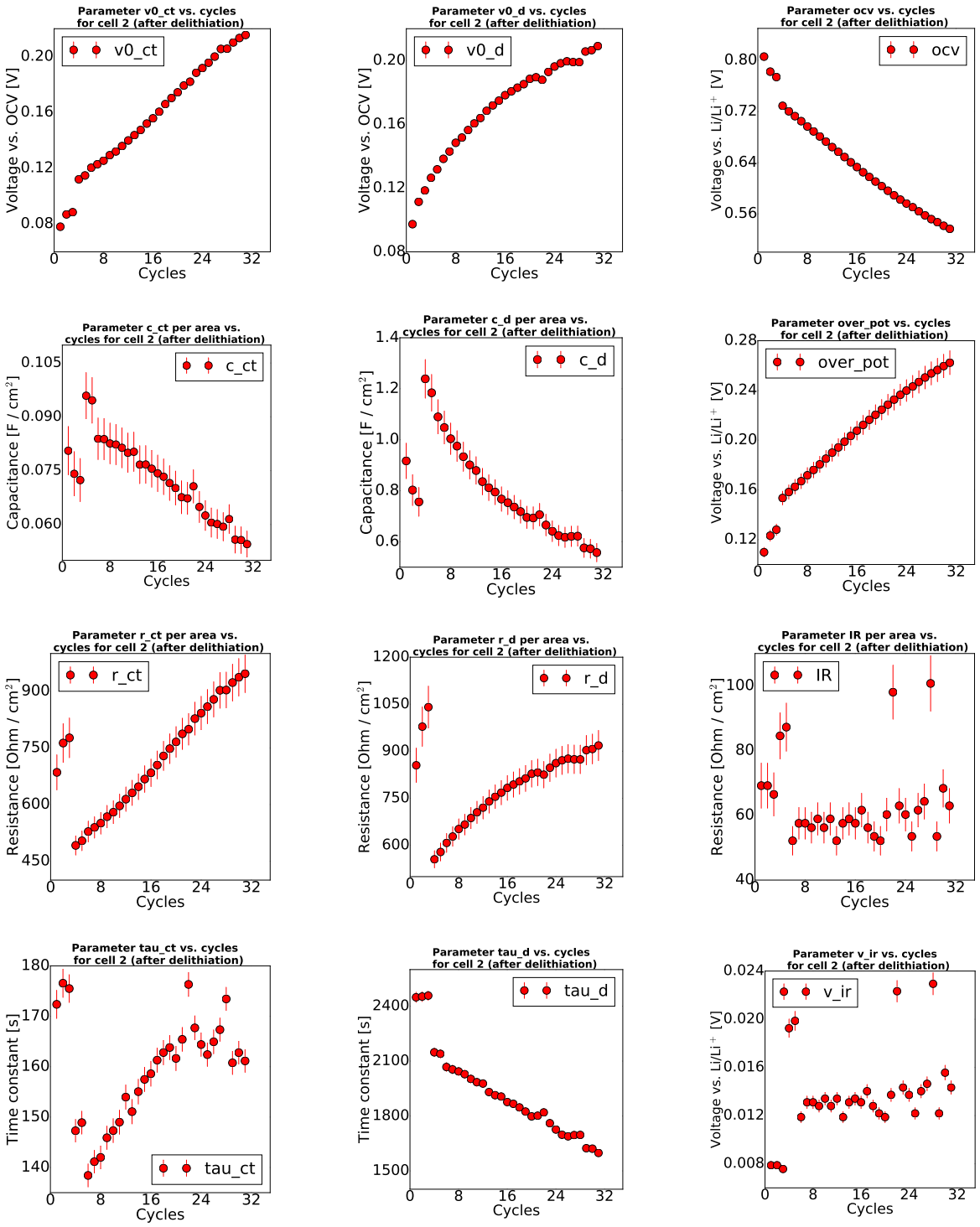

Figure 4.12: Fitted parameters vs. cycling for the cell 2 after delithiation. "tau_d", "tau_ct", "v0_d", "v0_ct" and "ocv" were fitted by `lmfit`, and their errors are the standard deviation, calculated by the least square minimization. "over_pot" is the magnitude of the total overpotential in the cell, calculated with the cut-off voltage subtracted from the fitted OCV. "ct" and "d" are charge transfer and diffusion. "tau" represents the time constant (τ). "r" and "c" are the resistance and capacitance. "IR" is the internal resistance. Resistance, capacitance and IR are per area of the 1.5 cm diameter disk.

Figure 4.13 displays the charge transfer and diffusion resistances from both the cell A1 and the cell 2, compared to the specific capacity per cycle. The black points are the cell A1 and the red the cell 2. The apparent resistance signify that the results from fitting OCV-relaxation is not a real resistance, but an analogue to the activities in a cell.

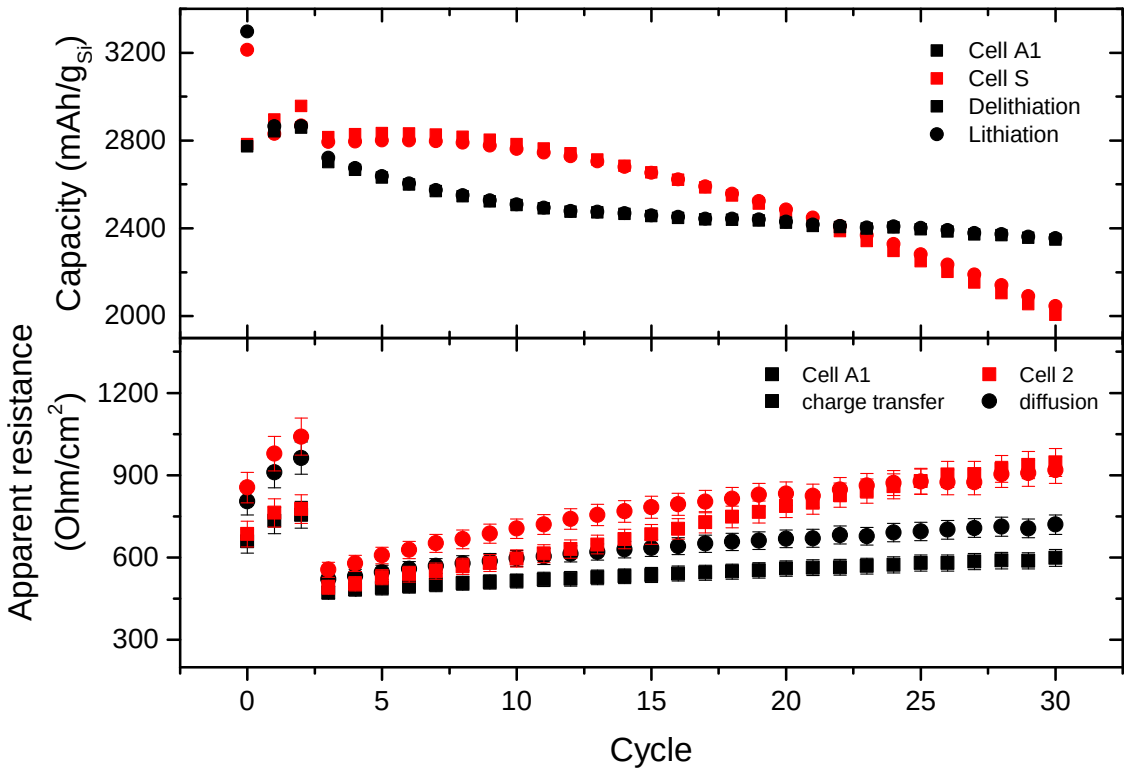

Figure 4.13: Comparison between fitted resistances from the cells A1 and 2, with specific capacity per cycle. Black points are associated with the cell A1.

4.2.2 Evaluation of Fitted Parameters After Delithiation

The model shows a satisfying fit with the measured relaxation voltage. However, when studying the residual plots in Fig. 4.8 and 4.9, the best fits did not start in the same point as the measured data. This happened for all cells after delithiation (appendix B). The model did not fit with the fastest reactions during the first 10~50 seconds. The charge transfer RC-circuit was originally supposed to model the fast reactions in the start of the relaxation process, after the IR-drop. Instead, Fig. 4.11 and 4.12 show that the charge transfer time constants were above 120 seconds for cycles with 1/10 C-rates, and above 160 for 1/20 C-rates (first three cycles). Assuming that

the charge transfer process would be completely stopped after five time constants, the modeled charge transfer process would last for about 700 seconds. The charge transfer time constants and the high residual during the first 50 seconds suggest that another process with a different time constant than the charge transfer was present, but not included in the model. Including a new RC-circuit could improve the fit.

Figure 4.10 separates the fit in Fig. 4.8 and 4.9 into the charge transfer and diffusion process. This demonstrates which process was dominating at what time. The charge transfer was indeed the fastest process. In Fig. 4.10 the charge transfer stopped around 700-1000 seconds, while the diffusion was much slower.

Figure 4.10 also points out that the ratio between charge transfer and diffusion processes was almost constant with cycling for the cell A1. This indicates that the additives in the cell A1 helped forming a stable SEI, thus avoiding the blocking of Li-ions. The charge transfer process increased slightly faster than the diffusion process for the cell 2. The charge transfer overpotential was bigger than the diffusion overpotential at cycle 30, indicating that the charge transfer resistance was the limiting factor for the cell 2.

Equation (2.12) and (2.14) point out that the charge transfer capacitance and resistance are inversely proportional when there's a change in surface area or thickness. The cell 2's parameters in Fig. 4.12 show that the charge transfer RC-pairs are inversely proportional. This was however not observed in Fig. 4.11. The charge transfer resistance was increasing with cycling and the capacitance stayed constant. In other words, the SEI's growth was smaller with cycling for the cell A1 than in the cell 2. This mean that lithium had a rather constant access to the cell A1's electrode area with cycling, compared to the cell 2 with its decreasing capacitance (available electrode area).

The diffusion capacitance decreased with cycling, implying that there was a lower concentration gradient of lithium in the core, compared to the surface. It is possible that a growing SEI-layer prevents Li-ions from moving from the core to the surface. The restraint of Li-atoms could be an explanation for why the charge transfer resistance was increasing with cycles in the cell A1, while the capacitance was constant. For the charge transfer resistance to be constant as well, the same amount of lithium after delithiation had to be present during the charge transfer process, every cycle. The decline of available Li-atoms per cycle would cause an increased charge

transfer resistance per cycle, and probably is what was observed in Fig. 4.11.

In Fig. 4.11 and 4.12, an increase of total overpotential per cycle was observed, which is conformed to the measured relaxation voltage data in Fig. 4.6. Even though OCV behaves as expected per cycle, the model still failed to fit the final relaxation potential. In Fig. 4.8 and 4.9, none of the ocv-lines were accurate enough. The diffusion process was still occurring after 2 hours, thus the "ocv"-asymptote should be lower than what is shown in Fig. 4.8 and 4.9. In fact, some of the fitted "ocv"-asymptotes were above the last measured point, which is illogical because the OCV is defined as the equilibrium voltage.

The comparison between specific capacity and resistance in Fig. 4.13 demonstrates how the apparent resistance obtained from the fitting of OCV can be used to analyze the cell's cycle life. Both diffusion and charge transfer resistance increased with cycling (rise in polarization), indicating a decrease of stored charge capacity. Figure 4.13 shows that the capacity was indeed decreasing with the increase of resistance. Additionally, the cell 2's resistances had a bigger slope than the cell A1's. This corresponded with the faster decline of capacity for the cell 2. However the reason why the cell 2 seemed more stable during the initial 10 cycles could not be explained by the resistance.

Figure 4.13 points out that fitting of the OCV with `fitting_cell_ocv` and a reasonable cell model could be used as a tool for analyzing activities occurring after delithiation. The suggested model was not sufficient to predict a satisfying OCV value, nor did it give a sufficient fit of the charge transfer process during the first 50 seconds. To improve the estimation of best parameter values, an enhanced model based on more research and theory is endorsed. It is likely to obtain an improved result if a new RC-circuit is added to the cell model. This change could shift the charge transfer fit to the first 50 seconds. This could also have a positive effect on the fitted OCV, as it would indicate the diffusion process in a better way. The result would be an improved fit in the start and at the end of the measured relaxation period. Another suggestion is to add more boundaries for the parameter iteration.

4.2.3 After Lithiation

Cycles 10 and 25 were selected for comparison of the cell 2 with the cell A1. The program was unable to fit cycles 1, 4 and 5. According to Fig. 4.3, cycles 10 and 25 looked stable for both the cells 2 and A1. The fits were generated with `cellpy`'s `fitting_cell_ocv` program, developed in this thesis (listing A.1 and A.2 in appendix). The OCV fits with residuals are shown in Fig. 4.14 and 4.15. The charge transfer and diffusion processes were separated and graphed in Fig. 4.16 with Eq. (2.23).

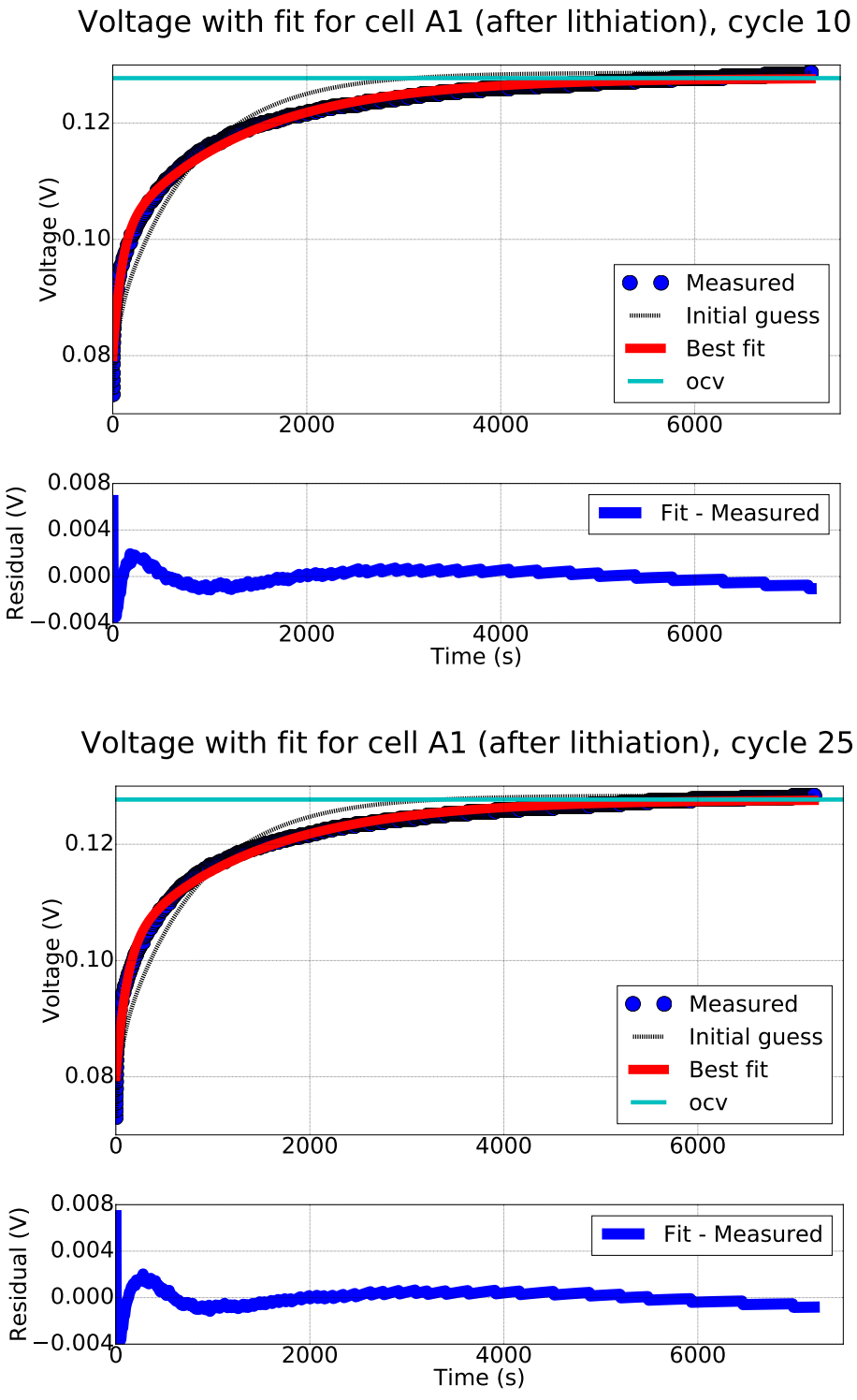

Figure 4.14: Fitted OCV-relaxation after lithiation for the cell A1, cycles 10 and 25. Generated with `cellpy`. The measurement accuracy was stated as 0.1 % of full scale range. The initial guess was plotted with Eq. (3.3). All initial guessed values were the best fitted parameters from the previous cycle. Lithiation current was 1/20 C-rate. IR-drop was excluded.

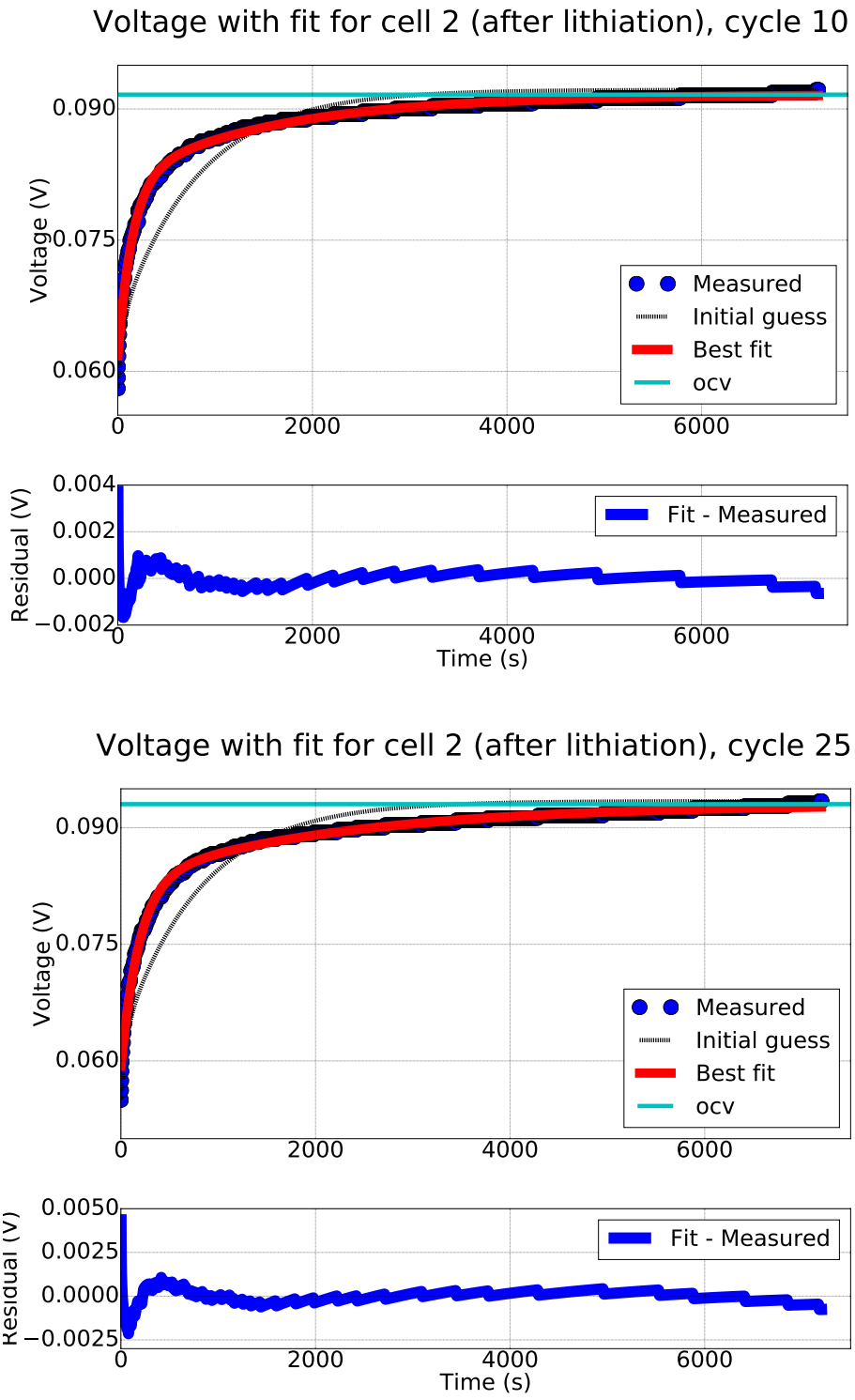

Figure 4.15: Fitted OCV-relaxation after lithiation for the cell 2, cycles 10 and 25. Generated with `cellpy`. The measurement accuracy was stated as 0.1 % of full scale range. The initial guess was plotted with Eq. (3.3). All initial guessed values were the best fitted parameters from the previous cycle. Lithiation current was 1/20 C-rate. IR-drop was excluded.

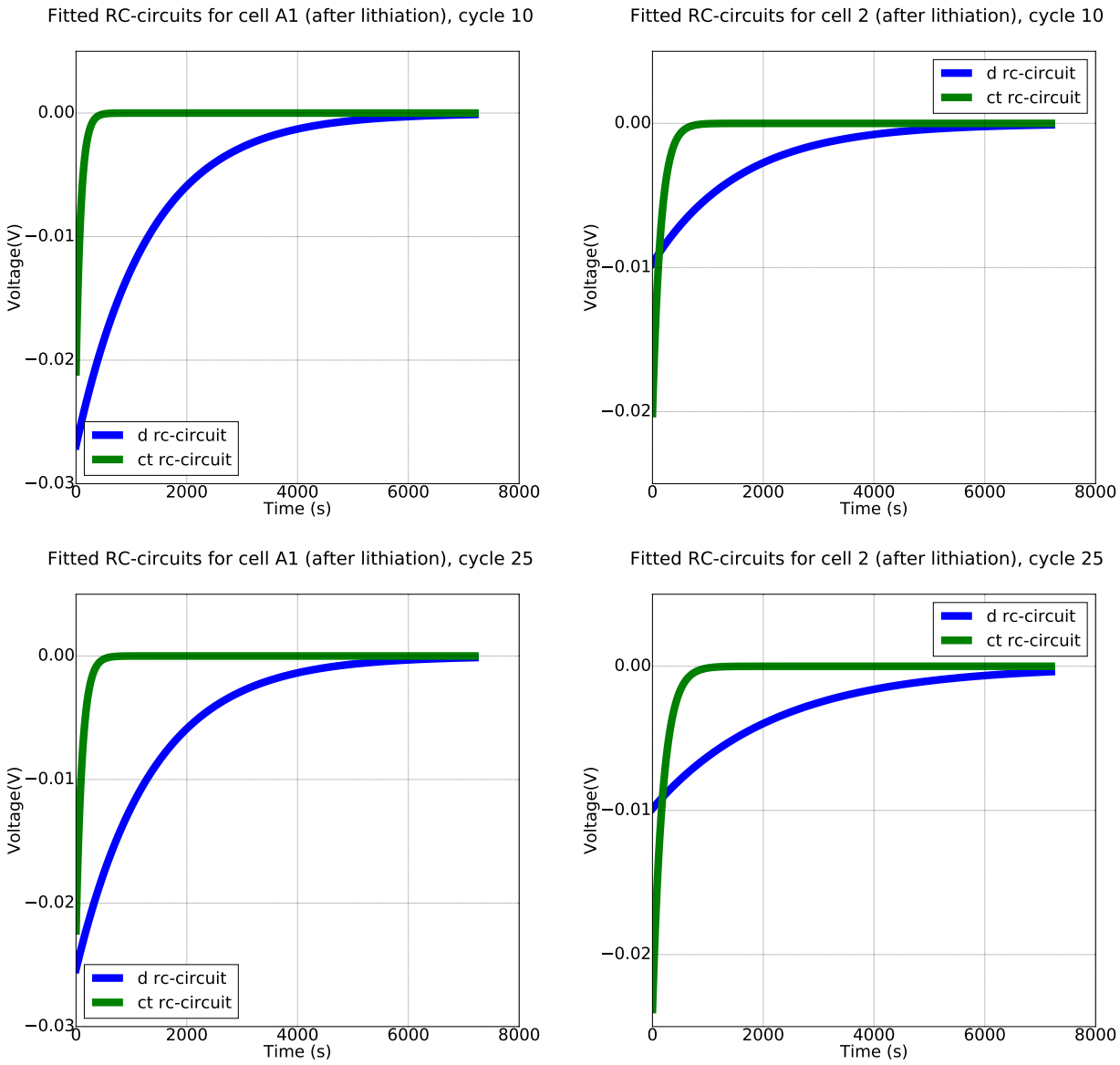

Figure 4.16: RC-circuits for cells A1 and 2 after lithiation for cycles 10 and 25. d and ct RC-circuit stands for diffusion and charge transfer. Both graphs were plotted with the fitting results from `cellpy` and Eq. (2.23). ct- and d-RC-circuits are both decaying towards OCV. d and ct decay towards zero in this graph because OCV was the reference. Lithiation current was 1/20 C-rate.

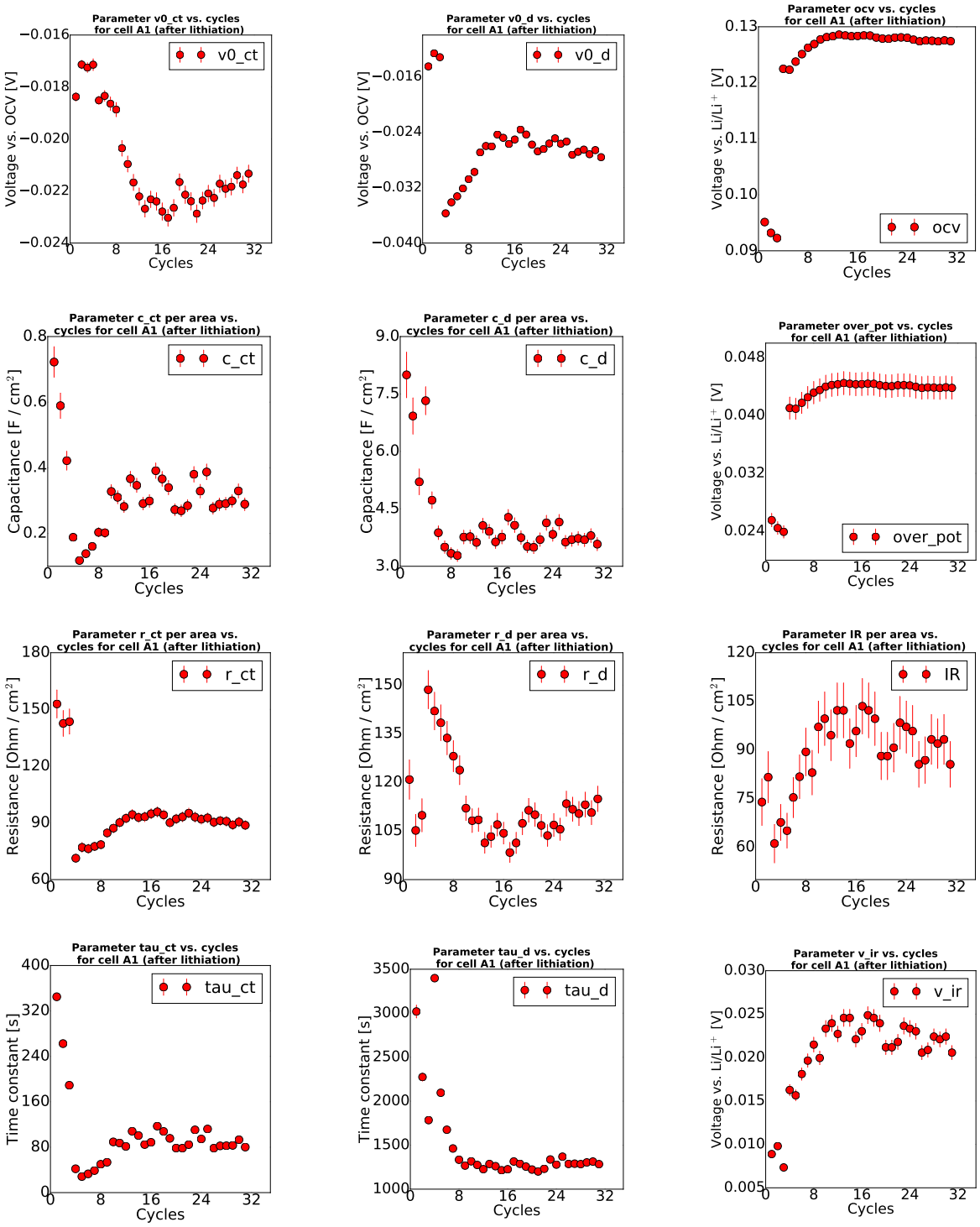

Figure 4.17: Fitted parameters vs. cycling for A1 after lithiation. "tau_d", "tau_ct", "v0_d", "v0_ct" and "ocv" were fitted by lmfit, and their errors are the standard deviation, calculated by the least square minimization. "over_pot" is the magnitude of the total overpotential in the cell, calculated with ocv subtracted from the cut-off voltage. "ct" and "d" are the charge transfer and diffusion. "tau" represents the time constant (τ). "r" and "c" are the resistance and capacitance, while "IR" is the internal resistance. Resistance, capacitance and IR are per area of the 1.5 cm diameter disk.

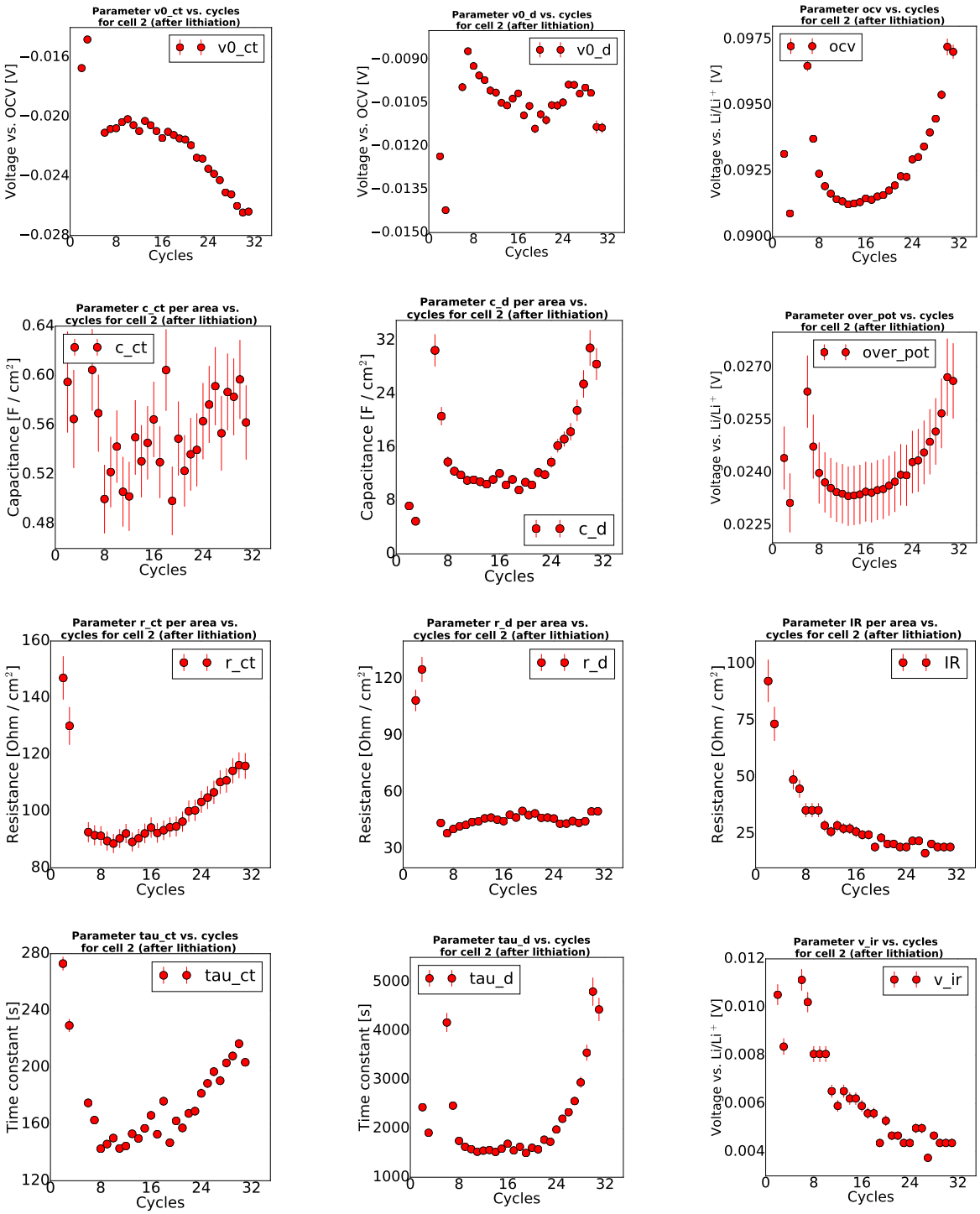

Figure 4.18: Change in fitted parameters with cycling for the cell 2 after lithiation. Cycles 1, 4 and 5 were excluded from the plots because of failed fitting. "tau_d", "tau_ct", "v0_d", "v0_ct" and "ocv" were fitted by lmfit, and their errors are the standard deviation, calculated by the least square minimization. "over_pot" is the magnitude of the total overpotential in the cell, calculated with "ocv" subtracted from the cut-off voltage. "ct" and "d" are the charge transfer and diffusion. "tau" represents the time constant (τ). "r" and "c" are the resistance and capacitance. "IR" is the internal resistance. Resistance, capacitance and IR are per area of the 1.5 cm diameter disk.

4.2.4 Evaluation of Fitted Parameters After Lithiation

The fits in Fig. 4.14 and 4.15 have low residuals during most of the relaxation period, but failed to fit the first 10-50 seconds. Additionally, the "ocv"-asymptote was too low. The voltage was not fully relaxed after 2 hours, yet the ocv-line in Fig. 4.14 and 4.15 was very close to, occasionally below, the last measured point. The program failed to iterate a satisfying estimation of the OCV after lithiation. However, the reason for a poorly-estimated OCV could be because of the reaction occurring about 0.09 V.

When analyzing the individual processes for cycle 10 and 25 in Fig. 4.16, the ratio between the charge transfer process and diffusion process for the cell A1 was rather constant, but not for the cell 2. The rate of diffusion process slowed down significantly more from cycles 10 to 25 than the charge transfer process. This is more visible in Fig. 4.17 and 4.18.

According to Fig. 4.18, the cell 2's time constant for diffusion increased rapidly compared to the charge transfer process. The exponential increase in duration of the diffusion process after cycle ~22 was, according to the fit, caused by the exponential growth of the diffusion capacitance. The diffusion capacitance can be interpreted as the Li-concentration gradient between the electrode's surface and core. The diffusion capacitance in Fig. 4.18 suggests that there was either an increase of lithium at the surface or decline of lithium in the core, or perhaps a combination of both. Nevertheless, the cell 2's diffusion overpotential and resistance looked less affected by the increase of capacitance.

The charge transfer capacitance of the cell 2 was somewhat constant with cycling, but the charge transfer resistance was increasing. This can most likely be explained by the growing SEI, blocking Li-ions from entering the electrode surface. The growing SEI-layer could also explain the increase of diffusion capacitance. The SEI restrained lithium diffusion and thus decreased the amount of lithium reaching the core.

The cell A1's parameters in Fig. 4.17 show a different behavior than the cell 2. During cycles 4 to 10, the charge transfer resistance increased, while the diffusion resistance decreased. The IR was also increasing during these cycles. The apparent parameters in Fig. 4.17 suggest that the cell was still undergoing a SEI-formation until cycle 10. However, the processes capacitances' were proportional to the increase in their corresponding resistance. This was unexpected when considering the equations (2.12) and (2.14). If an SEI was still being constructed, the charge

transfer capacitance was likely to decrease instead. The electrode thickness would increase with the formation of SEI, causing a decrease of capacitance. The parameter behaviors in Fig. 4.17 suggest a greater increase in active material's surface area instead of a rise in SEI thickness. This was probably caused by the unknown processes happening about 0.09 V.

Furthermore Fig. 4.17 indicates that the reaction occurring around 0.09 V stabilized after 7 to 8 cycles. To support this theory, notice that the last cycle's parameter values in Fig. 4.18 did not change as much compared to the previous 7-10 cycles. Figure 4.17 indicates that a material changed, and caused a larger overpotential after lithiation. As this was happening with all the cells after lithiation, it is not likely that the additives played a major role of this process - implying that it was probably the silicon, binders, carbon or Li-metal cathode which reacted about 0.09 V. Nonetheless, the information from the fitted parameters was not sufficient to make a valid conclusion regarding the reaction at 0.09 V.

A comparison between capacity and resistances per cycle was not displayed in this subsection because of the issues regarding 0.09 V. Further studies are recommended to investigate the correlation between capacity and fitted resistances after lithiation for the cell with and without additives. It could clarify why the capacity was more stable for the cell 2 than for the cell A1 during the first 8 cycles.

4.3 Electrochemical Impedance Spectroscopy Results

EIS experiments were performed on the cell EA from table 3.2. The cell's electrolyte included additives and was initially lithiated with 1/20 C-rate, then cycled with 1/10 C. Bio-Logic's cycle routines are shown in Fig. 3.6. The EIS results after delithiation and lithiation for cycle 1 and 9 are displayed as Nyquist plots in Fig. 4.19 and 4.20. When an EIS analysis after delithiation and lithiation is mentioned in this text, it refers to the EIS performed after the final OCV-relaxation (after cut-off voltage).

The frequency range of the EIS was 10 kHz to 10 mHz. Frequencies lower than 1 Hz after delithiation in Fig. 4.19 and 4.20 were not included because a Warburg impedance was observed for lower frequencies than 1 Hz. It was assumed that the diffusion process was included in the Warburg impedance.

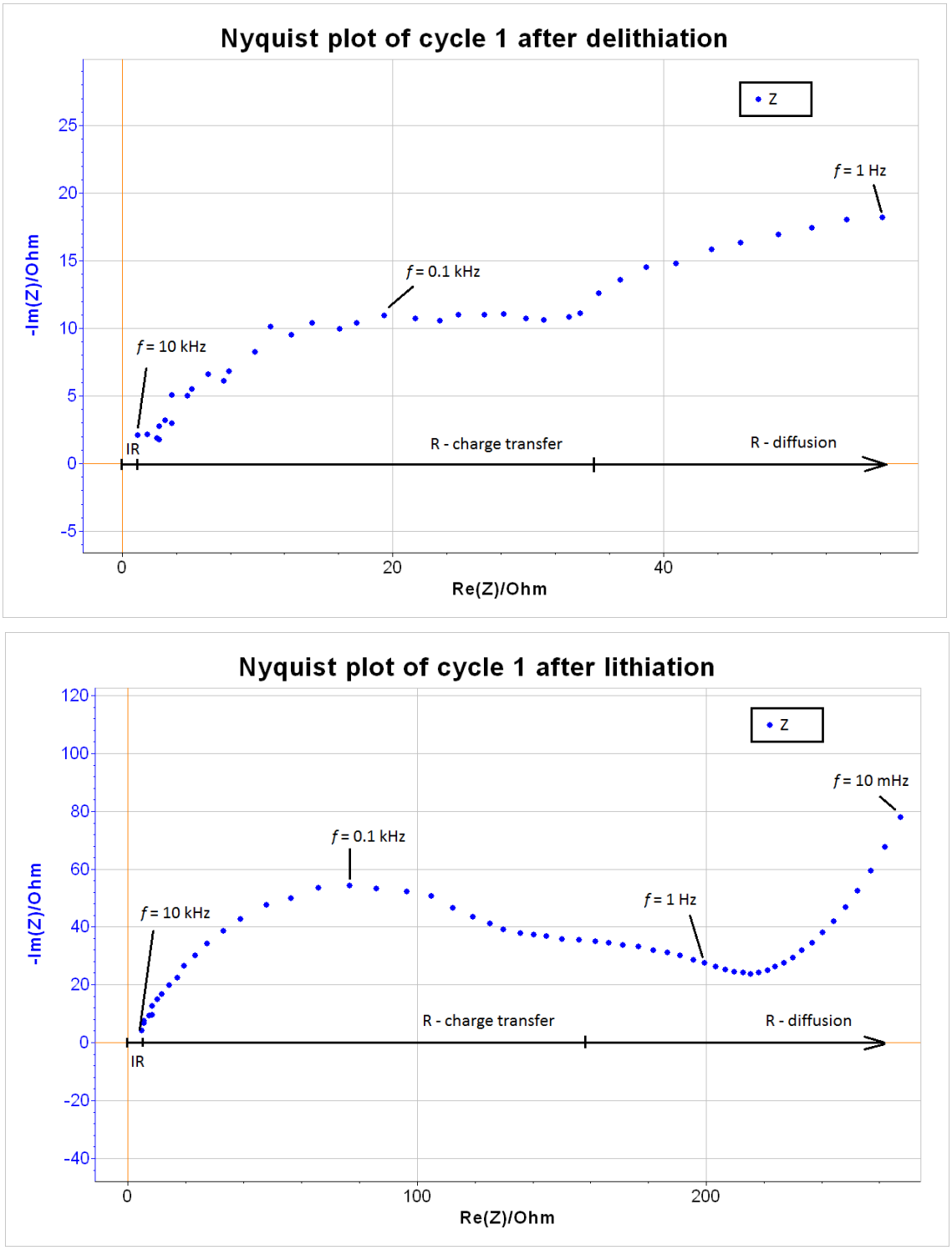

Figure 4.19: Nyquist plot of EIS data from cycle 1 for cell EA, after delithiation and lithiation. R = resistance, IR = internal resistance, f = frequency, Z = impedance from EIS.

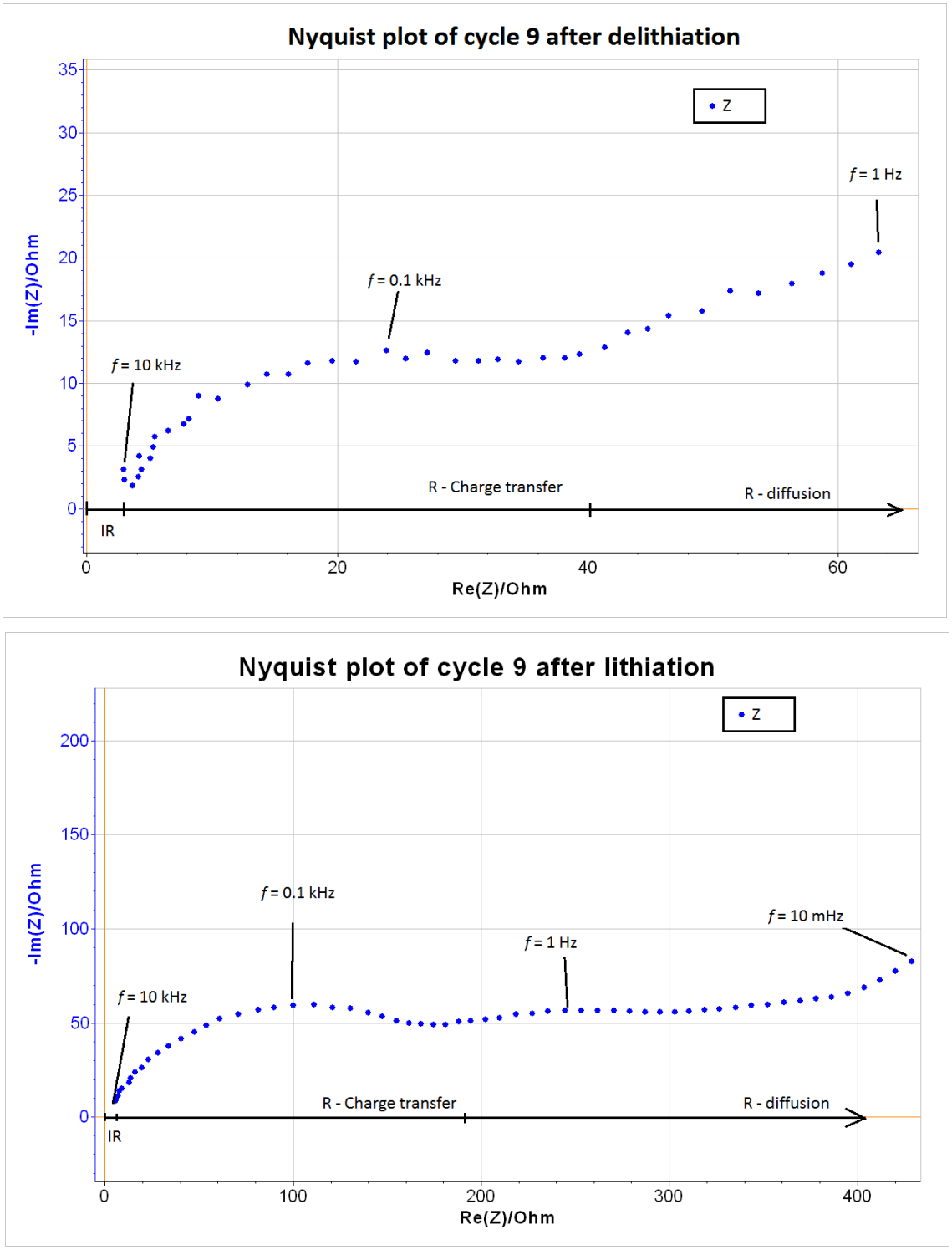

Figure 4.20: Nyquist plot of EIS data from cycle 9 for cell EA, after delithiation and lithiation. R = resistance, IR = internal resistance, f = frequency, Z = impedance from EIS.

The IR values from every cycle were graphically read from Nyquist plots like the ones in Fig. 4.19 and 4.20. The IR values were plotted in Fig. 4.21. All RC-parameters were also graphically read from the Nyquist plots for every EIS after delithiation and lithiation. The first semicircle in Fig. 4.19 and 4.20 was presumed to be the charge transfer process. The second semicircle was somewhat problematic to extract graphically from the Nyquist. Thus only the charge transfer parameters were extracted from the Nyquist plots and displayed in Fig. 4.22. The resistance is the semicircle's diameter. The capacitance was calculated with Eq. (3.8) by reading the maximum radial frequency of the semicircle (see subsection 3.3.2, page 46). All parameters shown in Fig. 4.21 and 4.22 are per electrode area (1.5 cm in diameter).

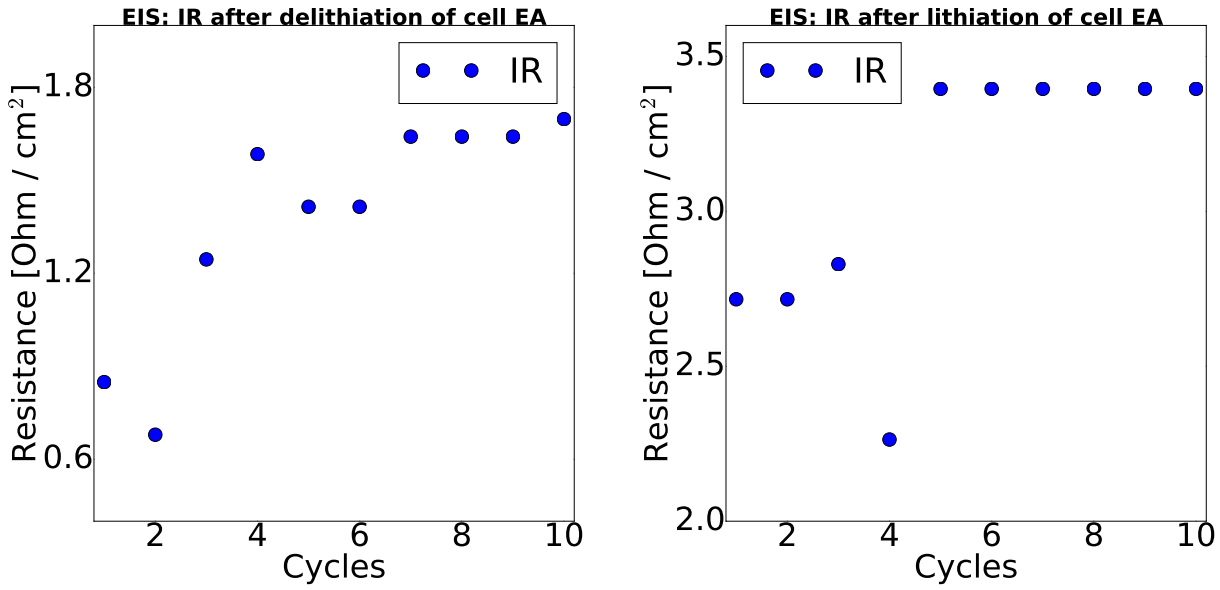

Figure 4.21: Internal resistance from the EIS study after delithiation and lithiation. The values were read graphically. The IR are per disk area. The EA cell's electrode disk had a diameter of 1.5 cm.

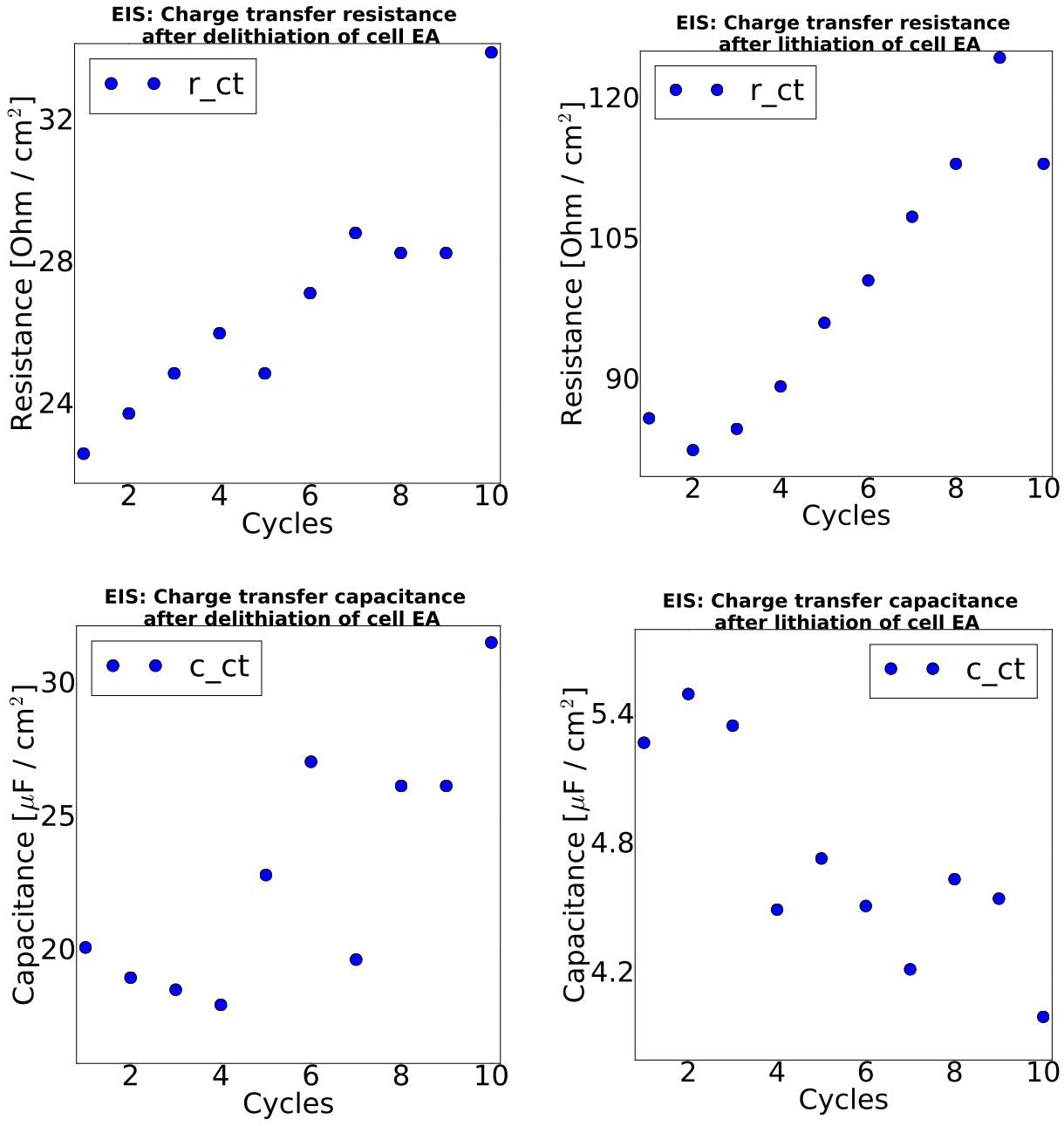

Figure 4.22: Resistance and capacitance from the EIS study after delithiation and lithiation. The RC-parameters are per disk area. The EA cell's electrode disk had a diameter of 1.5 cm.

4.3.1 Discussion of EIS

One semicircle in a Nyquist plot represents the time constant of a process. The cell model proposed in this thesis had two RC-circuits (two time constants). Two semicircles were therefore expected to be observed in a Nyquist plot of the EIS results. It was also assumed that the diffusion process was slower than the charge transfer, hence the diffusion process should be a bigger semicircle in a Nyquist plot. Two time constants were recognized in Fig. 4.19 and 4.20. However, one of these two was probably not the diffusion process, because it was assumed that the diffusion was in the Warburg impedance and could not be easily interpreted from the EIS study. The size of the charge transfer semicircle did not show a distinct increase from cycles 1 to 9, but the second semicircle increased with cycling.

The first lithiation process was operating at a 1/20 C-rate, and its EIS result was expected to look different from the other cycles. As seen in Fig. 4.19 and 4.20, there was a difference between cycles 1 and 9 after lithiation, but it was fairly small. The first cycle show a slight indication of a second semicircle after the charge transfer, before the Warburg. A second semicircle was also observed after lithiation in cycle 9, but larger than the one observed in the first cycle. The second semicircle was smaller than the charge transfer. It is possible that this semicircle could represent the impedance of the SEI layer. The second semicircle also grew with cycling, indicating that the SEI layer was increasing in size. If the second semicircle after lithiation was in fact the SEI layer, it is possible that the second semicircle observed after delithiation (around 1 Hz) was also the SEI layer.

Figure 4.21 indicates that the IR was slightly increasing with cycling up to cycle 5, then stayed constant. It was expected to see an increase of the charge transfer resistance in Fig. 4.22 because of the presumed increase of SEI-layer's thickness with cycling. The capacitance decreased after lithiation, but the capacitance after delithiation in Fig. 4.22 was increasing with cycling.

4.4 Correlation between EIS and Fitted Parameters

A focus in this study was to check correlation between an electrochemical impedance spectroscopy (EIS) and the parameters obtained from fitting OCV-relaxation data. Table 3.2 show that the mass of A1 and EA only differed with 1 μg. Additionally, both cells included additives in their electrolyte solutions. A1 was therefore chosen as the comparing cell to EA.

4.4.1 Lithiation

The fitted charge transfer resistance after lithiation in Fig. 4.17 and the charge transfer resistance from EIS after lithiation in Fig. 4.22 are displayed together in Fig. 4.23.

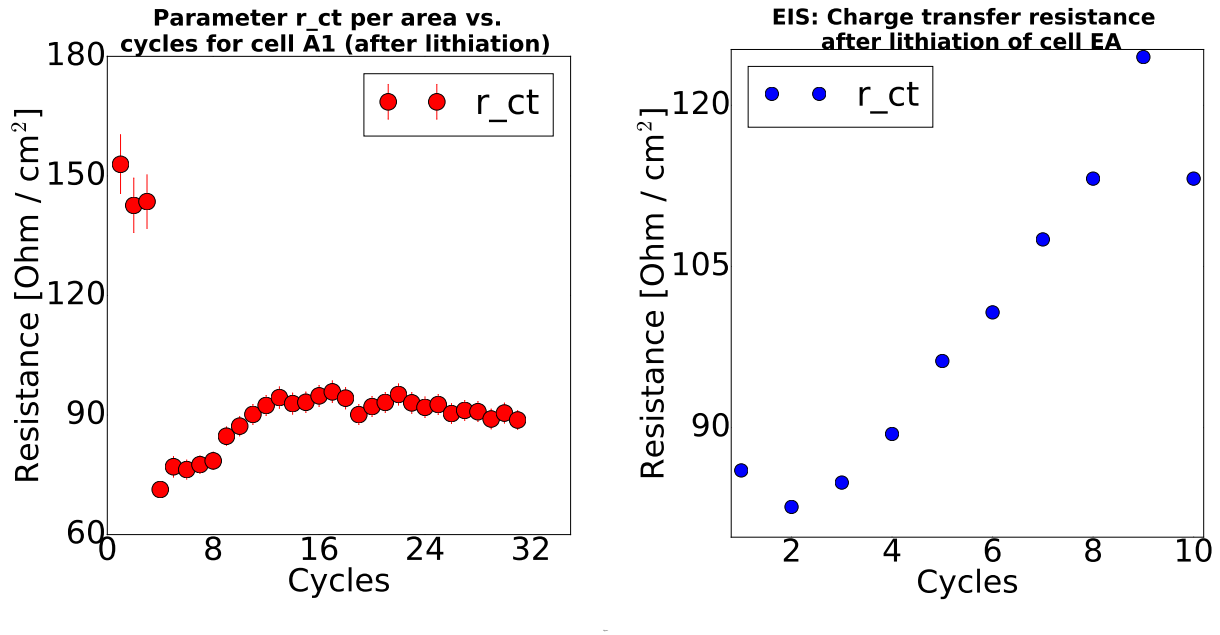

Figure 4.23: Correlation between resistances per cycle, after lithiation for the cell A1 and EA. r_ct = charge transfer resistance.

A1's charge transfer resistance increased from cycle 4 until cycle ~ 13. The C-rate from cycle 4 was C/10, same as the cell EA's C-rate from cycle 2. The EIS cell's charge transfer resistance also increased for 8 number of cycles. The cell EA had a larger resistance than A1. This could be explained by the fact that the cell EA was cycled in a room temperature environment, while the A1 cell had a fixed temperature of 30°C. A lower cell temperature should in theory increase the resistance in the cell, because the conductivity in Eq. (2.14) is temperature-dependent. The correlations between charge transfer resistances after lithiation for OCV fitted data and the EIS

study are therefore considered adequate. The fitted charge transfer and EIS capacitance are show in Fig. 4.24.

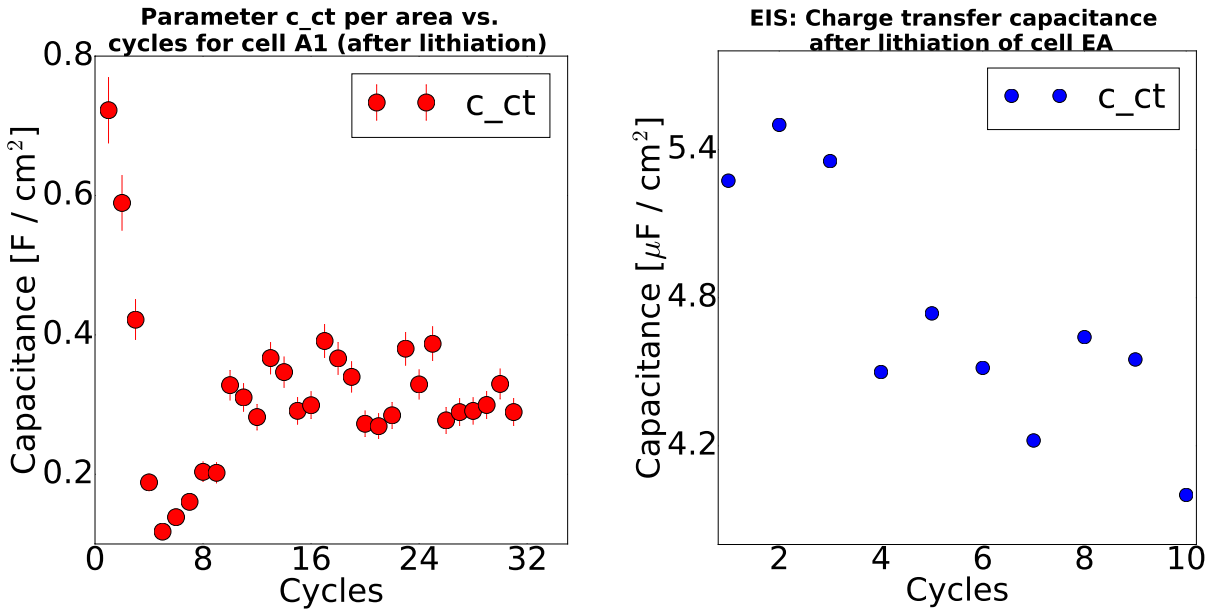

Figure 4.24: Comparison between fitted and EIS charge transfer capacitance (c_ct) after lithiation.

Although the charge transfer resistances after lithiation had a satisfying correlation, their capacitance did not compare sufficiently. The fitted capacitance differed from the EIS capacitance with a factor of 10,000. Additionally the capacitances were inversely proportional to each other. It can therefore be concluded that the charge transfer capacitance after lithiation from OCV fitted data, and the EIS results, are not comparable.

4.4.2 Delithiation

Figure 4.25 is a comparison between EIS and fitted RC-parameters after delithiation.

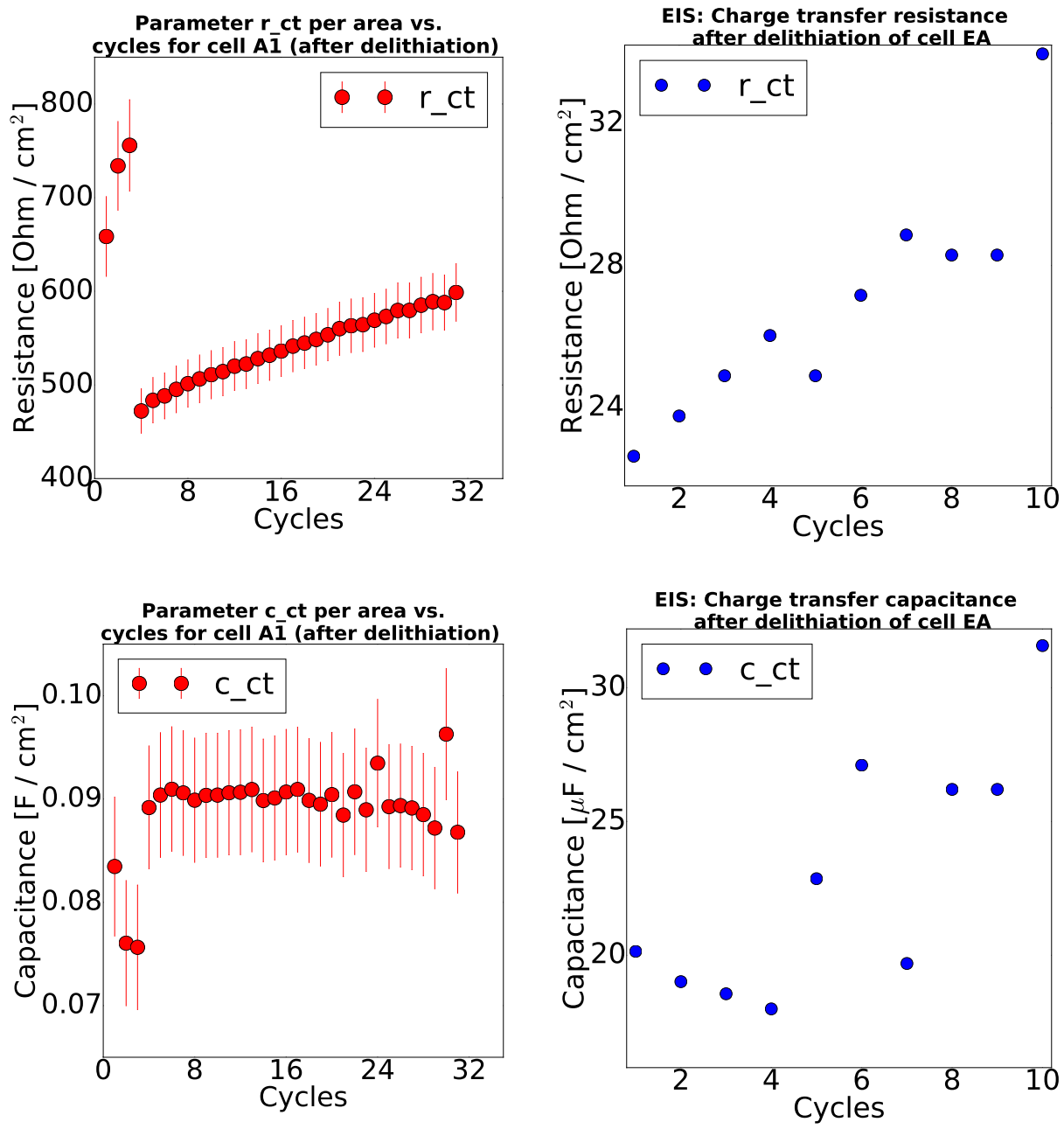

Figure 4.25: The cells A1 and EA's charge transfer RC-parameters after delithiation. The parameters are per electrode area (1.5 cm diameter). r_ct = charge transfer resistance, c_ct = charge transfer capacitance.

Charge transfer resistance found by fitting OCV data increased with cycling, just like the ones

from the EIS study, but their values were not alike. The fitted resistance was 20 times higher than the EIS results. The fitted charge transfer resistance was similar to the fitted diffusion resistance in Fig. 4.11, although a lower resistance than the diffusion process was expected. The capacitance in Fig. 4.25 shows non-correlating values or patterns. The fitted capacitance's and resistance's values after delithiation show a discrepancy between the fitted parameters and EIS results - though the resistances' increasing patterns had a decent correlation.

Figure 4.26 is the figure from page 75 (Fig. 4.13), but includes the EIS charge transfer resistance.

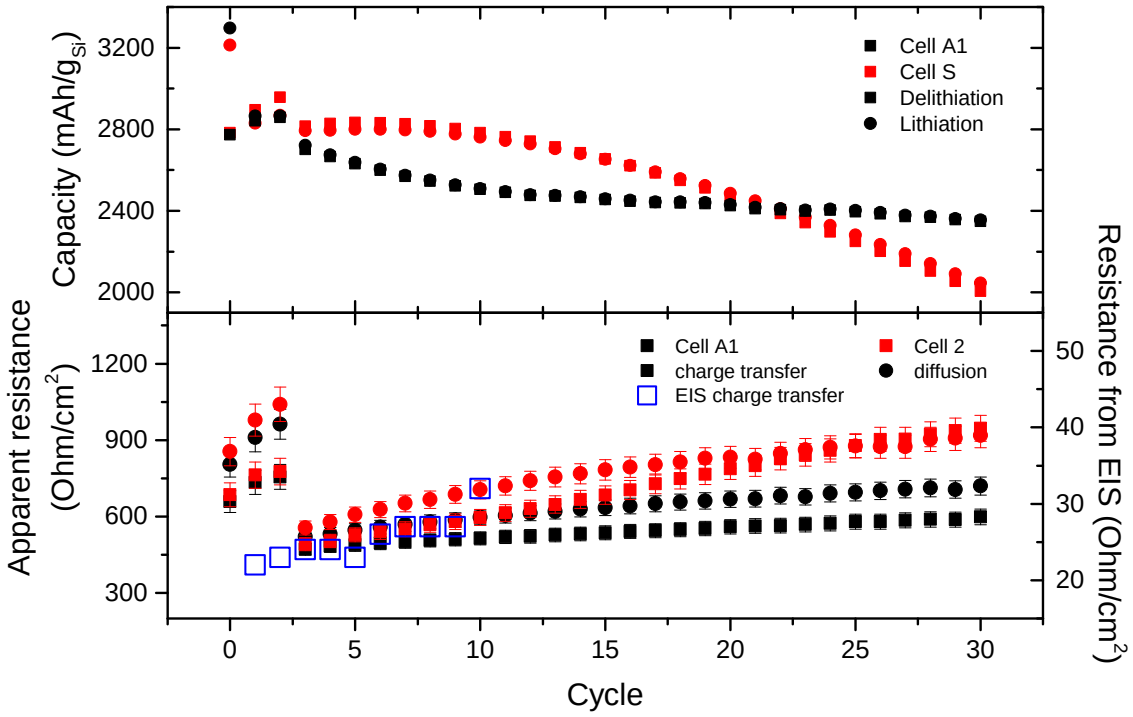

Figure 4.26: Comprehensive comparison of cycle life patterns with fitted parameters and EIS study. Black color indicates the A1 cell. The cells A1 and 2 starts at cycle 0, while the data obtained from EIS start at cycle 1. Alteration of 1 cycle to the right for the cells A1 and 2 has to be considered when comparing cell A1 and 2 with EIS.

Even though the EA cell had few cycles, compared to the other cells, those cycles showed a close correlation with the fitted resistances of the cell 2. Nonetheless, the cell 2 did not include additives in its electrolyte, while the EIS cell did. A possible explanation could be the difference in temperature. The cell A1 had a higher temperature than EA, thus the electrode material should have a higher ionic and electric conductivity, decreasing the resistance in the material. It is not

unlikely that the charge transfer resistance obtained from EIS on the cell EA (in room temperature) should've indeed increased faster than the A1 cell. From Fig. 4.26 it can be concluded that the charge transfer resistance obtained from fitting OCV data has a satisfying correlation with the EIS charge transfer resistance.

A difference in IR values calculated with Ohm's law (Eq. (2.15)) and IR obtained from the EIS study can be observed in Fig. 4.27. However, their cycle patterns looked comparable and stable after a few cycles. The cells' IR was therefore not a major reason for the decrease in capacity per cycle, seen in Fig. 4.26. This fortifies the charge transfer resistance's influence on the cell's cycle life.

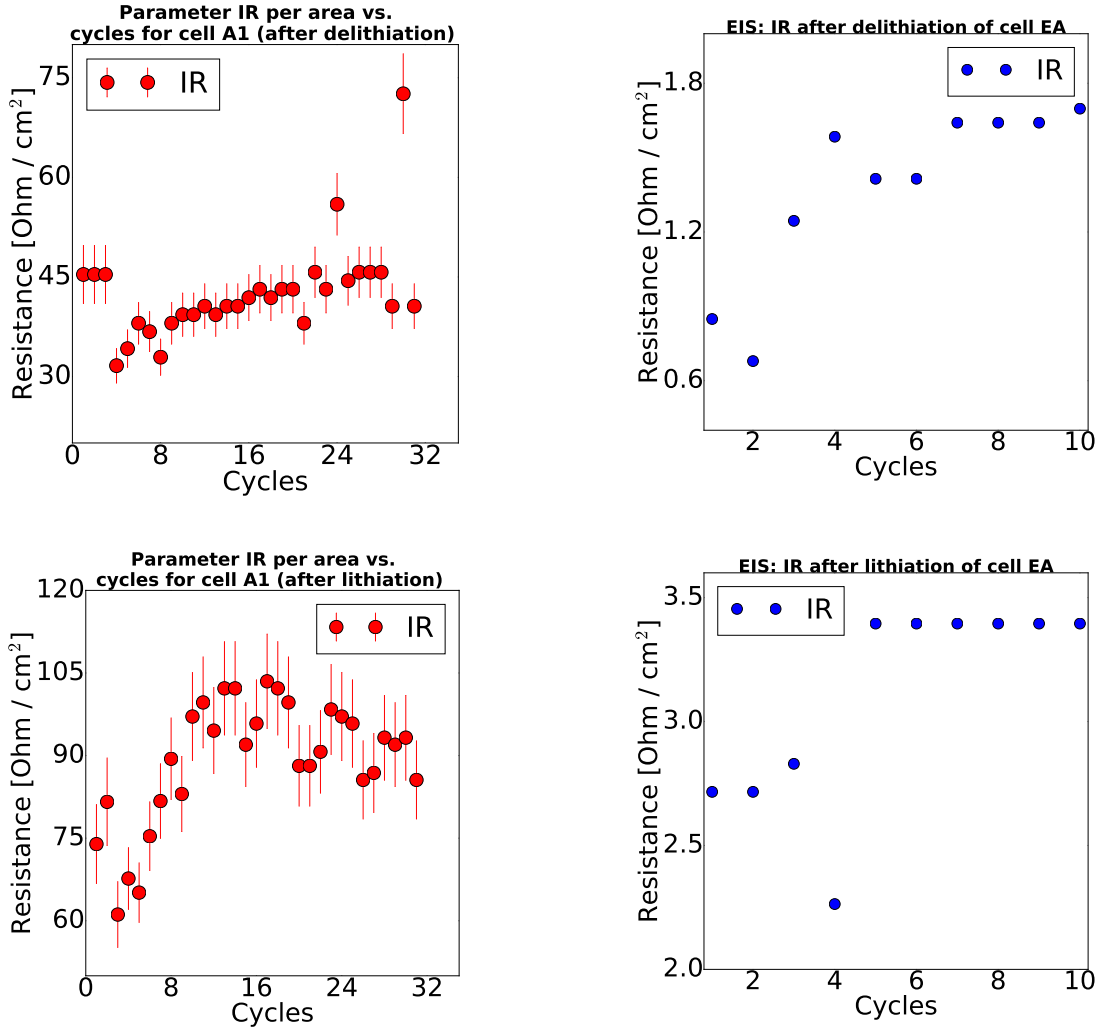

Figure 4.27: Comparison between IR for the cells A1 and EA. IR from A1 was calculated with Ohm's law (Eq. (2.15)). IR from EA was graphically extracted from Nyquist plots of the EIS results.

4.5 Summary and General Discussion

The relaxation models in Fig. 4.5 and 4.7 was derived from analysis of Arbin's OCV-relaxation data after delithiation and lithiation. The proposed model for after delithiation (Fig. 4.7) seemed reasonable with the recognized patterns from the fitted parameters in subsection 4.2.1. However, it was difficult to explain the proposed model in Fig. 4.5 with the fitted parameters after lithiation.

The program was not able to fit the first 50 seconds with the proposed cell model. This could be because of an insufficient cell model. Adding one more RC-circuit was suggested. Bugs in the program could also cause the poor fit during the first 50 seconds. In general, when writing a new program, tests are necessary to ensure that the program is working as it should. Unfortunately, no tests were produced for the program developed in this thesis. The program contains more than 1600 lines of codings, but none of them were tested. It can not be guaranteed that all the choices made during development of the program were properly thought-out. The absence of tests reduces the quality of the program's results.

Nonetheless, the results and discussions presented in this chapter show that it was possible to make sense from the program's fits of OCV-relaxation after delithiation, and could be useful for further research. However, it was somewhat difficult to find meaning in the relaxation fits, after lithiation. This was probably because the model was not designed to explain the presence of a new reaction during the open circuit-relaxation. The unexpected process after lithiation happened at around 0.09 V. It was observed in Fig. 4.17 that the reaction stabilized after ~6~9 cycles.

Besides the inability to fit some of the parameters of the OCV-relaxation after lithiation, the program was useful for analyzing the parameter changes over cycling. It was unexpected to see that both the resistance and capacitance of the charge transfer process increased, while the diffusion resistance and capacitance decreased with cycles where the potential was above 0.09 V after lithiation. From analyzing the fits in subsection 4.2.3, it appeared as if a structural change in the cell's materials was causing the unexpected behavior at about 0.09 V. Further studies are needed in order to conclude what the activities at about 0.09 V were.

Section 4.3 revealed that the EIS parameter's values did not correlate well with the fitted parameters, except from the charge transfer resistance after lithiation. The EIS study revealed two

time constants, which strengthen the proposed cell model in section 3.2. However, it also looked like the diffusion process was not observed in the Nyquist plot. The second semicircle observed in the Nyquist plots could be a diffusion process through the SEI layer. If this was the case, the cell model would not be two RC-circuits, but three instead. The inclusion of an additional RC-circuit could improve the fitting of the OCV-relaxation.

Figure 4.26 confirmed that the change in resistances had an adequate correlation with the cell's cycle life, and the EIS study uphold this observation. The fitted resistances could therefore be used to explain the capacity fade per cycle. In addition, the IR-drop found by using Ohm's law and the IR found from EIS did not compare in value, but had a similar pattern. The IR was rather constant with cycling, hence it did not affect the capacity fade, but instead supported the program's results.

Chapter 5

Conclusion

Polarization activities in a cell have been analyzed through fitting a cell model's relaxation voltage to the measured open circuit voltage (OCV)-relaxation data. Test cells were made (some with an improved electrolyte) and cycled with an Arbin BT2000 instrument. The proposed cell model was based on the Randles circuit and previous studies on equivalent circuits for a cell. The fitting procedure was made in Python for the package, `cellpy`. To validate the method developed in this thesis, an electrochemical impedance spectroscopy (EIS) was performed on a cell with improved electrolyte to compare with the fitted parameters.

The illustrations in Fig. 4.7 and 4.5 proposed an interpretation of the relaxation process after delithiation and lithiation. The figures were derived through analyzing Arbin's OCV-relaxation data. The analysis of the fitted parameters revealed an SEI formation during cycling. The fit was also useful to interpret an unpredicted activity, occurring about 0.09 V during OCV-relaxation after lithiation. However, it was disappointing to see that the fitted OCV value did not suit the fully relaxed voltage (OCV). The cell model was also unable to fit the first 50 seconds of the relaxation process. The charge transfer resistance acquired from the EIS study was compared with the fitted resistances and the cell's cycle life in Fig. 5.1.

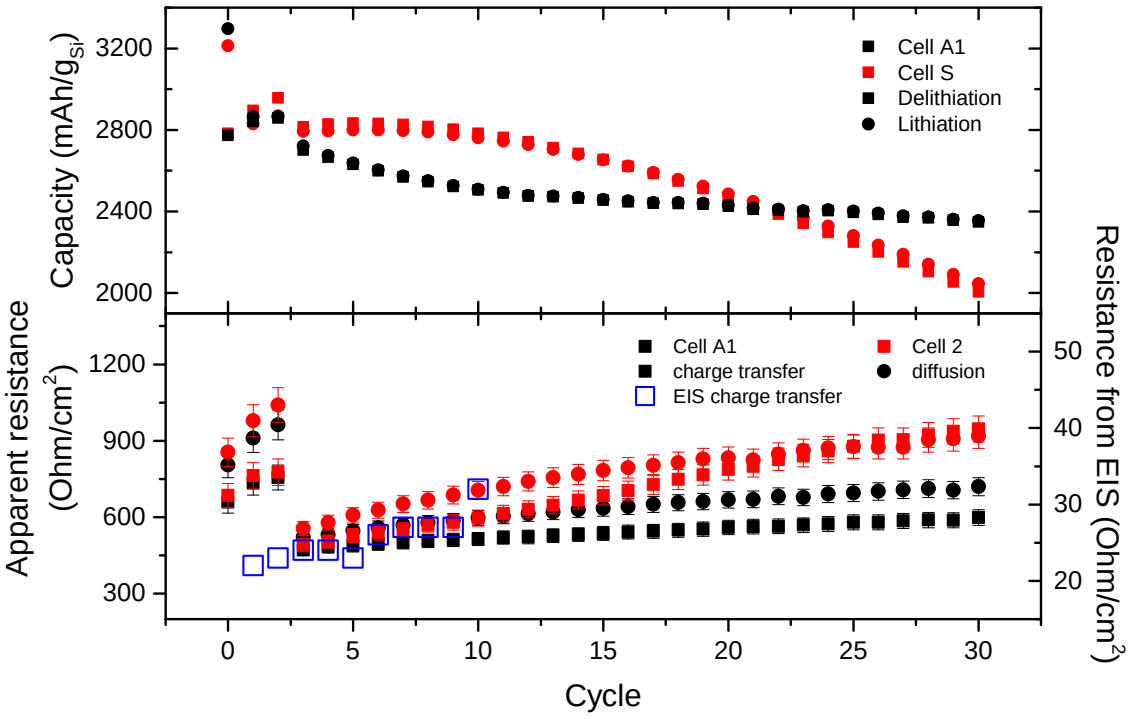

Figure 5.1: Cycle pattern of OCV fitted resistances for cell A1 and 2 after delithiation, compared with EIS charge transfer resistance and capacity. Black indicates cell A1 (with additives in electrolyte).

Figure 5.1 suggests a satisfying correlation between the cycle pattern of OCV charge transfer resistance and EIS-obtained charge transfer resistance after delithiation. However, the values of their charge transfer resistances and capacitances did not compare. The fitted charge transfer resistances after lithiation and the ones found from the EIS study had an adequate correlation in both values and cycle pattern. Nevertheless, the capacitance values after lithiation differed with a factor of 10,000, and no comparable cycle pattern was observed. The EIS IR values and calculated IR did not match, but their cycle patterns had a sufficient correlation.

Although the apparent parameter values did not compare with the impedance found in the EIS study, their charge transfer resistance patterns had an adequate correlation. Figure 5.1 supports the program's utility for cycle life analysis. Based on the results and discussions, the method developed in this thesis was concluded to be useful in analyzing the material behaviors regarding the charge transfer process. Further studies are necessary for additional utilization of the program.

Chapter 6

Further Studies

In subsection 4.1.1, the effect of storing a cell for a longer period before initial lithiation was investigated. The stored cell had 50 % lower capacity than expected capacity (from theoretical value), while the other cells had 20-35 % lower capacity. This indicated that the storage reduced the cell's capacity compared to younger cells. Nevertheless, the stored cell (cell S) was more stable with cycling, compared to the cell (cell 2) that was not stored and without additives. Further investigation on how storage of cells with and without additives affect the cells cycle life and performance is suggested.

The derived cell model in this thesis used existing theory, earlier studies and rough calculations. However, the results showed that the model was not sufficient for a good fit of the first 50 seconds of the OCV-relaxation. The fitted charge transfer process appeared as if it included an other process that was not accounted for. To improve the fit, a new RC-circuit was proposed with a guessed time constant of ~100 seconds. In addition, the guessed charge transfer time constant should be decreased to 10 seconds. Testing the program with different models and compare them with other experiments is recommended.

Further investigation of how to fully utilize the apparent resistance and capacitance acquired from the fitting process is urged. For instance, use Eq. (2.12) and (2.14) to find the dielectric constant (ϵ) and conductivity (κ), and compare these with the material properties of the compounds in the cell. If the program's fit and EIS result (or other methods) have a solid correlation, the calculation of ϵ and κ could help uncover materials presence during different situations. Conducting other studies with various charge and discharge techniques are also endorsed. Some examples are: using different C-rates, changing the temperature, performing galvenostatic intermittent titration technique (GITT) or potentiostatic intermittent titration technique (PITT).

The program was written by an engineer, and not a computer programmer, thus is a revision of the program advised. Implementation of unit- and integration tests of the program could help discover important bugs and flaws. For a better user interface, the program should be even more generalized and optimized. Making a graphical user interface that could show, alter and save plots of fitted results could be of great help for scientist with little programming experience. Additionally, combining experimental results (EIS) with an OCV-fit, and compute the statistical correlation between the measured and fitted results would improve `cellpy`'s benefits. Furthermore should a successful integration of lmfit's confidential interval be built in to the fitting process. This would make it easier to validate the covariance calculated by the minimization method.

Bibliography

[1] Erik J. Berg et al. 'Rechargeable Batteries: Grasping for the Limits of Chemistry'. In: *Journal of The Electrochemical Society* 162.14 (2015), A2468–A2475. DOI: 10.1149/2.0081514jes. URL: http://dx.doi.org/10.1149/2.0081514jes.

[2] Bruno Scrosati. 'History of lithium batteries'. In: *Journal of Solid State Electrochemistry* 15.7 (2011), pp. 1623–1630. ISSN: 1433-0768. DOI: 10.1007/s10008-011-1386-8. URL: http://dx.doi.org/10.1007/s10008-011-1386-8.

[3] Timothy D Bogart, Aaron M Chockla and Brian A Korgel. 'High capacity lithium ion battery anodes of silicon and germanium'. In: *Current Opinion in Chemical Engineering* 2.3 (2013), pp. 286–293. DOI: 10.1016/j.coche.2013.07.001. URL: http://dx.doi.org/10.1016/j.coche.2013.07.001.

[4] Naoki Nitta et al. 'Li-ion battery materials: present and future'. In: *Materials Today* 18.5 (June 2015), pp. 252–264. DOI: 10.1016/j.mattod.2014.10.040. URL: http://dx.doi.org/10.1016/j.mattod.2014.10.040.

[5] Fei Luo et al. 'Review - Nano-Silicon/Carbon Composite Anode Materials Towards Practical Application for Next Generation Li-Ion Batteries'. In: *Journal of The Electrochemical Society* 162.14 (2015), A2509–A2528. DOI: 10.1149/2.0131514jes. URL: http://dx.doi.org/10.1149/2.0131514jes.

[6] Y. Oumellal et al. 'The failure mechanism of nano-sized Si-based negative electrodes for lithium ion batteries'. In: *Journal of Materials Chemistry* 21.17 (2011), p. 6201. DOI: 10.1039/c1jm10213c. URL: http://dx.doi.org/10.1039/c1jm10213c.

[7] J. Vetter et al. 'Ageing mechanisms in lithium-ion batteries'. In: *Journal of Power Sources* 147.1–2 (2005), pp. 269–281. ISSN: 0378-7753. DOI: http://dx.doi.org/10.1016/j.jpowsour.2005.01.006. URL: http://www.sciencedirect.com/science/article/pii/S0378775305000832.

[8] T.R. Crompton. *Battery Reference Book*. Electronics & Electrical. Newnes, 2000. ISBN: 9780750646253. URL: https://books.google.no/books?id=q58IX4BM7-0C.

[9] R. Dell, D.A.J. Rand and Royal Society of Chemistry (Great Britain). *Understanding Batteries*. RSC paperbacks. Royal Society Of Chemistry, 2001. ISBN: 9780854046058. URL: https://books.google.no/books?id=-VJg6gLmy2UC.

[10] J.K. Park. 'Principles and Applications of Lithium Secondary Batteries'. In: *Principles and Applications of Lithium Secondary Batteries*. EngineeringPro collection. Wiley, 2012. Chap. 1-3. ISBN: 9783527650422. URL: https://books.google.no/books?id=papHH-urMVYC.

[11] James H Clark, R M Dell and D A J Rand. *Clean Energy*. RSC Clean Technology Monographs. The Royal Society of Chemistry, 2004, pp. X001–X004. ISBN: 978-0-85404-546-4. DOI: 10.1039/9781847550552. URL: http://dx.doi.org/10.1039/9781847550552.

[12] Sheng Shui Zhang. 'A review on the separators of liquid electrolyte Li-ion batteries'. In: *Journal of Power Sources* 164.1 (Jan. 2007), pp. 351–364. DOI: 10.1016/j.jpowsour.2006.10.065. URL: http://dx.doi.org/10.1016/j.jpowsour.2006.10.065.

[13] Larry R. Faulkner Allen J. Bard. 'Potentials and Thermodynamics of Cells'. In: *Electrochemical Methods: Fundamentals and Applications*. JOHN WILEY & SONS INC, 11th Dec. 2000, pp. 44–85. ISBN: 0-471-04372-9. URL: http://www.ebook.de/de/product/3254912/allen_j_bard_larry_r_faulkner_electrochemical_methods_fundamentals_and_applications.html.

[14] C.W. Pratt and K. Cornely. 'The Chemical Basis of Life. Energy and Metabolism'. In: *Essential Biochemistry*. Wiley, 2015, pp. 10–14. ISBN: 9781118441688. URL: https://books.google.no/books?id=F2wLnAEACAAJ.

[15] John Broadhead and Han C. Kuo. 'ELECTROCHEMICAL PRINCIPLES AND REACTIONS. ELECTROCHEMICAL PRINCIPLES AND REACTIONS'. In: Thomas B. Reddy David Linden. *Handbook of batteries. Handbook of batteries*. 3rd ed. 2002. Chap. 2, pp. 2.0–2.37. ISBN: 0-07-135978-8.

[16] M Endo et al. 'High power electric double layer capacitor (EDLC's); from operating principle to pore size control in advanced activated carbons'. In: *Carbon science* 1.3&4 (2001), pp. 117–128.

[17] J. OM. Bockris, M. A. V. Devanathan and K. Muller. 'On the Structure of Charged Interfaces'. In: *Proceedings of the Royal Society A: Mathematical, Physical and Engineering Sciences* 274.1356 (25th June 1963), pp. 55–79. DOI: 10.1098/rspa.1963.0114. URL: http://dx.doi.org/10.1098/rspa.1963.0114.

[18] E Gongadze et al. 'Classical Models of the Interface between an Electrode and an Electrolyte'. In: *COMSOL Conference*. 2009, pp. 14–16.

[19] Particle Sciences. 'An Overview of the Zeta Potential. Technical Breif'. In: *Particle Sciences* 2 (2012). URL: http://www.particlesciences.com/news/technical-briefs/2012/overview-of-zeta-potential.html (visited on 02/11/2016).

[20] Grant M. Ehrlich. *Handbook of batteries*. 3rd ed. 2002. ISBN: 0-07-135978-8.

[21] W. Blum and G. W. Vinal. 'The Definition of Polarization, Overvoltage and Decomposition Potential'. In: *Transactions of The Electrochemical Society* 66.1 (1934), p. 359. DOI: 10.1149/1.3498105. URL: http://dx.doi.org/10.1149/1.3498105.

[22] David Loveday, Pete Peterson and Bob Rodgers. 'Evaluation of organic coatings with electrochemical impedance spectroscopy'. In: *JCT coatings tech* 8 (2004), pp. 46–52.

[23] D.K. Schroder. *Semiconductor Material and Device Characterization*. Wiley, 2006. ISBN: 9780471749080. URL: https://books.google.no/books?id=OX2cHKJWCKgC.

[24] J.W. Nilsson and S.A. Riedel. *Electric Circuits*. Pearson/Prentice Hall, 2008. ISBN: 9780131989252. URL: https://books.google.no/books?id=sxmM8RFL99wC.

[25] FL. W. M. Haynes Boca Raton. *TABLE 3. Reduction Reactions Having E° Values More Negative than That of the Standard Hydrogen Electrode*. In: *CRC Handbook of Chemistry and Physics*. Ed. by CRC Press/Taylor & Francis. 97th (Internet Version 2017). 2016. (Visited on 03/11/2016).

[26] Pallavi Verma, Pascal Maire and Petr Novák. 'A review of the features and analyses of the solid electrolyte interphase in Li-ion batteries'. In: *Electrochimica Acta* 55.22 (Sept. 2010), pp. 6332–6341. DOI: 10.1016/j.electacta.2010.05.072. URL: http://dx.doi.org/10.1016/j.electacta.2010.05.072.

[27] Masakazu Haruta et al. 'Effects of SEI Formation Additives on Cycle Performance and Surface Morphology in Si-Flake-Powder Anodes'. In: *Meeting Abstracts* MA2016-02.3 (2016), p. 285. URL: http://ma.ecsdl.org/content/MA2016-02/3/285.abstract.

[28] Xin-Bing Cheng et al. 'A Review of Solid Electrolyte Interphases on Lithium Metal Anode'. In: *Adv. Sci.* 3.3 (Nov. 2015), p. 1500213. DOI: 10.1002/advs.201500213. URL: http://dx.doi.org/10.1002/advs.201500213.

[29] Y. Wu. *Lithium-Ion Batteries: Fundamentals and Applications*. Electrochemical Energy Storage and Conversion. CRC Press, 2015. ISBN: 9781466557345. URL: https://books.google.no/books?id=AymsCQAAQBAJ.

[30] M. Lannoo. 'The role of dangling bonds in the properties of surfaces and interfaces of semiconductors'. In: *Revue de Physique Appliquée* 25.9 (1990), pp. 887–894. DOI: 10.1051/rphysap:01990002509088700. URL: http://dx.doi.org/10.1051/rphysap:01990002509088700.

[31] Olindo Isabella Arno Smets Klaus Jager and Rene van Swaaij. 'Generation and recombination of electron-hole pairs'. In: *Solar Energy*. UIT Cambridge, 14th Jan. 2016. Chap. 7.5, p. 78. ISBN: 9781906860325.

[32] Qianfan Zhang, Yi Cui and Enge Wang. 'First-principles approaches to simulate lithiation in silicon electrodes'. In: *Modelling and Simulation in Materials Science and Engineering* 21.7 (2013), p. 074001. URL: http://stacks.iop.org/0965-0393/21/i=7/a=074001.

[33] Hong Liu and Zhong Lin Wang. 'Etching silicon wafer without hydrofluoric acid'. In: *Applied Physics Letters* 87.26 (2005), p. 261913. DOI: 10.1063/1.2158021. URL: http://dx.doi.org/10.1063/1.2158021.

[34] JC Burns et al. 'Introducing symmetric Li-ion cells as a tool to study cell degradation mechanisms'. In: *Journal of The Electrochemical Society* 158.12 (2011), A1417–A1422.

[35] Lei Pei et al. 'Development of a voltage relaxation model for rapid open-circuit voltage prediction in lithium-ion batteries'. In: *Journal of Power Sources* 253 (2014), pp. 412–418.

[36] Arbin Instruments. *Arbin-010 MITS Pro 4.0-BT2000 User Manual*. Arbin Instruments. May 2010. Chap. 9.4, pp. 17–18.

[37] Hélène Piret et al. 'Online Estimation of Electrical Impedance'. In: *7th International Workshop on Impedance Spectroscopy (IWIS)*. 2014.

[38] Princeton Applied Research. *Basics of Electrochemical Impedance Spectroscopy*. Application Note AC-1.

[39] Gamry Instruments. *Basics of Electrochemical Impedance Spectroscopy*. Application note Rev 1.0. 2010.

[40] Jan Petter Maehlen. *cellpy documentations*. Ed. by Jan Petter Maehlen. Documentations. 2016. URL: http://cellpy.readthedocs.io/en/latest/.

[41] SciPy. *scipy optimize curve fit*. Ed. by The SciPy community. 2016. URL: https://docs.scipy.org/doc/scipy-0.18.1/reference/generated/scipy.optimize.curve_fit.html (visited on 13/11/2016).

[42] Matt Newville et al. *lmfit-py: release 0.9.3*. Apr. 2016. DOI: 10.5281/zenodo.49428. URL: https://doi.org/10.5281/zenodo.49428.

[43] Ben Straub Scott Chacon. *Pro Git*. Apress, 18th Nov. 2014. xxi456 pp. ISBN: 9781484200766. URL: http://www.ebook.de/de/product/23510106/scott_chacon_ben_straub_pro_git.html.

[44] Vincent Driessen. *A successful Git branching model*. Ed. by Vincent Driessen. 5th Jan. 2010. URL: http://nvie.com/posts/a-successful-git-branching-model/ (visited on 13/11/2016).

Appendix A

Relevant Python Codes

Listed in this chapter are the most relevant Python codes for the fitting program developed in this thesis.

A.1 Open Circuit Voltage Script

The cell model's core is defined in `cell_ocv`, listed below. `relaxation_rc` calculates the relaxation voltage from a RC-circuit with Eq. (2.23). A function is defined by `def`, and its name is what follows, i.e. `def name_function(arguments):`. The purple text are documentations and the blue texts are python statements.

```
import numpy as np

def relaxation_rc(time, v0, tau_rc):
  """
  Calculates the relaxation function of an rc-circuit.

  Args:
    time (nd.array): Points in time [s].
    v0 (float): The initial voltage across the rc-circuit at t = 0 [V].
    tau_rc (float): The rc-circuit's resistance [Ohm].

  Returns:
    nd.array: The rc-circuit's relaxation voltage.

  """

  return v0 * np.exp(-time / tau_rc)
```

```
def ocv_relax_func(time, ocv, v0_rc, tau_rc):
  """Calculates the cell's relaxation voltage.

  Args:
    time (nd.array): Points in time [s].
    ocv (nd.array): Open circuit voltage [V].
    v0_rc (dict): Initial relaxation voltage for each rc-circuits [V].
    tau_rc (dict): The rc-circuit's time constant [s].

  Returns:
    nd.array: The relaxation voltage of the model
  """

  volt_rc = [relaxation_rc(time, v0_rc[rc], tau_rc[rc]) for rc in tau_rc.keys
    ()]

  return sum(volt_rc) + ocv


def guessing_parameters(v_start, i_start, v_0, v_ocv, contribute, tau_rc):
  """
  Initial parameter guess.

  Args:
    v_start (float): Voltage before IR-drop [V].
    i_start (float): Current right before open circuit [A].
    v_0 (float): Voltage after IR-drop [V].
    v_ocv (float): Guessed voltage at full relaxation [V].
    contribute (dict): The rc-circuits contributed part of v_0.
    tau_rc (dict): Guessed time constants across each rc-circuit

  Returns:
    dict: Guessed parameters.
  """

  if sum(contribute.values()) != 1.0:
  raise ValueError('The sum of contribute does not add up to 1.')

  v_rlx = v_0 - v_ocv   # voltage after IR-drop
  # Initial RC-circuit voltage
```

```
  v0_rc = {rc: v_rlx * rc_contri for rc, rc_contri in contribute.items()}

  v_ir = v_start - v_0
  r_ir = v_ir / i_start
  r_rc = {key: v0 / i_start  for key, v0 in v0_rc.items()}
  c_rc = {k: t / r for k, r in r_rc.items() for i, t in tau_rc.items() if i ==
    k}
  return {'r_rc': r_rc, 'r_ir': r_ir, 'c_rc': c_rc, 'v0_rc': v0_rc}
```

Listing A.1: "cell_ocv" script. Returns the relaxation voltage and guess initial parameters.

Equation (3.3) is returned from `ocv_relax_func` in listing A.1. This is the main part of the `cell_ocv` script.

A.2 Fitting OCV

The following listing from the script `fitting_cell_ocv` are the main fitting part of the program developed in this thesis. Only the most important code-lines are displayed in listing A.2.

```
import numpy as np
from cell_ocv import *
import lmfit


def relax_model(t, **params):
  """Fitting of parameters with lmfit.

  This function is made into a lmfit.Model object and used for parameter
   iteration.

  Args:
    params (lmfit.Parameters): A lmfit object that contain a dictionary of
   parameters like v0, ocv and tau.
    t (nd.array): Points in time [s].

  Returns:
    nd.array: Expected relaxation voltage based on the model.
  """

  # the ocv voltage (equilibrium voltage) has to be same length as time, t.
  ocv_array = np.ones(len(t)) * params['ocv']
```

```
  # time constant for each rc-ciruit
  tau_rc = {key[4:]: val for key, val in params.items() if key.startswith('tau
    ')}

  # initial voltage for each rc-circuit
  v0_rc = {key[3:]: val for key, val in params.items() if key.startswith('v0')
    }

  return ocv_relax_func(t, tau_rc=tau_rc, ocv=ocv_arr, v0_rc=v0_rc)


def define_model(filepath, filename, guess_tau, contribution, c_rate=0.05,
         ideal_cap=3.579, mass=0.86, v_start=None):
  """Reading data, creating Model object from relax_model and set param_hints.

  Reading the .csv file with all the cycling data.
  The user may initialise the use of lmfit. If user does not know the
  parameters, some defaults are set. Filepath and filename has to be given.

  Removing "nan" is inspired by 'stackoverflow'_

  Args:
    filepath (str): The exact path to the folder where the data lies.
    filename (str): The ocv relaxation filename for up- or downwards relax.
    guess_tau (:obj: 'dict' of :obj: 'float'): User guessing what the time
    constant for each rc-circuit might be.
    contribution (:obj: 'dict' of :obj: 'float'): Assumed contribution
    from each rc-circuit. Help guessing the initial start voltage value
    of the rc-circuit.
    c_rate (float): C-rate of discharge or charge.
    ideal_cap (float): Theoretical capacity of the cell.
    mass (float): Mass of the active material. Given in [mg].
    v_start (float): Cut-off voltage (before IR-drop).

  Returns:
    :obj: 'Model' of :obj: 'relax_model', :obj: 'list' of :obj:
    'nd.array', :obj: 'list' of :obj: 'nd.array': Model of relax_model
    with it's guessed parameters as hints. One list of time, and one of
    voltage, both with len equal to number of cycles. Each element in
    list represent number of cycle - 1.

  .._stackoverflow:
```

```
    http://stackoverflow.com/questions/11620914/removing-nan-values-from-an-
    array

    """

    try:
      r_filepath = r'%s' % filepath
      r_filename = r'%s' % filename
      data_write = os.path.join(r_filepath, r_filename)
      data_read = pd.read_csv(data_write, sep=';')
      data = manipulate_data(data_read)
    except ImportError:
      print "Folder- or filename not found."
      raise
    if not guess_tau:
      guess_tau = {'d': 500, 'ct': 50}
    if not contribution:
      contribution = {'d': 0.8, 'ct': 0.2}

    # Extracting time and voltage from data.
    time = []
    voltage = []
    for i, sort in data.iteritems():
      sort_t = np.array(sort[:]['time'])
      sort_v = np.array(sort[:]['voltage'])
      sort_t = sort_t[~np.isnan(sort_t)]
      sort_v = sort_v[~np.isnan(sort_v)]
      sort_time = np.sort(sort_t)

      # checking if relaxation down or up
      if sort_v[-1] > sort_v[0]:
        sort_volt = np.sort(sort_v)
      else:
        sort_volt = np.sort(sort_v)
        sort_volt[:] = sort_volt[::-1]
      time.append(sort_time)
      voltage.append(sort_volt)
    v_ocv = voltage[0][-1]
    v_0 = voltage[0][0]

    i_start = (c_rate * ideal_cap * mass) / 1000
    if v_ocv < v_0:
```

```
    # After charge
    if not v_start:
    v_start = 1.
  else:
    # After discharge
    if not v_start:
    v_start = 0.01

  init_guess = guessing_parameters(v_start, i_start, v_0, v_ocv, contribution,
     guess_tau)

  r_model = lmfit.Model(relax_model, missing='raise')

  for name in guess_tau.keys():
    r_model.set_param_hint('tau_%s' % name, value=guess_tau[name], min=0)

  if v_ocv < v_0:
    # After charge (relax downwards)
    r_model.set_param_hint('v0_%s' % name, value=init_guess['v0_rc'][name],
    min=0)
  else:
    r_model.set_param_hint('v0_%s' % name, value=init_guess['v0_rc'][name],
    max=0)
  r_model.set_param_hint('ocv', value=v_ocv)
  r_model.make_params()
  print "Initial parameter hints are based on first cycle"
  r_model.print_param_hints()
  print "To define more boundaries: >>> " \
      "example_model.set_param_hint('name_of_parameter', min=min_value, " \
      "max=max_value)"
  return r_model, time, voltage


def fit_with_model(model, time, voltage, guess_tau, contribution, c_rate,
  change_i, ideal_cap=3.579, mass=0.86, v_start=None, v_err=0.01):
  """Fitting measured data to model.

  Some default parameters are set if user have not specified any.

  Args:
    model (lmfit.Model): The cell model.
    time (:obj: 'list' of :obj: 'nd.array'): Element in list equals the time
```

```
    of cycle number - 1.
    voltage (:obj: 'list' of :obj: 'nd.array'): Element in list equals
    the voltage of cycle number - 1.
    guess_tau (:obj: 'dict' of :obj: 'float'): User guessing what the time
    constant for each rc-circuit might be.
    contribution (:obj: 'dict' of :obj: 'float'): Assumed contribution
    from each rc-circuit. Help guessing the initial start voltage value
    of the rc-circuit.
    c_rate (:obj: 'list' of :obj: 'float'): The C-rate which the cell was
    discharged or charged with before cycle = change_i.
    change_i (:obj: 'list' of :obj: 'int'): The cycle number where the
    C-rate (AKA Current) is changed. len(c_rate) = len(change_i) + 1
    ideal_cap (float): Theoretical capacity of the cell.
    mass (float): Mass of the active material. Given in [mg].
    v_err (float): Voltage measurement accuracy in V. Default: Arbin BT2000.
    v_start (float): Cut-off voltage (potential before IR-drop).

  Returns:
    :obj: 'list' of :obj: 'lmfit.ModelResult', :obj: 'list' of :obj:
    'dict': Results of fitting from each cycle in a list with and
    calculated R and C parameters based on fit from result.
  """

  i_start = []
  step = 0
  for i in range(len(time)):
    # Checking if cycle number i is in change_i
    if i in change_i:
    step += 1
    i_start.append((c_rate[step] * ideal_cap * mass) / 1000)
  if not guess_tau:
    guess_tau = {'d': 500, 'ct': 50}
  if not contribution:
    contribution = {'d': 0.8, 'ct': 0.2}

  # performing initial fit and saving in a list.
  result_initial = lmfit.model.fit(voltage[0], t=time[0], weights=1./v_err)
  result = [result_initial]

  # calculating and saving parameters based on fit in previous sentence.
  best_para = [result[0].params]
  v0_ir_0 = abs(voltage[0][0] - v_start)
```

```
r_ir_0 = v0_ir_0 / i_start[0]
r_ir = {'IR': r_ir_0}

# Total magnitude of overpotential is the fitted ocv and start voltage.
tot_overpot_ini = {'over_pot': abs(best_para[0]['ocv'] - v_start)}

best_rc_ini = {'r_%s' % key[3:]: abs(v0_rc / i_start[0])
for key, v0_rc in best_para[0].valuesdict().items()
if key.startswith('v0')}

best_c_ini = {'c_%s' % key[4:]: tau_rc / best_rc_ini['r_%s' % key[4:]]
        for key, tau_rc in best_para[0].valuesdict().items()
        if key.startswith('tau')}
best_rc_ini.update(best_c_ini)
best_rc_ini.update(r_ir)
best_rc_ini.update(tot_overpot_ini)
best_rc_para = [best_rc_ini]

# performing the rest of the fitting based on previous best parameters.
for cycle_i in range(1, len(time)):
  temp_start_voltage = voltage[cycle_i][0]
  temp_end_voltage = voltage[cycle_i][-1]

  # Guessing new values when current has changed.
  if i_start[cycle_i] is not i_start[cycle_i - 1]:
    temp_initial_guess = guessing_parameters(v_start, i_start[cycle_i],
                         temp_start_voltage,
                         temp_end_voltage,
                         contribution, guess_tau)
    for name in guess_tau.keys():
      model.set_param_hint('tau_%s' % name, value=guess_tau[name])
      if temp_end_voltage < temp_start_voltage:
        # After charge (relax downwards)
        model.set_param_hint('v0_%s' % name,
                    value=temp_initial_guess[v0_rc'][name], min=0)
      else:
        model.set_param_hint('v0_%s' % name,
                             value=temp_initial_guess[v0_rc'][name], max=0)
        model.set_param_hint('ocv', value=temp_end_voltage)
        model.make_params()
        result_cycle = model.fit(voltage[cycle_i], t=time[cycle_i],
                       weights=1. / v_err)
```

```
    else:
      # fitting parameters for cycle with previous cycle's best fit.
      result_cycle = lmfit.model.fit(voltage[cycle_i],
                      params=best_para[cycle_i - 1],
                      t=time[cycle_i], weights=1. / v_err)

    # Saving fitted results in the same list as initial fit.
    result.append(result_cycle)
    best_para.append(result_cycle.params)

    # Total magnitude of overpotential is the fitted ocv and start voltage.
    tot_overpot = {'over_pot': abs(best_para[cycle_i]['ocv'] - v_start)}

    # calculating r and c from fit
    r_ir_temp = abs(temp_start_voltage - v_start) / i_start[cycle_i]
    best_rc_cycle = {'r_%s' % key[3:]:
    abs(v_rc / i_start[cycle_i])
    for key, v_rc in
    best_para[cycle_i].valuesdict().items()
    if key.startswith('v0')}
    best_c_cycle = {'c_%s' % key[4:]:
    tau_rc / best_rc_cycle['r_%s' % key[4:]]
    for key, tau_rc in
    best_para[cycle_i].valuesdict().items()
    if key.startswith('tau')}
    best_rc_cycle.update({'IR': r_ir_temp})
    best_rc_cycle.update(best_c_cycle)
    best_rc_cycle.update(tot_overpot)
    best_rc_para.append(best_rc_cycle)

  return result, best_rc_para, i_start
```

Listing A.2: The main functions in `fitting_cell_ocv`. The `relax_model` function was defined as a Model-class by lmfit. lmfit use `relax_model` to perform the iteration of parameters. The `relax_model` calls `ocv_relax_func` from `cell_ocv` listed in A.1.

Appendix B

Fitting of OCV

This appendix display fitted OCV data and the best parameters of all cells.

B.1 Cell A1

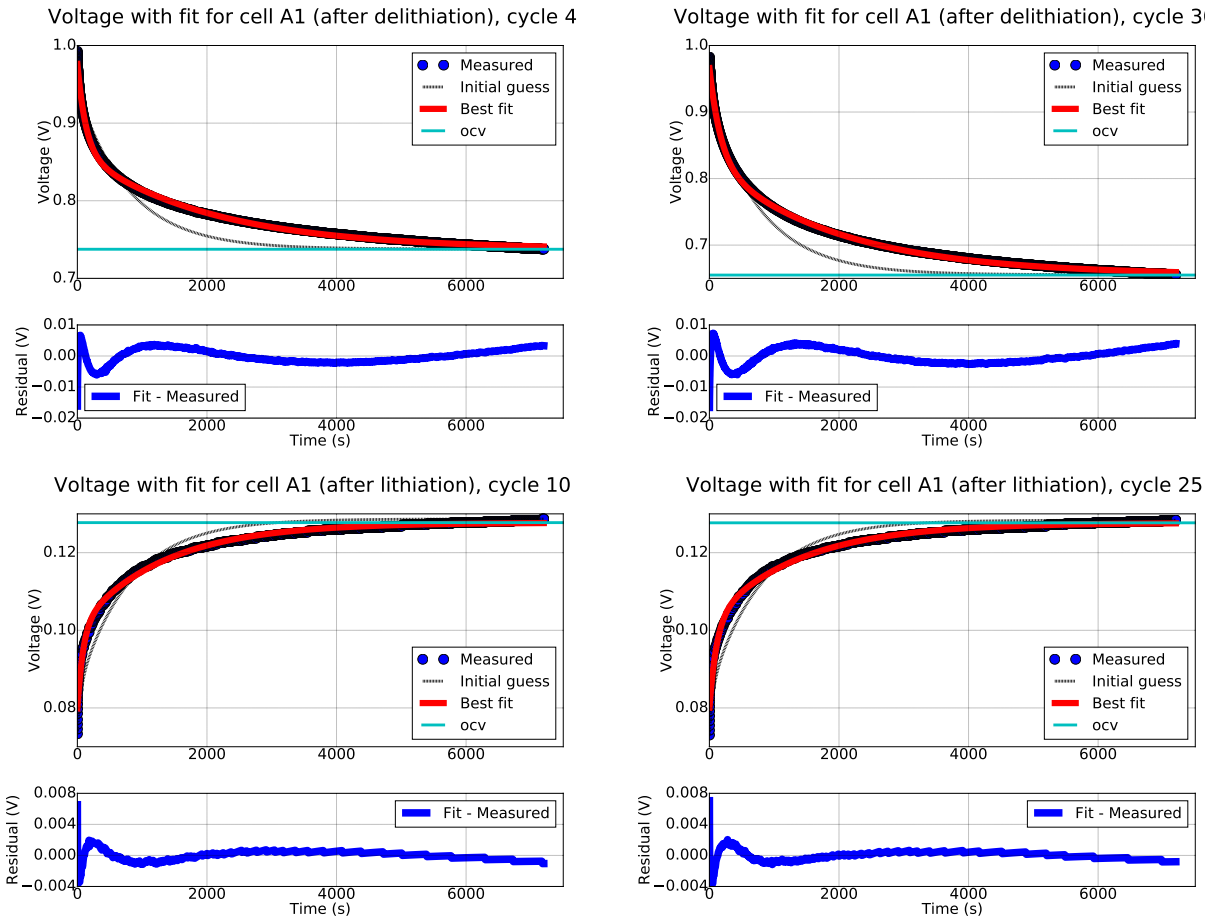

Figure B.1: Fitted OCV data for cycle 4 and 30 after delithiation and cycle 10 and 25 after lithiation.

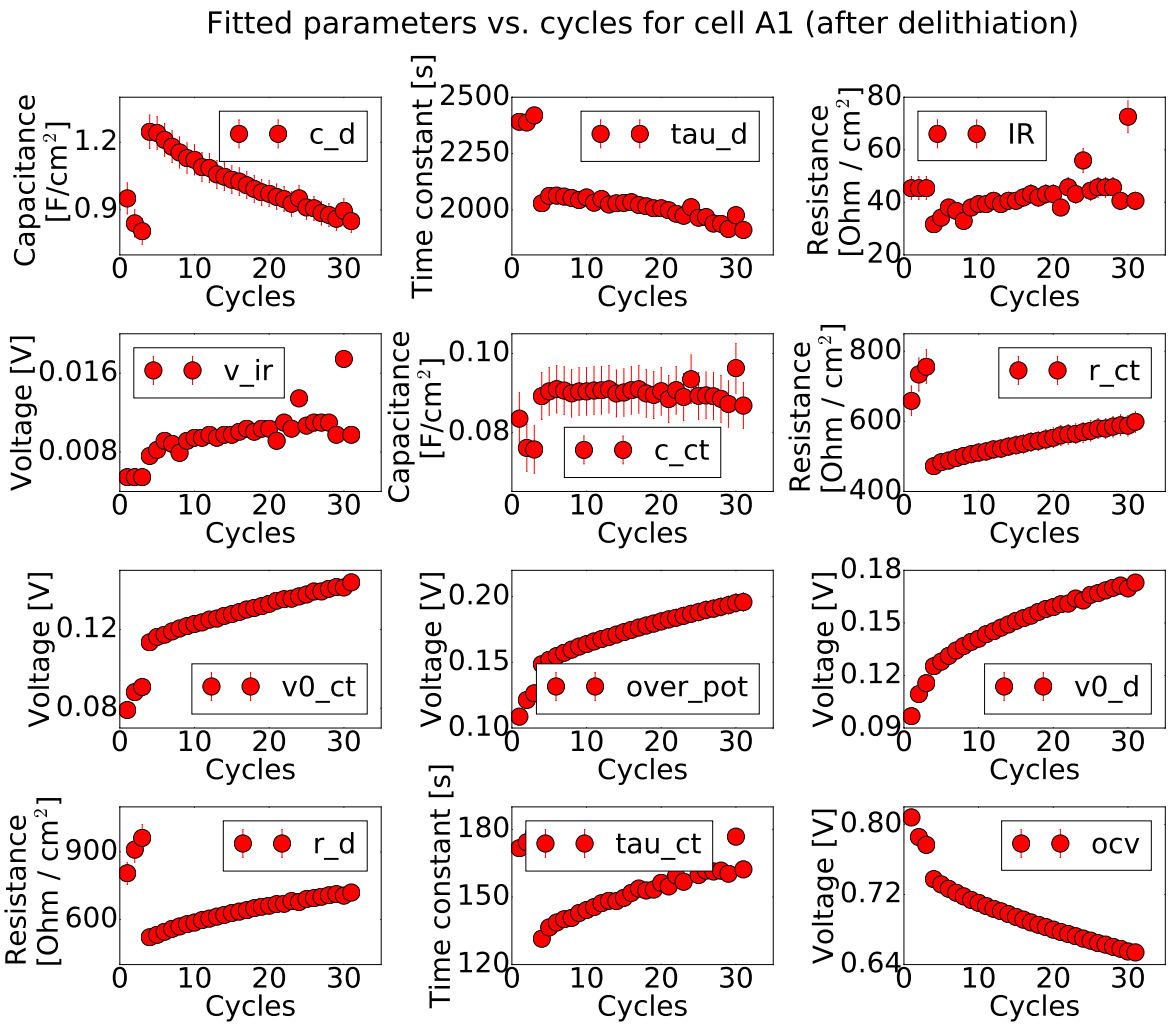

Figure B.2: All fitted parameters for cell A1 after delithiation.

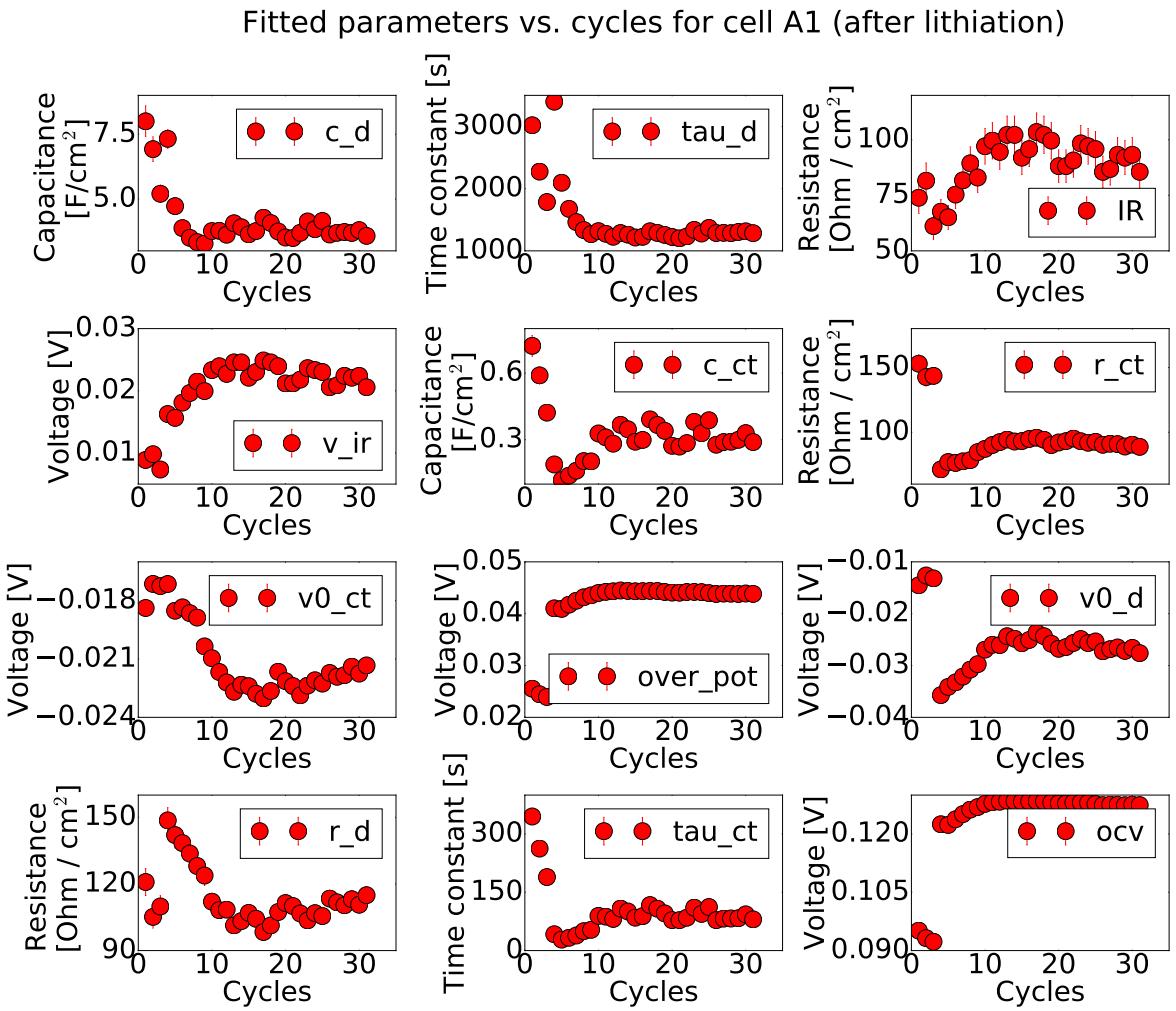

Figure B.3: All fitted parameters for cell A1 after lithiation.

B.2 Cell A2

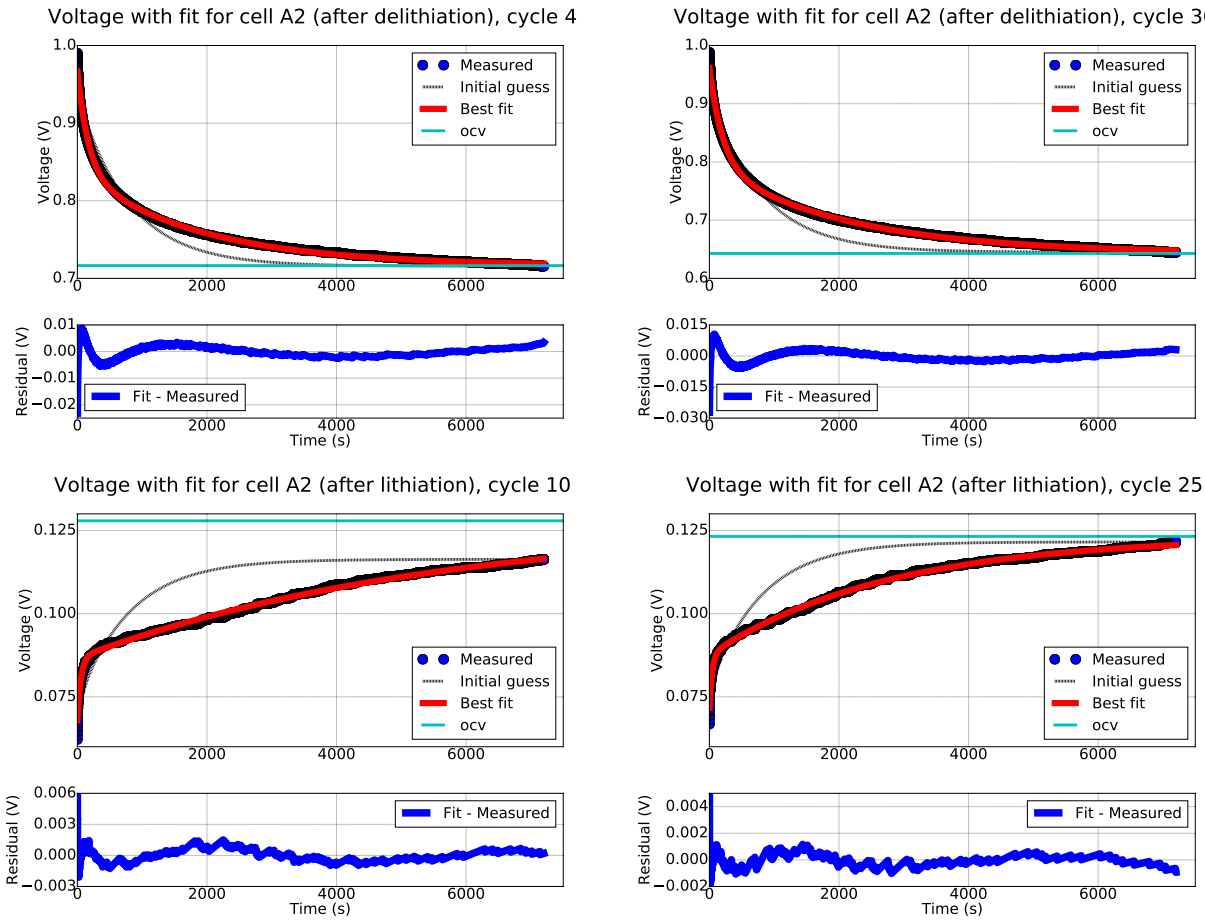

Figure B.4: Fitted OCV data for cycle 4 and 30 after delithiation and cycle 10 and 25 after lithiation.

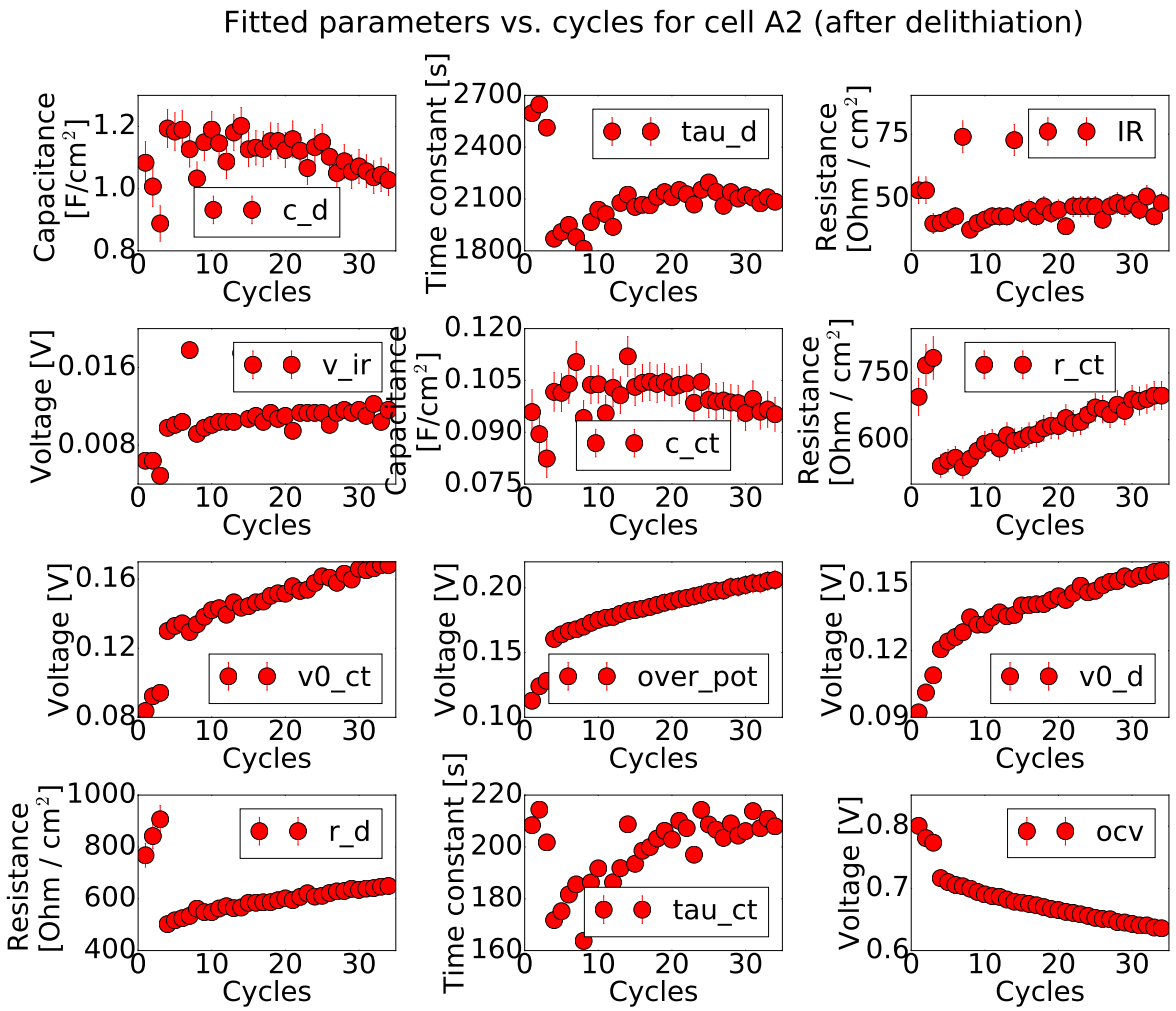

Figure B.5: All fitted parameters for cell A2 after delithiation.

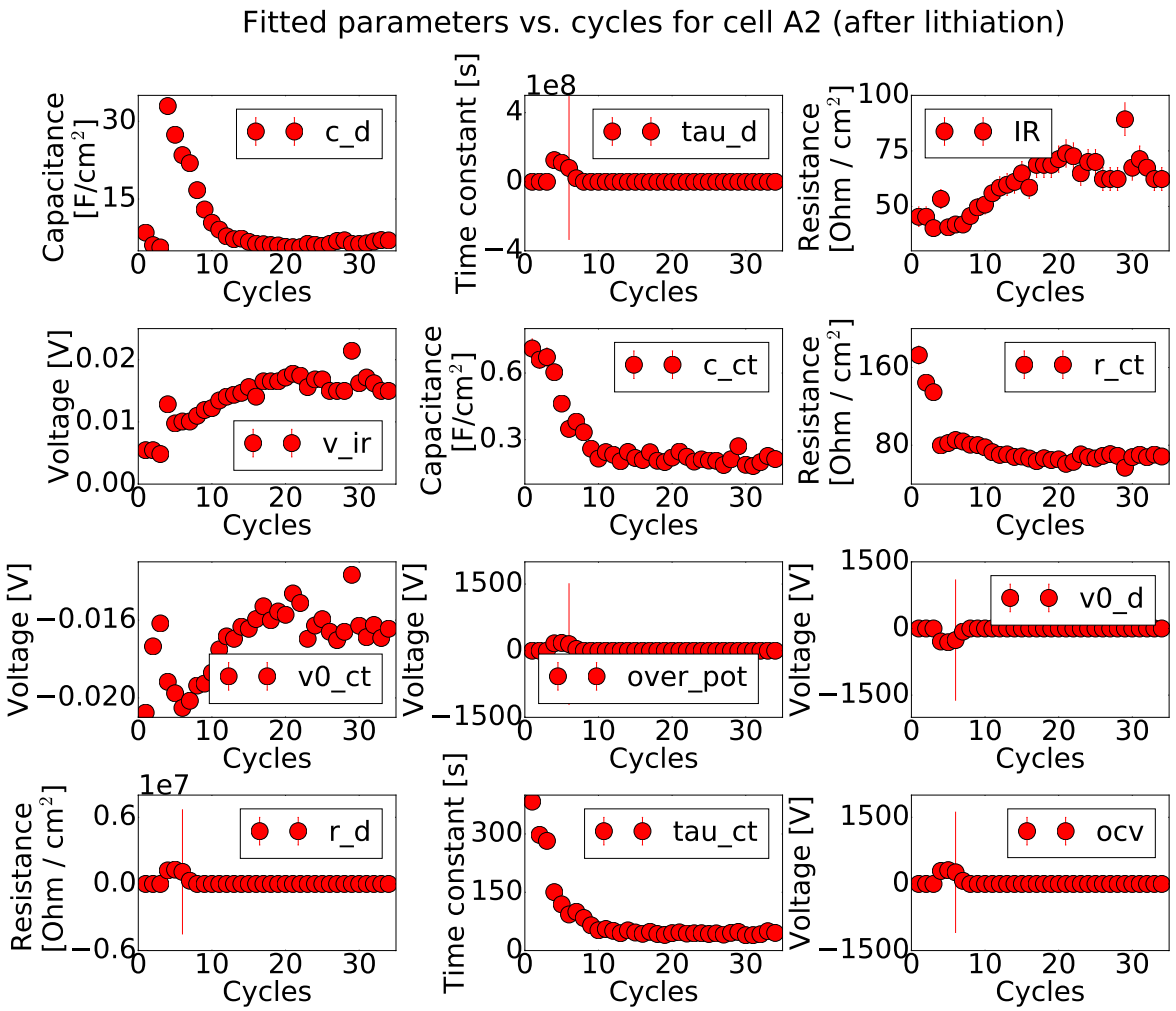

Figure B.6: All fitted parameters for cell A2 after lithiation.

B.3 Cell 1

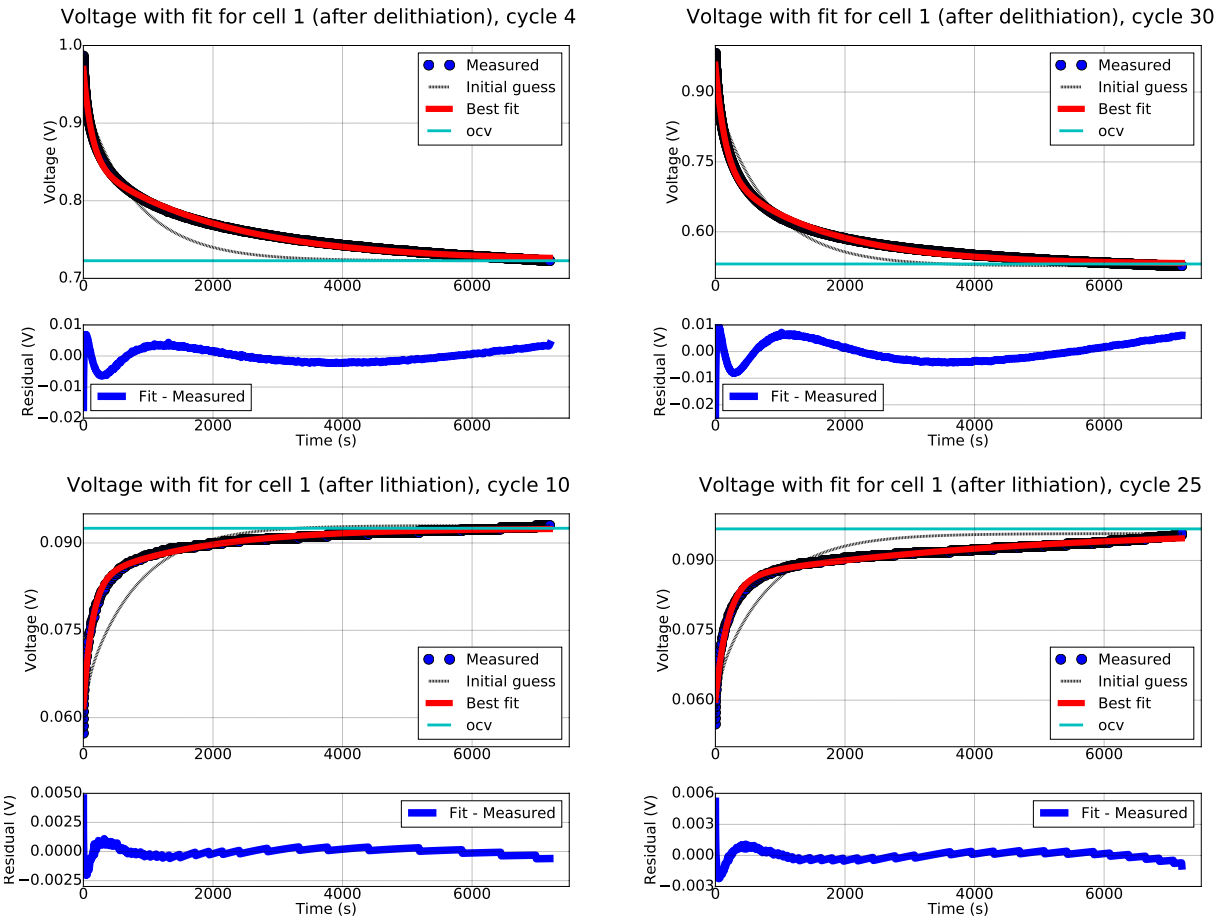

Figure B.7: Fitted OCV data for cycle 4 and 30 after delithiation and cycle 10 and 25 after lithiation.

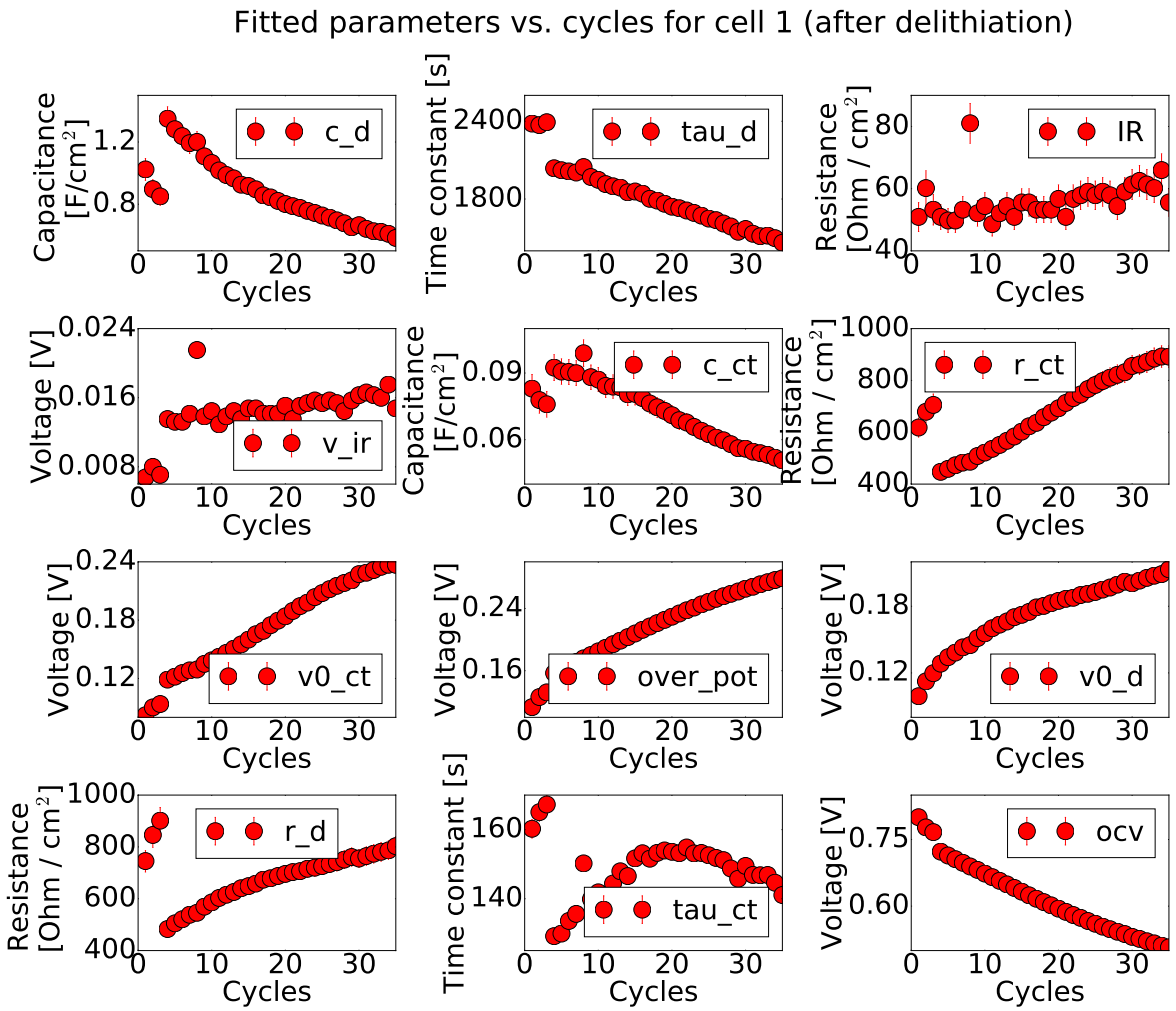

Figure B.8: All fitted parameters for cell 1 after delithiation.

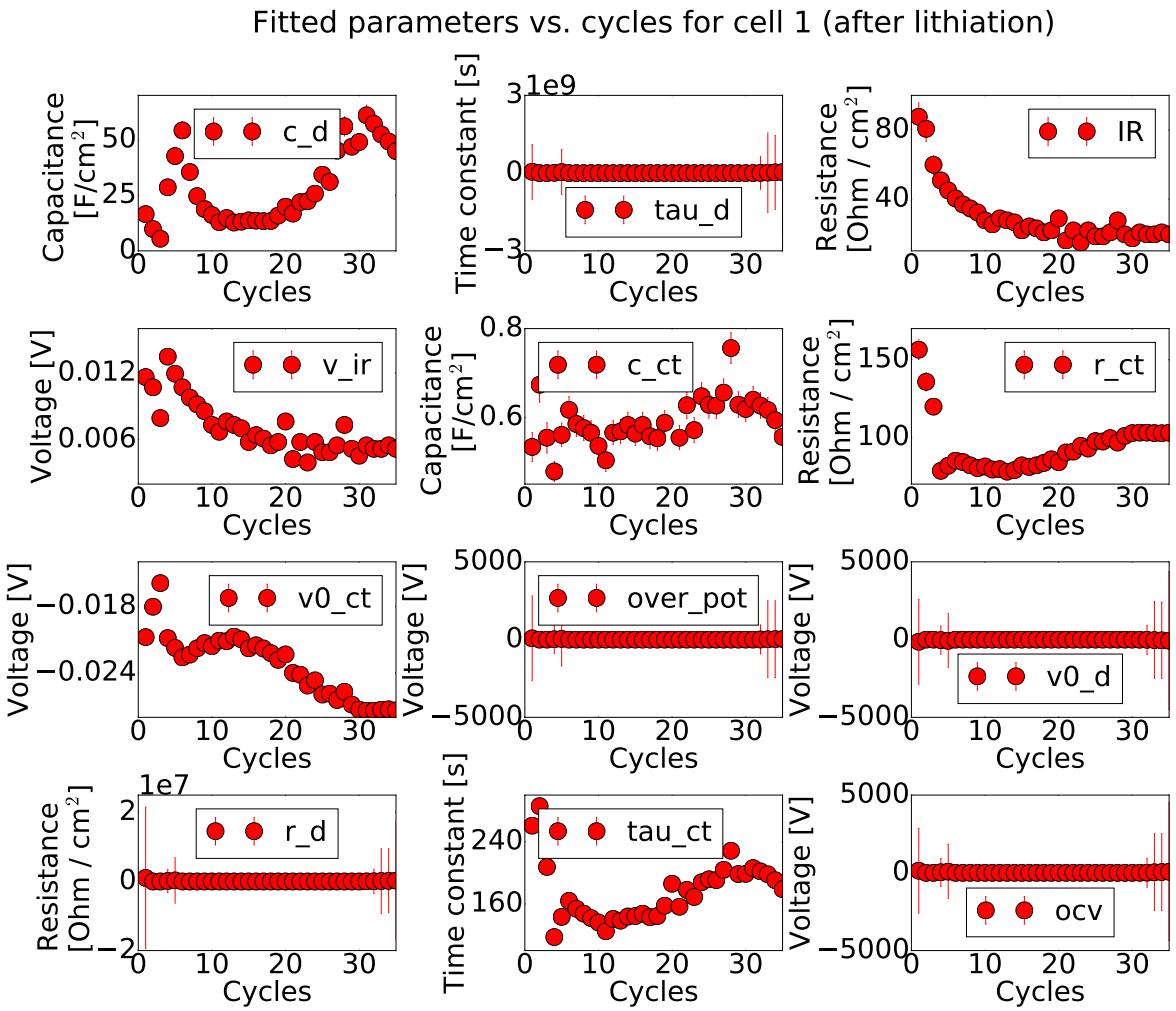

Figure B.9: All fitted parameters for cell 1 after lithiation.

B.4 Cell 2

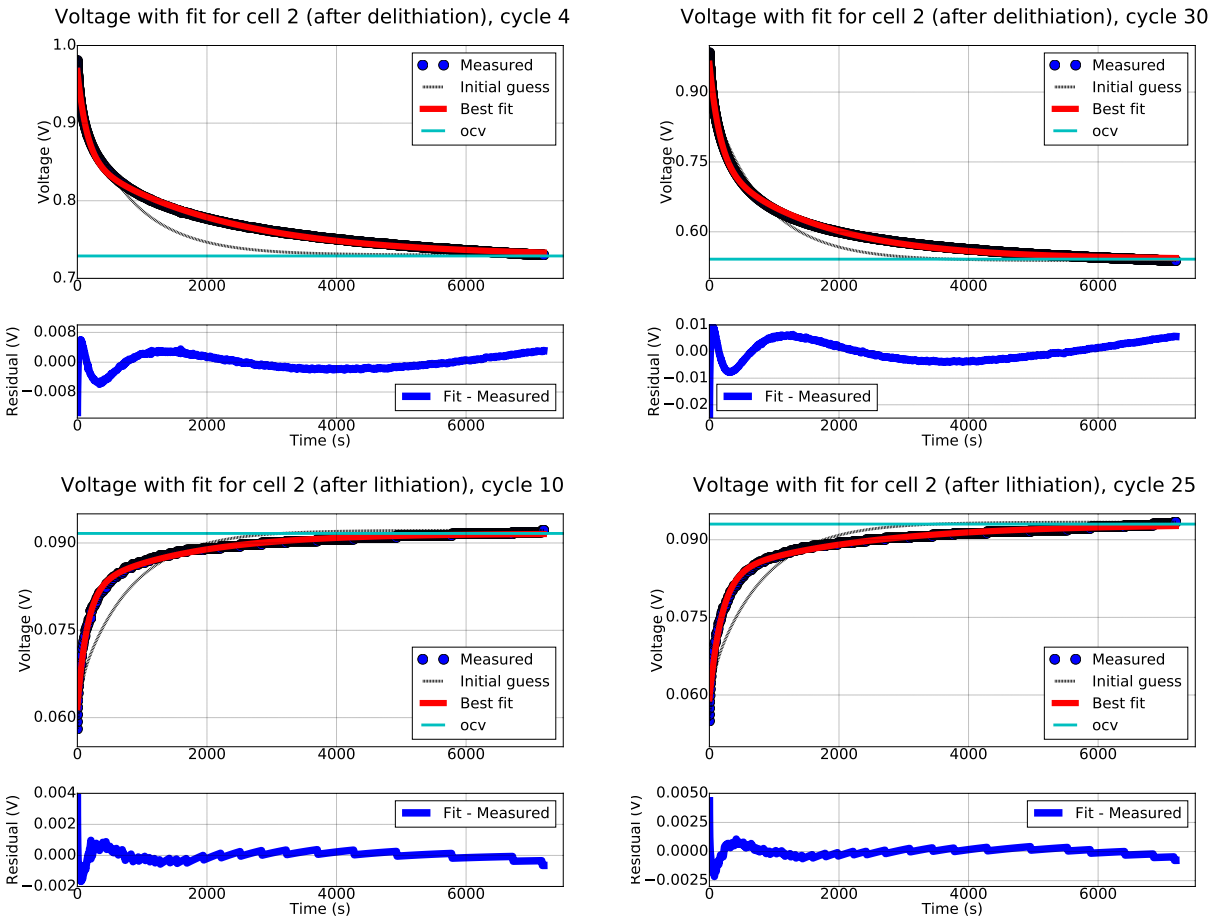

Figure B.10: Fitted OCV data for cycle 4 and 30 after delithiation and cycle 10 and 25 after lithiation.

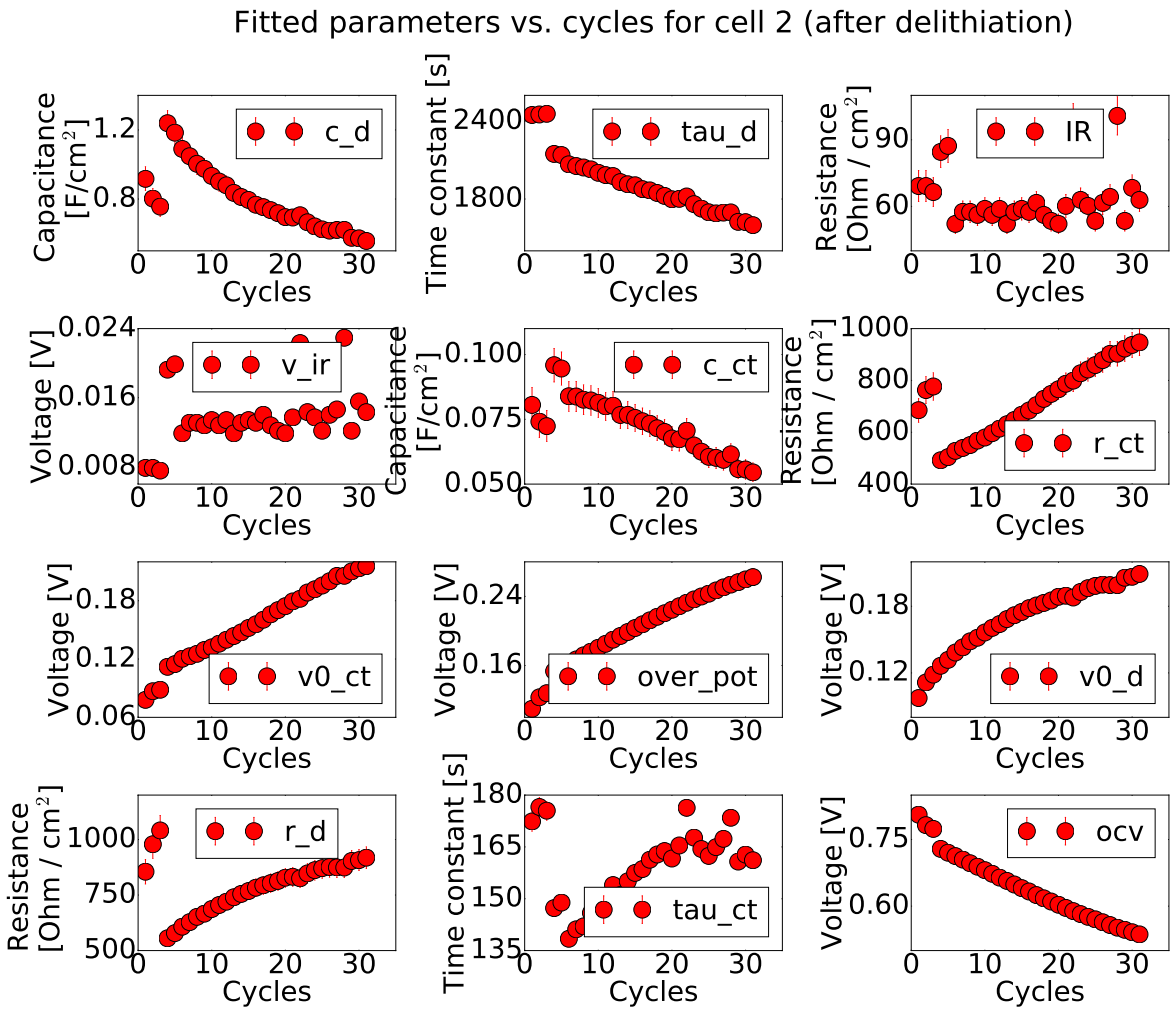

Figure B.11: All fitted parameters for cell 2 after delithiation.

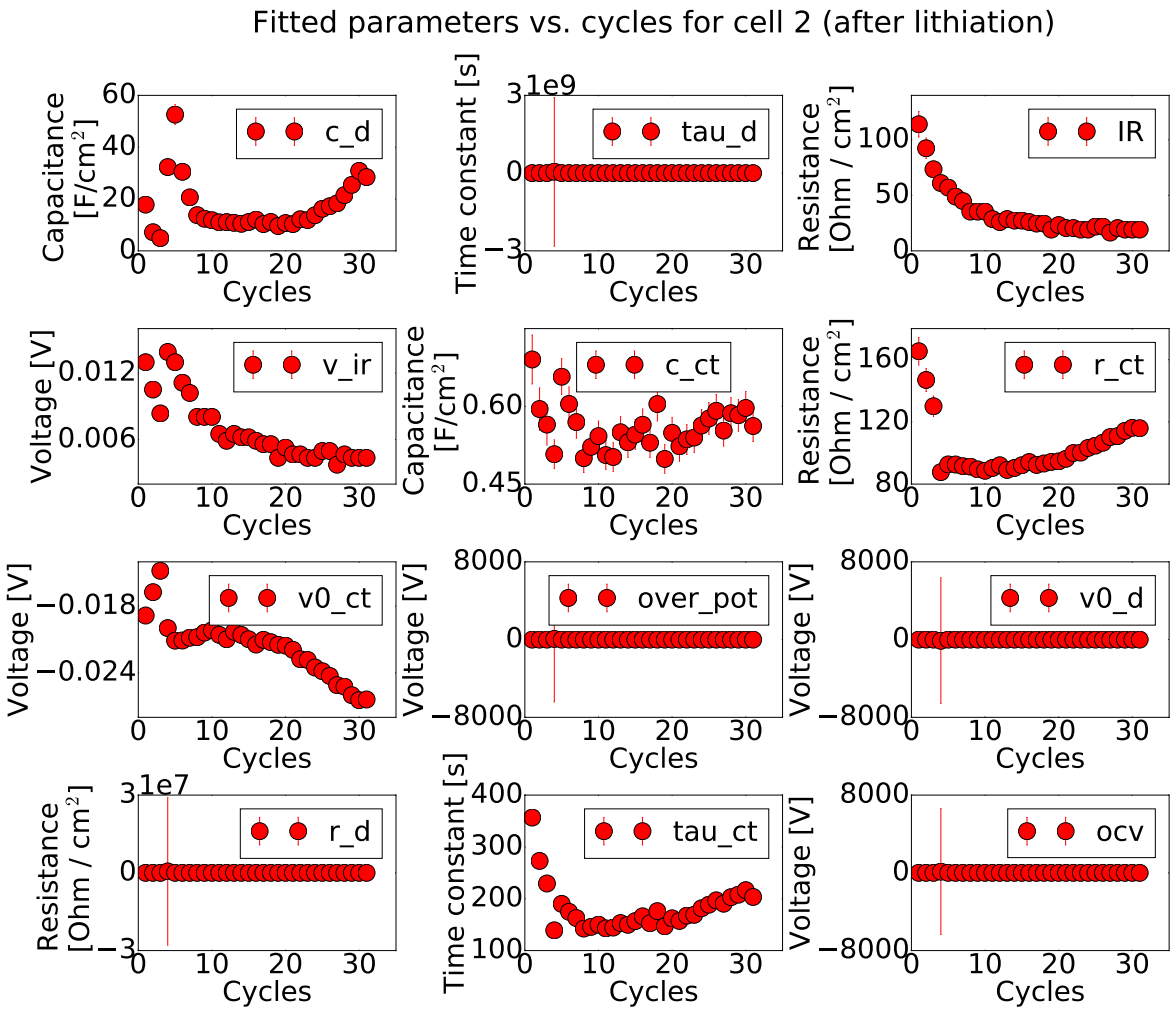

Figure B.12: All fitted parameters for cell 2 after lithiation.

B.5 Cell 3

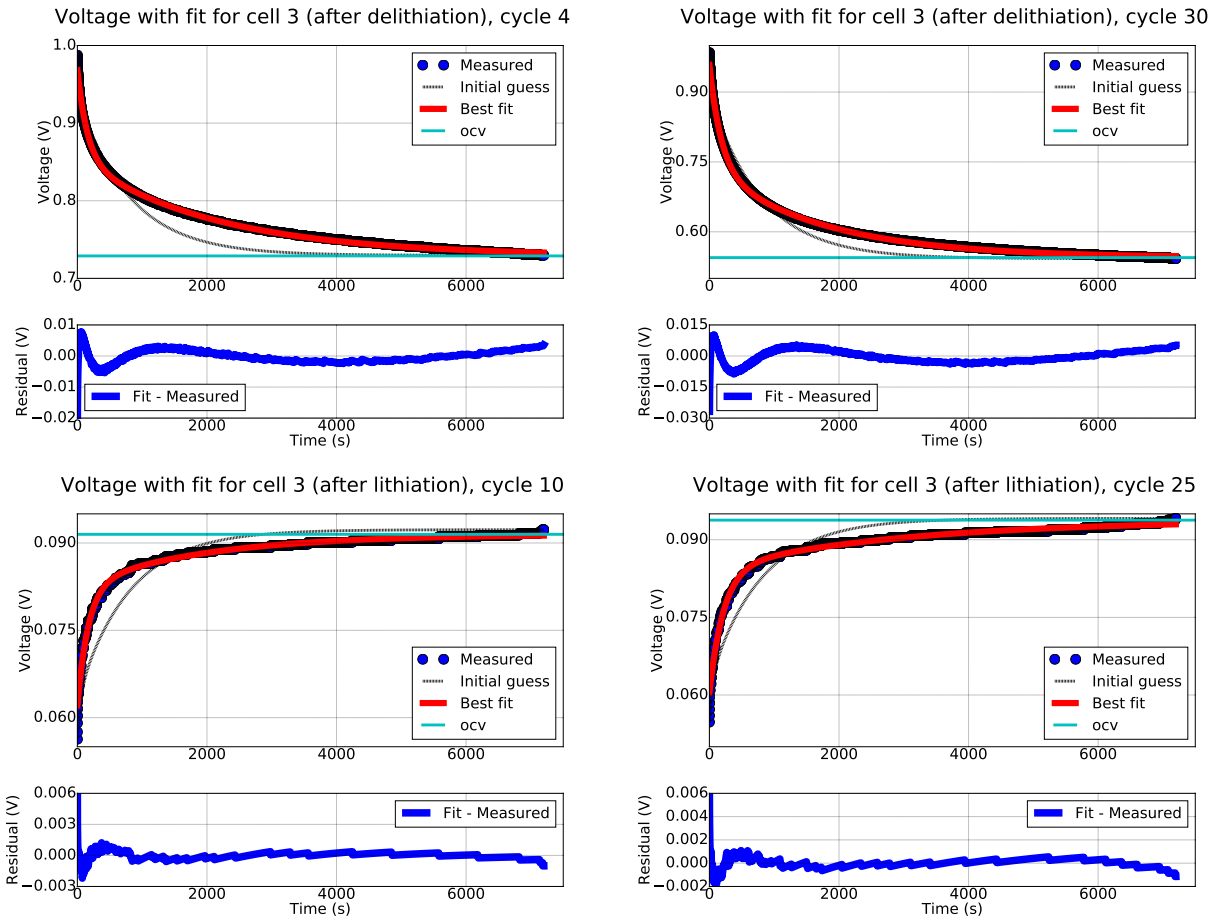

Figure B.13: Fitted OCV data for cycle 4 and 30 after delithiation and cycle 10 and 25 after lithiation.

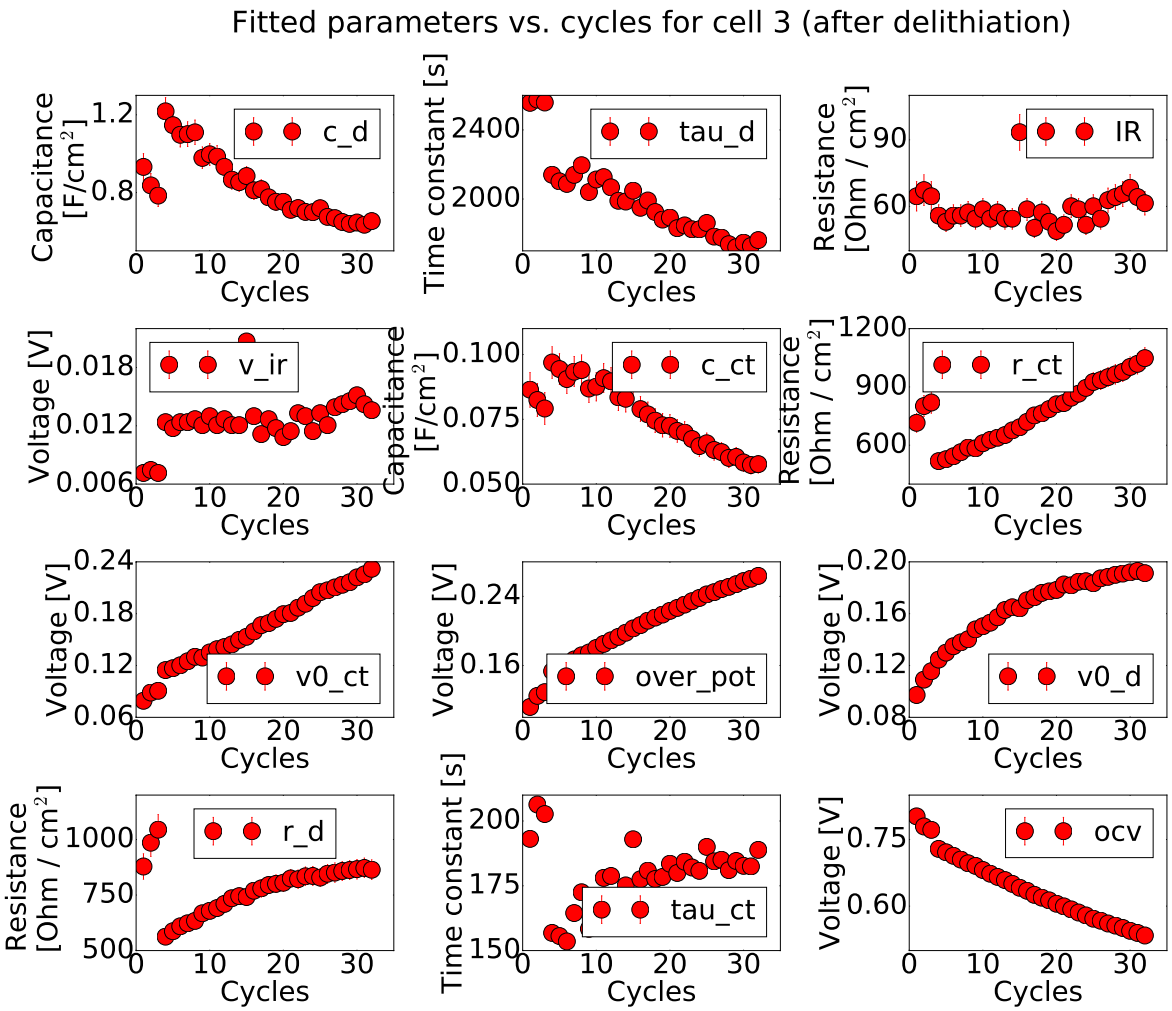

Figure B.14: All fitted parameters for cell 3 after delithiation.

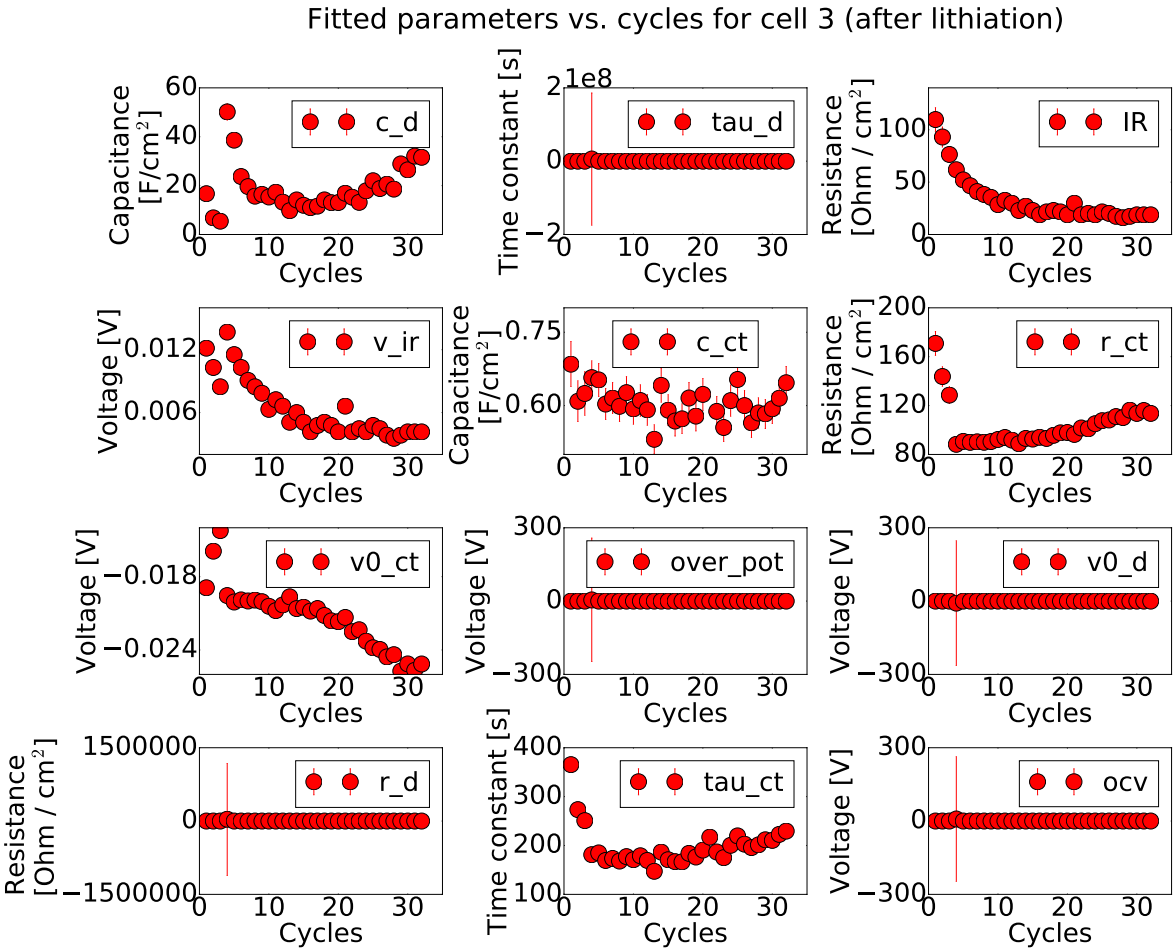

Figure B.15: All fitted parameters for cell 3 after lithiation.

B.6 Cell S

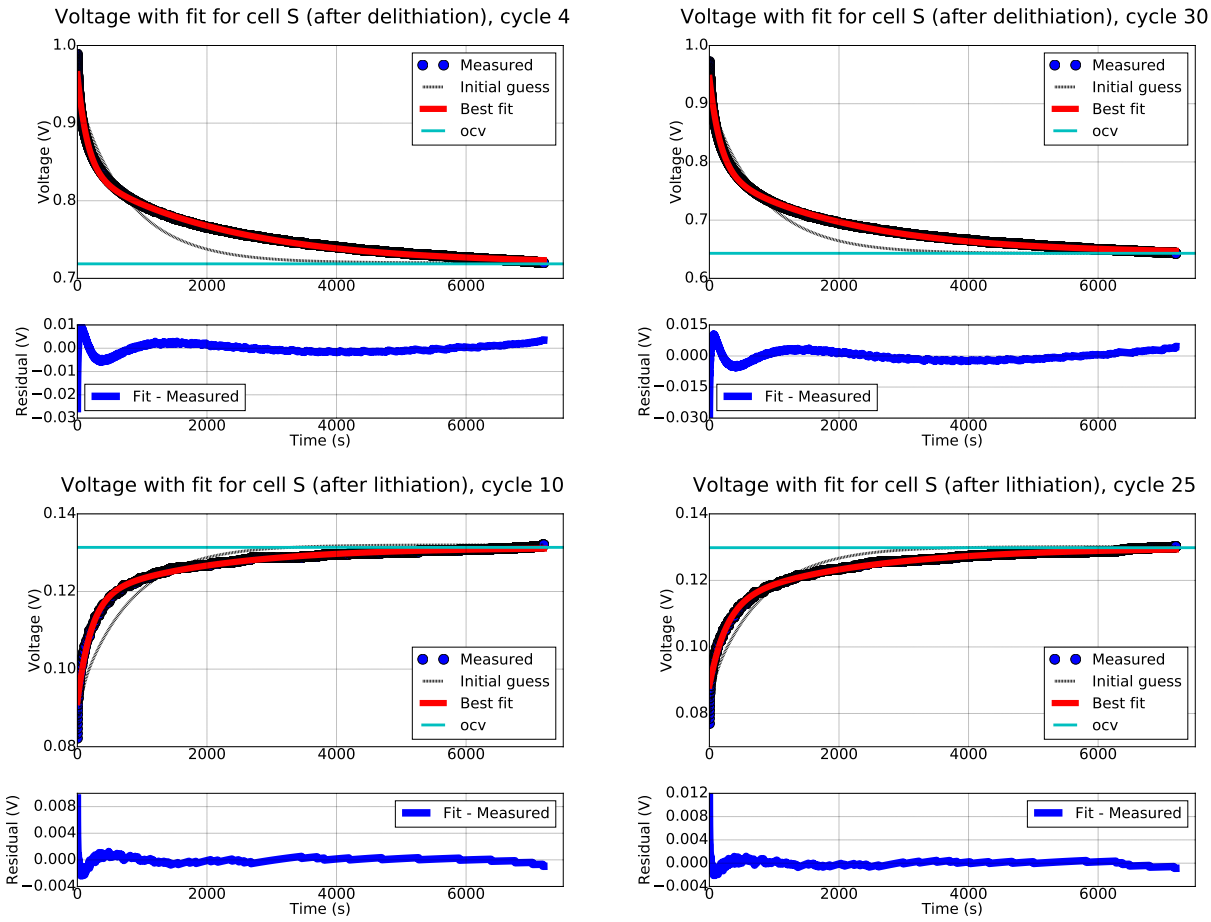

Figure B.16: Fitted OCV data for cycle 4 and 30 after delithiation and cycle 10 and 25 after lithiation.

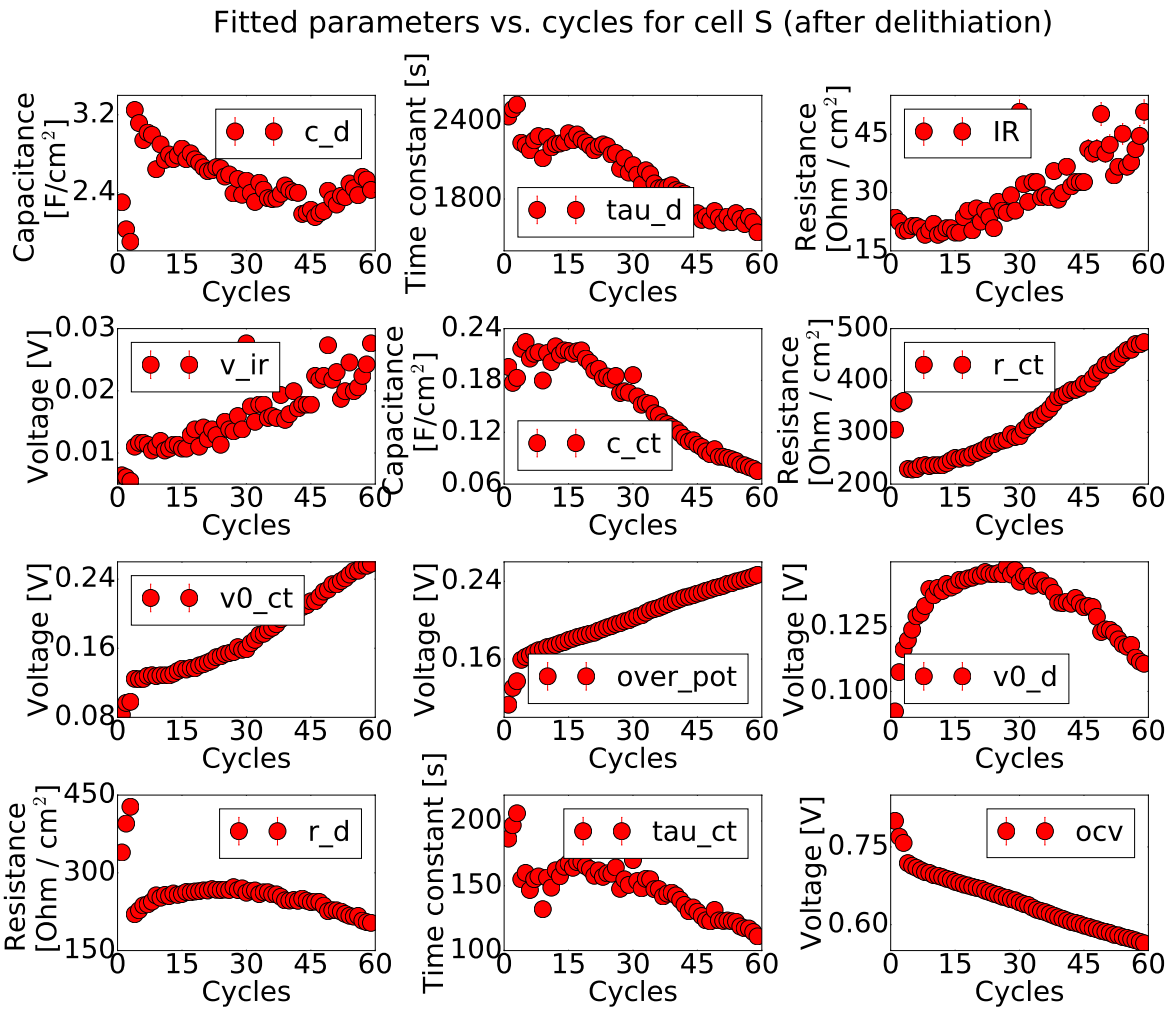

Figure B.17: All fitted parameters for cell S after delithiation.

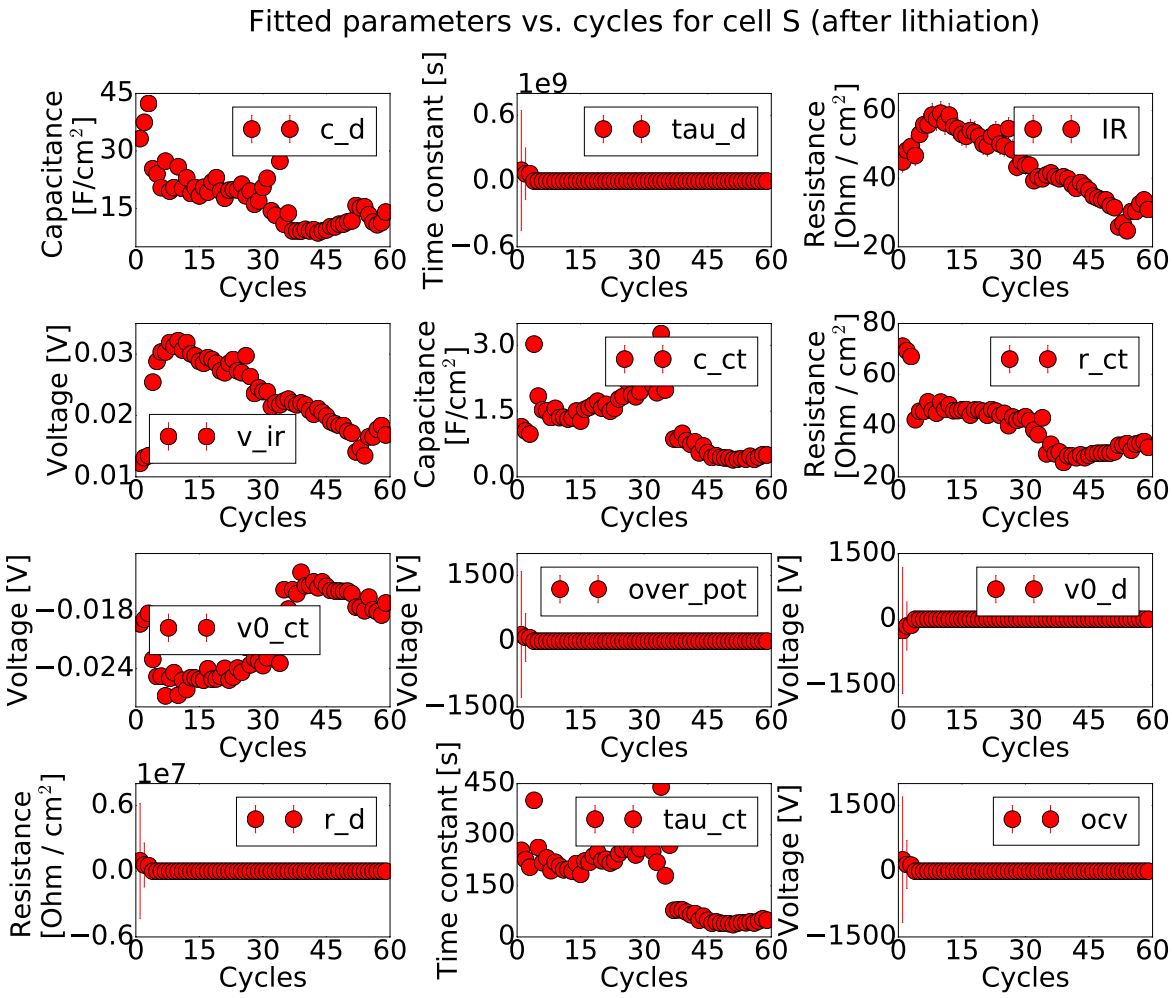

Figure B.18: All fitted parameters for cell S after lithiation.

Appendix C

EIS Data

All raw data were graphically extracted from Nyquist plots like the ones in Fig. 4.19 and 4.20.

Table C.1: Graphically extracted resistance and capacitance parameters from Nyquist plots after delithiation. Only charge transfer process and IR. c_ct = charge transfer capacitance, r_ct = charge transfer resistance.

process/cycle	1	2	3	4	5	6	7	8	9	10
ir [Ohm/cm$\hat{2}$]	0.8	0.7	1.2	1.6	1.4	1.4	1.6	1.6	1.6	1.7
cct [µF/cm$\hat{2}$]	20	19	19	18	23	27	20	26	26	32
rct [Ohm/cm$\hat{2}$]	22	23	24	24	23	26	27	27	27	32

Table C.2: Graphically extracted resistance and capacitance parameters from Nyquist plots after lithiation. Only charge transfer process and IR. c_ct = charge transfer capacitance, r_ct = charge transfer resistance.

process/cycle	1	2	3	4	5	6	7	8	9	10
ir [Ohm/cm$\hat{2}$]	2.7	2.7	2.8	2.3	3.4	3.4	3.4	3.4	3.4	3.4
cct [µF/cm$\hat{2}$]	5.3	5.5	5.4	4.5	4.7	4.5	4.2	4.6	4.5	4.0
rct [Ohm/cm$\hat{2}$]	83	80	82	87	93	97	104	110	121	110

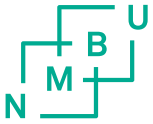

Norges miljø- og biovitenskapelig universitet
Noregs miljø- og biovitskapelege universitet
Norwegian University of Life Sciences

Postboks 5003
NO-1432 Ås
Norway